The Consolidation of Rapid Laser Deconsolidated Composite Tapes

Master Thesis

Dave A. van Winden

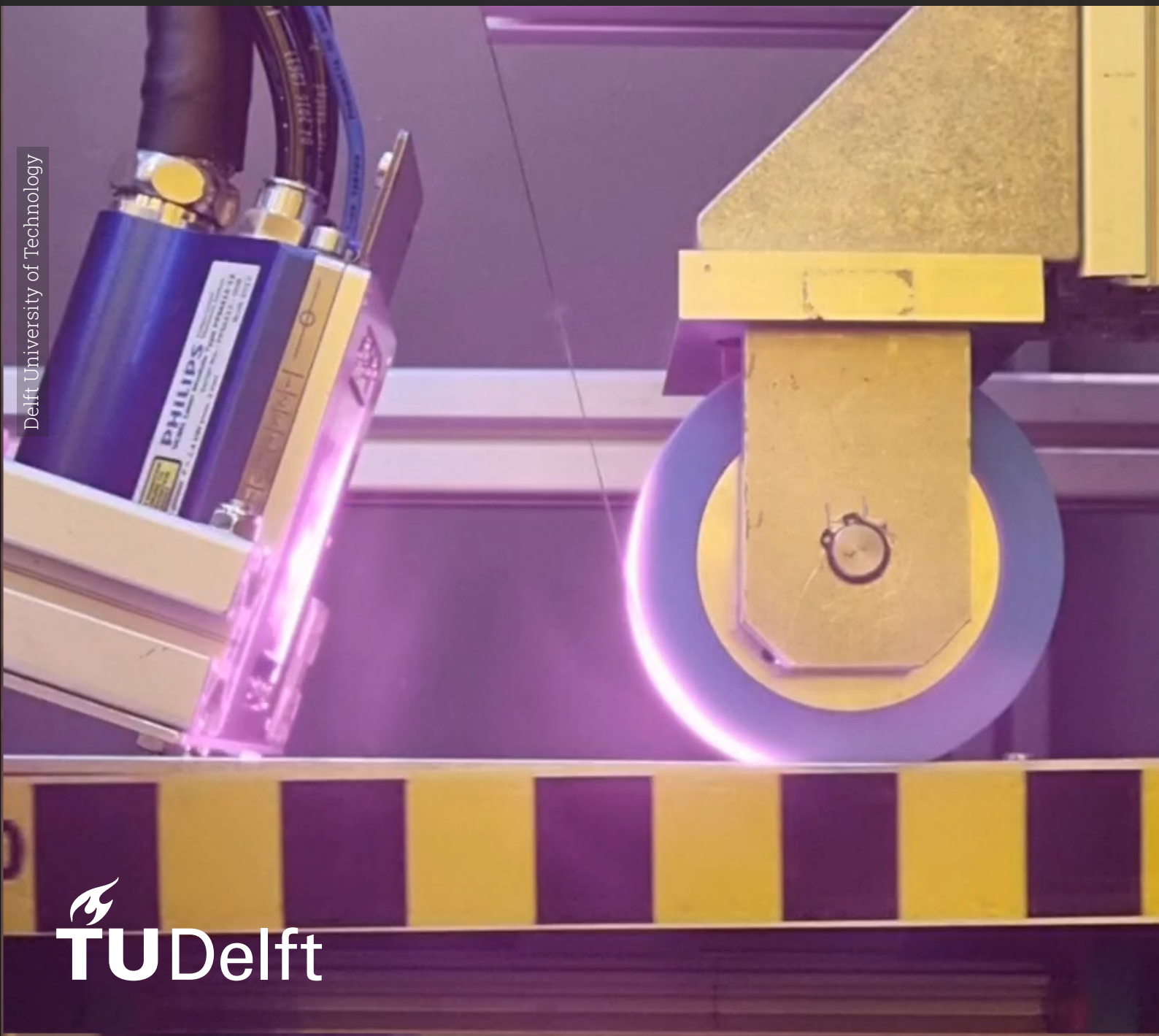

Delft University of Technology

TU Delft

The Consolidation of Rapid Laser Deconsolidated Composite Tapes

Master Thesis

by

Dave A. van Winden

Student Name	Student Number
Dave A. van Winden	4668324

Instructor:	Dr. Ir. D.M.J. Peeters
Instructor:	Dr. Ir. J.J.E. Teuwen
Project Duration:	August, 2022 - May, 2023
Faculty:	Faculty of Aerospace Engineering, Delft

Cover: Operation of the designed, constructed and utilized experimental set-up.

TU Delft

Summary

Laser assisted fiber placement (LAFP) is a promising automated manufacturing technique that can be utilized to manufacture larger thermoplastic composite aerospace structural components. The manufacturing technique would allow for a decrease in manufacturing cycle times and the end product is better recyclable than the currently used thermoset composite autoclave process. The LAFP manufacturing quality is promising but there are still some unknowns. For LAFP manufacturing quality to meet aerospace standards, additional research on the in-situ consolidation should be performed.

Research on LAFP has shown that deconsolidation of thermoplastic composite tapes occurs during the rapid heating phase. During the increase in temperature, various mechanisms occur that change the micro- and meso-structure of the tapes. The observed changes in structure, called deconsolidation forms, are increase in thickness, surface roughness, void content and waviness. It was identified that the deconsolidation forms have a negative effect on the bond forming ability as intimate contact forming is affected. Experimental studies have shown that it is possible to resolve the deconsolidation of the tapes when pressure and temperature is applied for a considerable amount of time. However, during LAFP the temperature and pressure time history for re-consolidation is limited. This time limit is expected to have a negative influence on the consolidation quality. The research objective was to acquire knowledge on the consolidation of rapid laser deconsolidated thermoplastic composite tapes by developing a novel experimental set up that can achieve variable laser-assisted fiber placement process parameters and analysing the produced specimens.

The research objective was split up into two research activities. First, the goal was to design and construct an experimental set-up that has the capability to make specimens undergo LAFP temperature and pressure histories. Secondly, utilizing the set-up to investigate the effect of LAFP process parameters on the rapid laser heating deconsolidation forms. The experimental set-up is utilized to produce CF/PEEK tape samples that have undergone six different combinations of placement speed (in the range of 40 mm/s to 200 mm/s) and consolidation pressure (in the range of 160 kPa to 600kPa). Post process, roughness, degree of effective intimate contact (DEIC), void content and thickness of the six data points where characterized using microscopy. The results of the characterization have been used to acquire knowledge on consolidation of rapid laser deconsolidated thermoplastic composite tapes.

The set-up that has been designed and constructed is capable of mimicking LAFP temperature and pressure histories. First the incoming tape is heated with a vertical-cavity surface-emitting laser (VCSEL), after which it moves through a shadow zone to be consolidated between a silicon roller and a moving tool surface that provides the linear placement movement. The experimental set-up has been designed and constructed to meet the research goal, while also maintaining flexibility for future modifications and advancements.

Deconsolidation resolvement is dependent on the re-compaction of the fiber bed and flow of the matrix material. Both placement speed and pressure increase have shown to yield a positive effect on the resolvement of deconsolidation. The process temperature was set equal between data points before the shadow zone at the visible nip point. The increase in placement speed and roller deformation due to pressure, shorten the time in the shadow zone, resulting in a higher nip-point temperature. The higher nip-point temperature allows for an increase in matrix mobility during consolidation. The increase in pressure, combined with the higher matrix mobility allow for the re-compaction and flow of the matrix to occur. Within the tested process parameter realm, initial severe deconsolidation can be resolved, leaving a certain level of decompaction and cavities to be resolved. The optimum process parameters have not been found in this study.

Acknowledgement

I would like to express my sincere gratitude to my supervisors Daniël Peeters and Julie Teuwen for their invaluable support, guidance, and confidence throughout my master thesis. Their expertise, encouragement, and constructive feedback have made this journey not only academically rewarding but also a pleasurable and memorable experience. I appreciate their method of guiding me, where I was given the freedom to make my own decisions while receiving valuable suggestions that helped me to achieve my research objectives.

I am particularly grateful to my supervisors for helping me select such an awesome thesis topic that has challenged me throughout my research journey. Their creativity, insights, and vision have motivated me to explore new ideas and push the boundaries of my capabilities and knowledge.

I would also like to extend my appreciation to the technicians who provided practical solutions and equipment for my experimental setup in the ASM flight hall. In particular, Dave and Johan's help has been invaluable, and I am grateful for their assistance.

I would like to thank the faculty of aerospace engineering at TU Delft for providing me with the opportunity to pursue a master's degree in Aerospace Structures and Materials, manufacturing track. The resources and facilities provided by the department have been essential to my success.

Finally, I would like to acknowledge my girlfriend, Elise Scheers, for her support, encouragement, and opinions during this journey. I am grateful for her love and support.

Finishing this challenging academic journey, which took a lot of hard work, time, and energy, with this thesis has been the perfect way to cap off my time at TU Delft. Thank you all for making my master thesis a truly enriching and rewarding experience.

Contents

List of Figures

List of Tables

Nomenclature

Abbreviations

Abbreviation	Definition
AR	As-received
CF	Carbon fiber
DEIC	Degree of effective intimate contact
LAFP	Laser assisted fiber placement
LSCM	Laser scanning confocal microscope
NIR	Near-infrared
PEEK	Polyether ether ketone
prepreg	Pre-impregnated (composite)
RMS	Root mean square
RQ	Research question
SQ	Sub-question
TP	Thermoplastic
VCSEL	Vertical-cavity surface-emitting laser

Symbols

Symbol	Definition	Unit
P	Pressure	[Pa]
R_a	Mean roughness	[μm]
R_q	Root mean square roughness	[μm]
sh	shore hardness [-]	
T	Temperature	[°C]
T_g	Glass transition temperature	[°C]
T_m	Melting temperature	[°C]
T_{m_i}	Infinite melting temperature	[°C]
T_p	Processing temperature	[°C]

1

Introduction

Reducing climate impact is becoming more and more important, all the while the aviation industry is growing. Due to the growth of annual commercial air traffic [1–3] in combination with the promise to reduce aerospace industry emissions [4], aircraft should reduces their emissions. One of the methods to lower aircraft emissions, is to reduce the weight of the aircraft. In the recent decades there has been an increase in the use of fiber reinforced composite materials for aircraft structures in an effort to decrease the weight [5, 6].

Currently, the majority of the structural composite parts are produced from thermoset composites. These composites have long cycle times, limited shelf life, limited recyclability and require the operation of massive autoclaves [7, 8]. For these reasons, more interest is directed towards the use of thermoplastic components. Thermoplastic composite components can be formed by melting plies or bundles of thermoplastic pre-preg together and consolidating the material into shape. The main benefit of thermoplastic composite manufacturing compared to thermosets is that they do not require post curing, witch reduces cycle time. Additionally thermoplastic composites allow for more recyclability, have greater fracture toughness and impact resistance, are repairable and allow to be welded [7, 8].

In order to extend the use of thermoplastic composite to large structural components, a promising automated manufacturing method, laser assisted fiber placement (LAFP), is considered. During LAFP the incoming material is melted using a laser, whereafter it is directly consolidated to the substrate material using a roller. This manufacturing method thus uses in-situ consolidation, which allows for continuous production of near net shaped aircraft structural components. Currently, the LAFP process has not been able to deliver sufficient manufacturing quality, a void content of 1.6% [9] is currently achievable and 1% is acceptable. Additional research regarding the consolidation quality is required before laser assisted fiber placement can pose a solution to the aerospace industry emissions reduction. The goal of this research is therefore to identify and perform research on knowledge shortcoming in the consolidation of thermoplastic composite material in the LAFP process.

First a literature study is performed in chapter 2, following the literature, research gaps are identified and the research is defined in chapter 3. In chapter 4 the design and construction of the experimental set-up will be explained. In chapter 5, the details of the experiments that will be performed are provided, followed by the results and discussion in chapter 6. Finally the work will be concluded in chapter 7 and recommendations for future work are suggested in chapter 8.

2

Literature Study

The literature study chapter provides an overview of the research conducted in advance of the current master thesis. The purpose of the study is to identify existing gaps in understanding and establish a framework for the current research. This review begins with a general introduction to laser-assisted fiber placement (LAFP), followed by more focused topics such as consolidation, deconsolidation, and the effects of deconsolidation on the consolidation phase.

2.1. Laser Assisted Fiber Placement

Laser assisted fiber placement is an additive manufacturing process for thermoplastic (TP) composite tapes. In this process a TP composite tape and the substrate are heated above their melting temperature using a laser heater. Thereafter the tape and substrate are consolidated under the pressure of a roller, which is considered in-situ consolidation. A visual representation of the manufacturing process is provided in Figure 2.1. The tapes are placed one-by-one, to eventually form the end product.

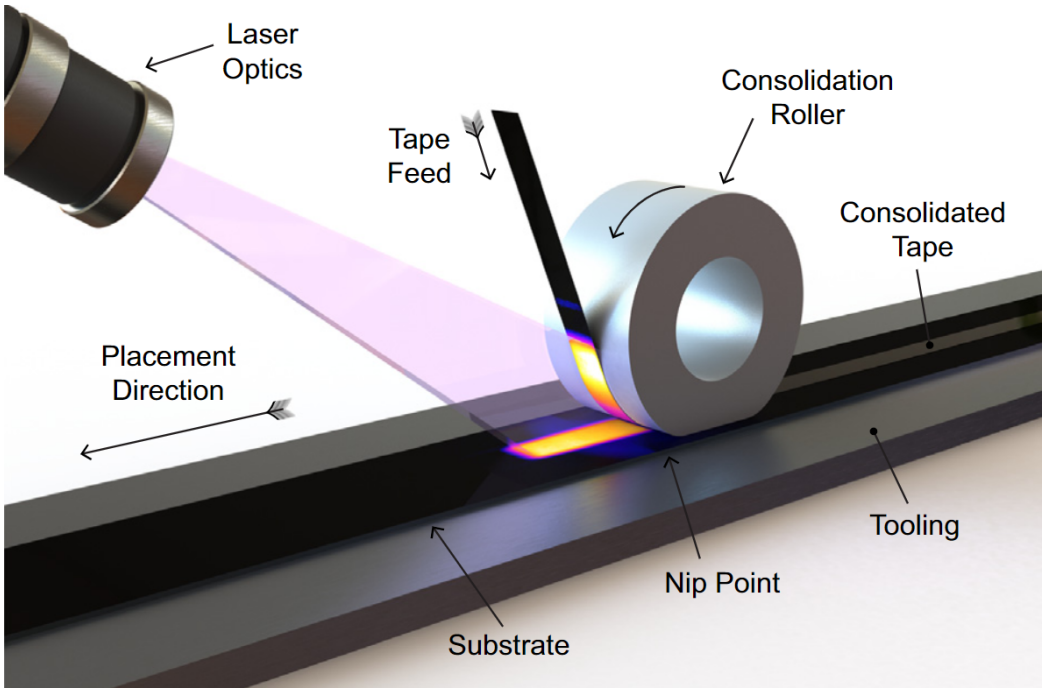

Figure 2.1: Working principle of LAFP process with visualization of the expected irradiance and typical laser beam propagation [10].

The process of in-situ consolidation during LAFP involves various mechanisms that ultimately lead to a consolidated material. These mechanisms operate within three distinct phases of the LAFP process: heating, consolidation, and release. In Figure 2.2, a schematic side view of the LAFP process is depicted, which highlights each of these phases and provides qualitative information on two critical process parameters - temperature and pressure. The mechanisms that act during each phase have a significant impact on the tape and substrate, and determine the final properties of the material.

This section provides the necessary background information on LAFP by delving into each of the three LAFP phases: heating, consolidation, and release. A thorough understanding of these phases is essential to achieve the desired quality and properties of the final composite structure.

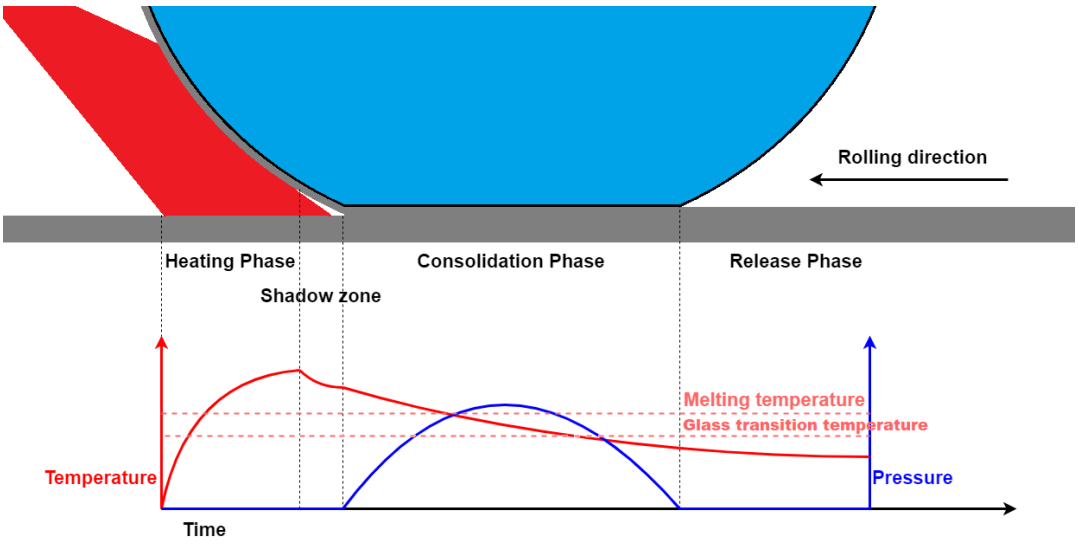

Figure 2.2: Overview of the different phases during LAFP.

2.1.1. Heating Phase

The first phase of the LAFP process is the heating phase, during which both the tape and substrate are heated using a laser heater. No external pressure is applied in this phase. It is critical to ensure that the surfaces of the tape and substrate are heated above their melting temperature at the start of the subsequent consolidation phase, known as the nip-point. However, just before the nip-point, the surfaces are in the shadow zone, where the laser cannot directly heat the material, and the temperature starts to decrease. Therefore, to avoid cooling below the melting temperature in the shadow zone, the surfaces must be heated slightly above the melting temperature during the heating phase. Depending on the roller type, laser location and placement speed, the shadow duration can be in the range of 3.5 to $96.0ms$ [11].

The heating phase is relatively short (0.2 to $0.7s$ [11]), and the material must be heated at a high heating rate (600 to $2500°C/s$) to achieve the desired temperature within this time frame. During the rapid increase in temperature, various mechanisms occur that change the micro- and meso-structure of the tapes [12, 13]. For example, volatiles and voids can expand, fibers can decompact, etc. Collectively these mechanisms are referred to as deconsolidation.

Two types of lasers have been mainly utilized and studied for LAFP: carbon dioxide (CO_2) and near-infrared (NIR) lasers. In particular, NIR lasers operate within a spectrum that directly heats the carbon fibers in the composite, while the matrix material remains transparent. This method of heating prevents the oxidation and burning of the matrix material, which can occur when using the CO_2 laser [14]. Additionally, NIR lasers offer advantages such as higher heat flux, improved efficiency, and greater control compared to CO_2 lasers [15]. Initially, laser heaters suffered from difficulties in shaping and focusing the heating spot. However, through addressing issues such as beam divergence, Stokes et al. were able to focus the NIR laser beam into a rectangular spot with uniform intensity, enabling homogeneous

heating of the tape and substrate during LAFP [15].

Classic NIR lasers are effective in providing good controllability, but their intensity distribution control is still limited. Therefore, Vertical Cavity Surface Emitting Lasers (VCSELs) have been developed for this purpose. A large array of single micro VCSELs are produced onto a chip. Multiple chips are placed in emitter lines, and these emitter lines can be stacked to form scalable arrays. VCSELs have the ability to control each individual emitter line, allowing for control of the laser intensity in sections of the heating spot [16–18]. Each emitter line contains two individually controllable lines, where the intensity is controlled by an electronic driver that sets the power per line. A change in power, or turning the line off/on takes place in the order of milliseconds [16, 17]. In Figure 2.3 an example of an heating profile is presented. When the laser placement as presented in Figure 2.4 is applied, both the tape and substrate can be heated individually, with intensity profiles in the placement direction.[16, 18].

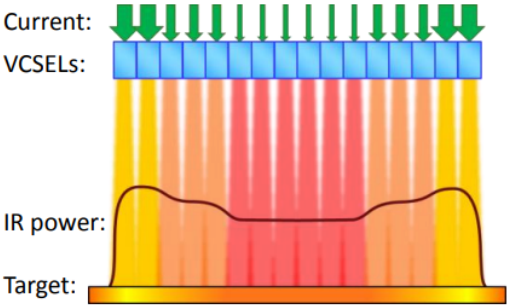

Figure 2.3: Controllable heating profile by individually controllable emitter lines [18].

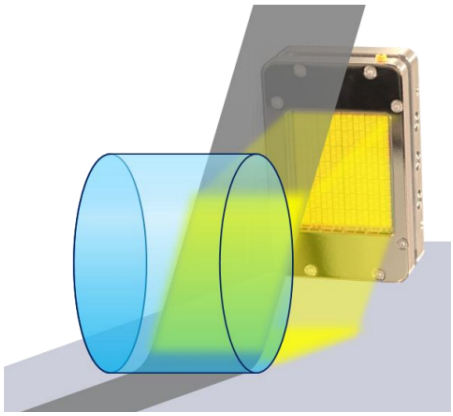

Figure 2.4: Applicability of a VCSEL heater on LAFP [18].

2.1.2. Consolidation Phase

After the heating phase, the material moves into the consolidation phase. The purpose of the consolidation phase is to properly consolidate the previously heated material. The pressure on the tape and substrate is increased and due to heat dissipation the temperature is reduced. If proper bonding is able to occur during the consolidation phase, the tape and substrate are fully consolidated into one single laminate [14, 19]. During the consolidation phase, not only the pressure but also the temperature of the TP at the interface plays an important role. Contact forming, bonding and crystallization are affected by the temperature history during the consolidation phase. The aforementioned tape deconsolidation that occurs in the heating phase hinders the intimate contact development [20]. The duration of the consolidation phase is a function of placement speed and roller contact area. The roller contact area is dependent on the roller stiffness and the compaction force. A more deformable roller provides a larger contact area with lower compaction pressure, compared to a harder roller [21]. The roller deformation affects the shadow zone as well, where the shadow zone decreases in length with increasing deformability [14].

Kok et al. [22] studied the effect of roller stiffness and compaction pressure and found that using a more deformable silicon roller increased the contact area and decreased the shadow zone length, resulting in a higher nip-point temperature for the same heating phase parameters. Two graphs from Kok et al. illustrating the effect of roller deformation on temperature history and nip-point temperature are shown in Figure 2.5 .

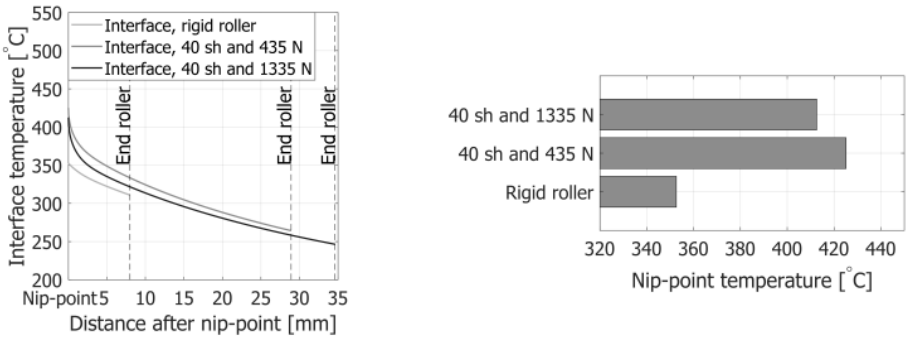

Figure 2.5: The effect of roller stiffness on (left) temperature history and roller area, and (right) nip-point temperature [22].

2.1.3. Release Phase

After the consolidation phase, the material enters the release phase where it is no longer under pressure from the roller. The material continues to cool down due to heat dissipation. The temperature at the start of the release phase is critical because if the matrix temperature is still above the T_g, deconsolidation and crystallization may continue to occur [23]. As the material cools, thermally induced stress may begin to form within the laminate [14].

2.2. Consolidation

This section aims to provide an in-depth understanding of the consolidation phase mechanisms and their role in achieving the desired manufacturing quality. The quality of the final product is commonly evaluated based on factors such as crystallinity, void content, fracture toughness, and interlaminar shear strength [24]. Void formation and compression, as well as intimate contact development and autohesion, are among the key phenomena that influence consolidation and ultimately determine the manufacturing quality [20]. In this subsection, we will first discuss void formation and compression, followed by the bonding mechanisms that define consolidation, intimate contact development and autohesion. Finally, we will examine the impact of various processing parameters on consolidation behavior.

Void Formation and Compression

The presence of voids is known to significantly impact the mechanical performance of advanced composite structures [25]. Consequently, in (de)consolidation studies, the final void content is commonly considered the most important quality parameter. The void content in the final product is dependent on both the base material quality and the manufacturing process [24, 26]. In safety-critical structures used in aircraft applications, the void content must be less than 1% to meet acceptance criteria [27]. Two types of voids are considered: intralaminar and interlaminar voids, as depicted schematically in Figure 2.6. Intralaminar voids are formed inside the plies and are mostly a result of the production process of as-received tapes. Interlaminar voids, on the other hand, are located between tapes and are formed during the LAFP manufacturing process.

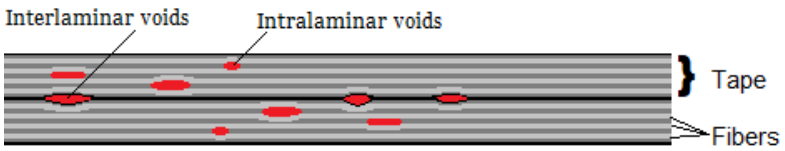

Figure 2.6: Schematical representation of intra- and interlaminar voids.

Intralaminar Voids

Intralaminar voids originate from the as-received tape and are included during its production. Efforts have been made to improve tape quality, which has led to a reduction in intralaminar void content in recent decades [28, 29]. However, the intralaminar void content can increase during the heating phase

due to the growth of existing voids and the formation of new ones from dissolved volatiles [30].

Interlaminar Voids
Interlaminar voids are formed during the consolidation of the tape and substrate [25], and can originate from inadequate pressure application, tape surface roughness, tape surface dry spots, and tape deformation. The tape (surface) structure has shown to also influence void formation [31], and additional mechanisms for interlaminar void development include void transfer and compression/decompression [32]. Void transfer occurs when existing or newly formed intralaminar voids travel to the surface of the tape, causing interlaminar voids [33].

Void Compression
Void compression occurs during the application of compressive force in the consolidation phase. The matrix material should be above T_g for the polymer chains to be mobile and allow the void volume to decrease. Early work approximated the compression behavior of voids using the ideal gas law [34], which shows that pressure and volume have an inverse relationship with respect to each other and that a decrease in temperature has a direct effect on the decrease in void volume. However, more recent research has recognized that limited matrix mobility [35] has an effect on this approach. A void filling model has been suggested that is dependent on volatile pressure in voids, fiber bed response, compaction load, and resin pressure due to squeeze flow [36]. The main take away from these studies is that both pressure and temperature have an positive effect on the compression of voids, with temperature allowing for matrix mobility and increased pressure is necessary to reduce void volume. However an increase in processing temperature can result in a higher final void content due to deconsolidation effects [20, 37].

Bonding Mechanisms

The final mechanical performance of a laminate depends on the bond quality between plies, which plays a crucial role in determining interlaminar shear strength, fatigue life, compression strength, and transverse tensile strength [25]. The bond between the composite tape and substrate is developed in steps, which are depicted in Figure 2.7. First intimate contact at the interface is required [38, 39] which is achieved with deformation of the surface. Through diffusion and entanglement of polymer chains at the interface, a process known as autohesion [40], the matrix material of both tapes are bonded.

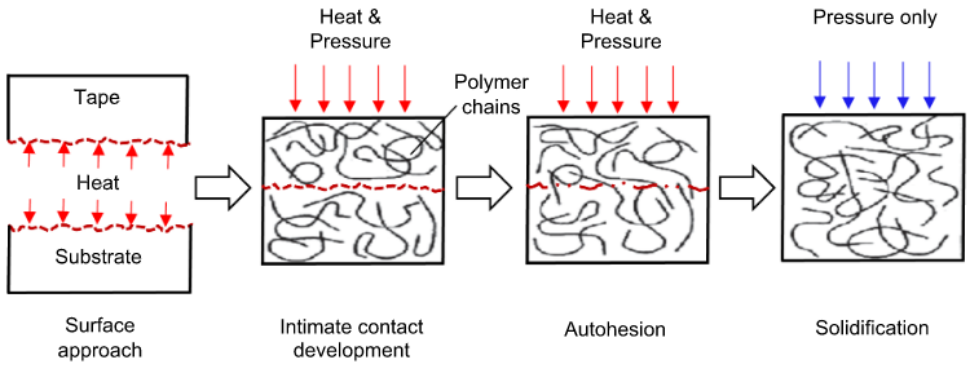

Figure 2.7: The in-situ consolidation of thermoplastic composite material at their interface [24].

Intimate Contact Development
The initial and crucial step in the bonding process is the formation of intimate contact. Optimal bond strength is achieved when the entire interface area is in intimate contact, as any areas lacking contact, such as those with interlaminar voids, will not develop a bond. Unbonded areas cannot transfer load and may even act as a site for damage initiation [19]. Intimate contact formation requires matrix material mobility [41]. Interface temperature dropping below melting point during consolidation leads to increased matrix viscosity and prevents further development of intimate contact.

For decades, the modelling of intimate contact development has been based on flattening surface asperities through transverse squeeze flow. Dara and Loos established the foundations for such models

in 1985 [42]. Since then, numerous studies have attempted to improve accuracy using this approach [43–45]. However, while these widely accepted models are used to predict the expected degree of intimate contact, they have limited prediction accuracy [11, 22, 46]. Kok et al. [22] were the first to point out that a model based on transverse squeeze flow of surface asperities is inadequate for accurately predicting the degree of intimate contact of LAFP. The suggested reason for this is the deconsolidation of the tape and substrate, leading to changes in the micro- and meso-structure of the surface that squeeze flow cannot model accurately. Deconsolidation will be further explained in section 2.3, and the effect on the deconsolidation phase in section 2.4

The degree of intimate contact is an important parameter for measuring bonding quality [20]. Therefore, it is crucial to know how to measure intimate contact and determine the degree of intimate contact experimentally. In the literature, C-scan [42, 47], ultrasonic inspection [45], X-ray [48], and micrograph imaging of the surface [19] or cross-section [41, 49] have been used to measure intimate contact. The choice of technique partially depends on the definition of the degree of intimate contact. C-scan, X-ray, and ultrasonic inspection identify the non-contact area. The remaining contact area is divided by the total area to obtain a fraction representing the degree of intimate contact. In contrary, the micro graph imaging of the interface area of Çelik at al. measured the resin content of the surface instead of the non-contact-area. Çelik at al. introduced ”effective” intimate contact, where only the contact area that contains resin is considered for intimate contact area. Here the degree of ”effective” intimate contact (DEIC) is calculated as the resin contact area divided by the total area.

Autohesion
Autohesion is a self-diffusion mechanism that bonds neat thermoplastics to itself [42]. The bonding occurs without any external force as long as the polymer interface is in intimate contact and the polymer chains are mobile. Unlike external pressure, time and temperature play a vital role in autohesion [42]. Above the T_g, polymer chains have limited mobility while above the T_m, they can freely move, making autohesion possible. Semi-crystalline polymers such as PEEK can normally only perform autohesion above T_m, where the material is fully amorphous and semi-crystallinity doesn't hinder polymer chain movement [50, 51]. On the other hand, amorphous polymers can perform autohesion below T_m and above T_g [50, 51]. Due to the heating phase of LAFP, the semi-crystalline PEEK at the surface is expected to be in an amorphous state, allowing autohesion to occur below T_m. Stokes-Griffin and Compston [11] found that semi-crystalline polymers heated above their infinite melting temperature (T_{m_i}) were also able to perform autohesion below T_m. For PEEK, T_{m_i} is considered to be between 385 and 395 °C [52, 53].

Crystallinity
The crystallinity of the polymer is an important physical characteristic for mechanical performance. The degree of crystallinity at the interface and in the tape affects interlaminar shear strength [54, 55], tensile strength [56], impact resistance [57, 58], and shrinkage [22, 24]. The final product's crystallinity depends on the initial crystallinity of the prepreg and the temperature history of the process. As-received tapes already have a certain degree of crystallinity, and during the heating phase of the LAFP process, the crystallinity is decreased if the processing temperature is above T_{m_i}. In the following consolidation and release phases, the crystallinity increases again if the process temperature is between T_g and T_m. A lower crystallinity tape is expected to melt faster, making diffusion easier, while a higher crystallinity tape is more difficult to melt, hindering diffusion, and resulting in a higher degree of crystallinity in the end product. The crystallinity of the polymer should be taken into account during LAFP. Ideally the heating phase should be able to melt the crystals at the interface for proper diffusion to take place. Lastly the cooling rate during both the consolidation and release phases also affects the amount of crystallization that can take place.

Processing Parameters

The LAFP process utilizes several process parameters to achieve the desired part quality and mechanical performance. Among these parameters, placement speed, compaction force, nip-point temperature, and tool temperature are considered the most significant. The process parameters and their qualitative contribution to the process are discussed.

Placement speed determines the productivity, consolidation time and heating time of the LAFP machine. Increasing the placement speed reduces the consolidation time which negatively impacts bond forming ability [21] and thus mechanical performance [20]. An increase in placement speed results in a less significant temperature decrease during the shadow zone. The placement speed is limited by the laser heating capacity and ability to consolidate the material.

Compaction force is critical in developing intimate contact and controlling the void content. An increase in compaction force results in more intimate contact development and a decrease in void volume.

Nip-point temperature, which is a result of the laser settings and placement speed, affects the state of the interface surface during consolidation. A higher nip-point temperature leads to a more mobile polymer but also increased deconsolidation effects [13, 20]. The temperature is limited by material properties, release temperature and LAFP machine capabilities.

Tool temperature, which is the temperature of the tooling, is shown to have a positive effect on mechanical properties [59, 60] due to increased autohesion and crystallization time. Increased tooling temperature does result in higher void content [60, 61].

The effect of each process parameter on important product quality parameters is summarized in Table 2.1. It is important to consider these effects when adjusting the process parameters.

Table 2.1: Influence of process parameters on quality parameters. The upward (↑) or downward (↓) arrow indicates the increase or decrease of the quality parameter due to the increase of the process parameter. The colour of the cell indicates whether that effect is positive(green) or negative(red) for the quality. The horizontal bar (-) and yellow cell indicate there is no effect.

	Autohesion	**Crystallinity**	**Interlaminar bond strength**	**Interlaminar voids**	**Intralaminar voids**
Placement speed ↑	↓[20, 21]	↓[20, 21]	↓	↑	↑
Compaction force ↑	↑[22, 41, 42]	-	↑	↓	↓
Nip-point temperature ↑	↑[19]	↑	↑	↓[22]	↓[62]
Tool temperature ↑	↑	↑	↑[59, 60]	-[22]	↑[60, 61]

2.3. Deconsolidation

Deconsolidation is a term used to describe the adverse changes that occur in the micro- and meso-structure of a TP composite material when exposed to high temperatures without the application of pressure. During the LAFP process, deconsolidation occurs in the heating phase, when the composite tape is heated without the application of pressure. This alteration in micro- and meso-structure has a negative impact on the consolidation of the tape and substrate, resulting in decreased bond quality. In the past, deconsolidation was observed in TP composites when well-consolidated tapes were re-heated without the application of pressure [63]. Such occurrences were typical in manufacturing processes such as induction welding, resistance welding, and stamp forming. However, it was believed that deconsolidation would not occur during LAFP due to the short heating phase. Recent studies have shown that deconsolidation can actually occur during LAFP [22]. Moreover, due to the high heating rate, the deconsolidation mechanisms in LAFP have been found to be different from typical deconsolidation [13]. In this section, the deconsolidation mechanisms in general will be discussed, followed by a specific focus on laser-induced deconsolidation.

Deconsolidation Mechanisms

Deconsolidation during high heating rates differs from low heating rate deconsolidation; however, the fundamental mechanisms are overlapping. From the literature, the primary deconsolidation mecha-

nisms identified are:

- Decompaction of the fiber reinforcements due to residual stresses [64, 65].
- Void growth caused by gas thermal expansion, movement, and coalescence [36, 66, 67].
- Thermal expansion and viscoelastic behavior of the matrix [68].
- Thermal expansion of dissolved moisture [69].

These deconsolidation mechanisms lead to micro- and meso-structural changes in the composite tape, resulting in an increase in surface roughness, volumetric void content, tape thickness, and fiber waviness [22, 70]. A cross-sectional image of deconsolidated tapes is shown in Figure 2.8.

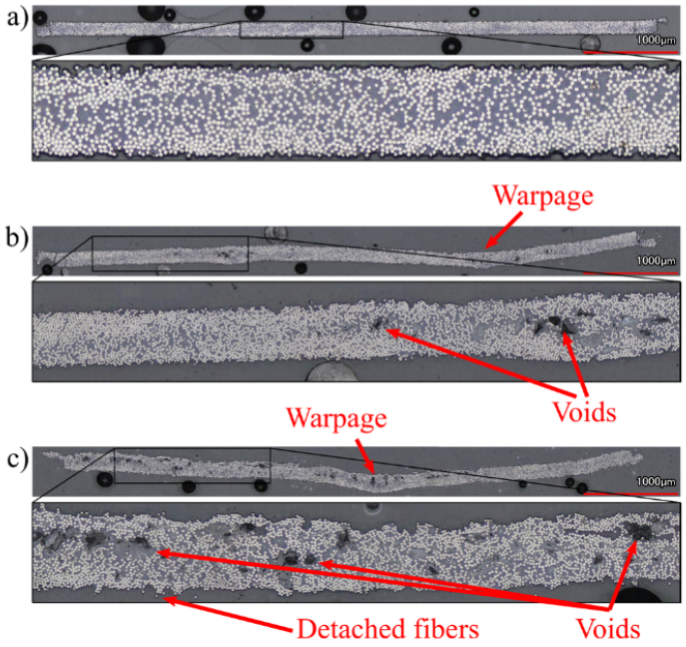

Figure 2.8: Cross-sectional images of a) as-received tape, b) slightly laser-deconsolidated tape, and c) highly laser-deconsolidated tape.[20] Here waviness is considered to be warpage.

Residual stresses are introduced during the production of prepreg tapes, which can be released as decompaction and waviness once the matrix is above T_g. According to Wolfrath et al. [64], elastic springback of the fiber preform is the main contributor to decompaction. The mobility of the matrix in combination with fiber movement allows for the growth of voids, where a less viscous matrix results in more void growth. Ye et al. [71] found that decompaction and subsequent void growth result in increased tape thickness, and the extent of the thickness increase is dependent on the heating time. Void growth occurs when the external pressure is lower than the decompaction pressure within the tape, indicating that fiber reinforcement decompaction leads to void growth. Additionally, decompaction is a cause of part of the surface roughness, as fiber decompaction and matrix mobility can result in loose dry fibers at the tape surface [69].

Besides decompaction, thermal expansion of gas and dissolved moisture can also result in an increased void content. However, Ye et al. [66] found that the void growth due to thermal expansion is insignificant compared to the void growth resulting from decompaction. Lu et al. [67] found that once the matrix is above T_m and matrix elasticity has disappeared, voids have the ability to migrate and coalesce to form larger voids. Furthermore, some voids can even move out of the composite due to void migration, lowering the void content [36, 67].

Rapid Laser Heating Deconsolidation

Deconsolidation during rapid laser heating of TP composite tapes is a recent finding. The first study to observe laser (assisted fiber placement) deconsolidation was conducted by Kok et al. [22], who

reduced the pressure on the tape during consolidation to capture the deconsolidated state. However, this method resulted in partial consolidation of the tape against the tool, making it difficult to accurately represent the tape state after the heating phase.

To address this issue, Çelik et al. [13] performed a different experimental study using a laser line scanner and thermal camera to measure the surface and temperature profile of the tape in-situ during laser heating. Their experimental setup, shown in Figure 2.9, utilized the VCSEL to mimic different placement speeds in a stationary setup.

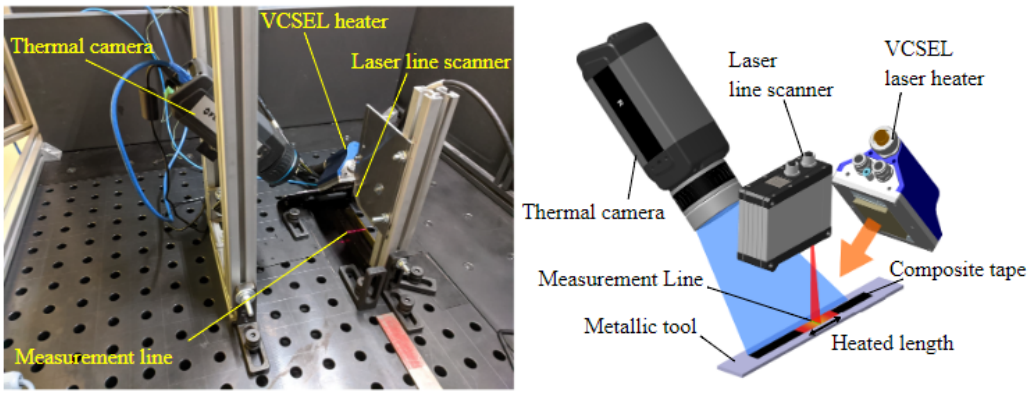

Figure 2.9: Experimental setup used by Çelik et al. to in situ capture laser deconsolidation [13].

This study found that laser heating causes significant micro- and meso-structure changes, including increased out-of-plane deformation, waviness, arc-length width, and surface roughness. The heating spot length had a significant effect on arc-length width, waviness, and surface roughness, while heating time had a significant effect on arc-length width and surface roughness. It was also identified that the heat distribution in the tape has a correlation with the meso-scale changes, with non-uniformity in the heat distribution intensifying the local deconsolidation mechanisms. This is illustrated in Figure 2.10, where the direct correlation between deconsolidation mechanisms and forms of deconsolidation are visualized.

It should be noted that this study has been able to identify that laser heated deconsolidation is significantly different from conventional deconsolidation. Laser heating is radiation heating that directly heats the fibers, instead of the conventional conduction/convection heating where the whole composite is heated. As a result, the fiber distribution in the composite has an effect, with more closely grouped fibers collectively becoming warmer than more spread out fibers. Currently, the fiber distribution in TP prepreg tapes is not homogeneously distributed, resulting in non-uniform temperature distribution.

The results of this experimental study have provided a greater understanding of how deconsolidation evolves during the heating phase and the state of the tape at the nip-point. However, there are some limitations to the experimental method that differentiate the setup from reality. In this study, an as-received tape was heated, which represents the tape being placed down on the substrate in LAFP. It is not known how deconsolidation evolves at the substrate, knowing that the substrate has already been heated and consolidated before, which might have an effect on the deconsolidation mechanisms. Furthermore, in this study, the tape had the freedom to move out of plane and was not under tension, which is not the case for LAFP. The tape in LAFP would be under slight tension, and the back pressure of the roller would have an influence on the ability to move out-of-plane. With this in mind, the deconsolidation as quantified by Çelik et al. could be overestimated.

Y. Blommert presented his master thesis work at Delft University of Technology, investigating the effect of tape pre-tension on deconsolidation [72]. Blommert compared his experimental results with those of Celik et al. and found that tape pre-tension reduced the deconsolidation effects to some extent. Choudhary and Çelik et al. [23] performed experiments on a composite tape that was constrained out-of-plane using kapton tape. This resulted in a more homogeneous temperature distribution and

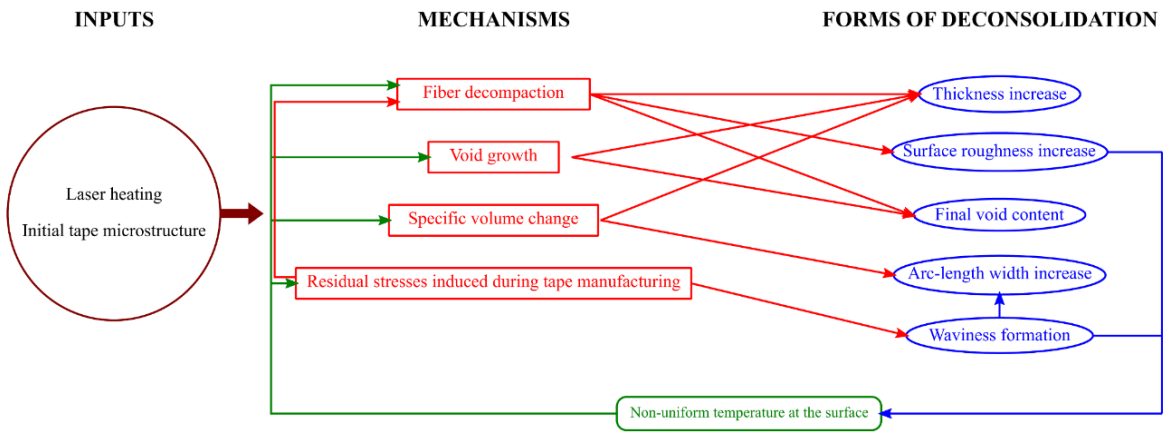

Figure 2.10: The effects of deconsolidation mechanisms and forms of deconsolidation [13].

less severe local deconsolidation. It was thus found that the deconsolidation quantification from previous research results could be overestimated as tape constrained was not taken into account properly.

Additionally, both Blommert and Kok et al. [22] performed research on the effect of resin-rich surface tapes with regards to deconsolidation. It was observed that having a resin-rich surface on the composite tapes, contains the fibers during heating more efficiently [22]. This may benefit the intimate contact development. Blommert found a positive effect on the intimate contact development, leading to reduced deconsolidation effects.

2.4. The Effect of Laser Deconsolidation on the Consolidation Phase

The understanding of the effect of rapid laser deconsolidation on consolidation behavior during LAFP is incomplete. Only a few studies have been conducted on the resolvement of laser deconsolidation and the effect of process parameters on deconsolidation resolvement [20, 73]. It is evident from previous research that current modeling and understanding of consolidation and bond formation are insufficient to account for deconsolidation. The primary issue in the current modeling and understanding of consolidation after deconsolidation is the impregnation of the resin-poor surface layer due to dry surface fibers. This section discusses the current understanding of intimate contact development of deconsolidated tapes, followed by the mechanisms of deconsolidation resolution and the influence of process parameters.

Intimate Contact Development of Laser Deconsolidated Tapes

Kok et al. [22] observed that deconsolidation leads to the emergence of dry fibers at the surface of the composite tape. While squeeze flow is a crucial mechanism for intimate contact development, it is not sufficient due to the presence of dry fibers at the contact interface. Kok et al. proposed a 1D impregnation model, in this model the fiber bed is compressed and the matrix is redistributed between the new fiber distribution. However, it underestimated the degree of intimate contact, possibly due to its simplicity. A more advanced 2D model that includes squeeze flow and impregnation in all directions was suggested. Additionally, Kok et al. recognized that the dry fibers at the surface are partially impregnated, which aids in achieving a higher degree of impregnation. Çelik et al. [19] also found that squeeze flow alone is not enough to explain intimate contact development. They proposed a combination of through thickness and in-plane percolation flow along with squeeze flow, as shown in Figure 2.11. Zone two can develop effective intimate contact through squeeze flow, but zones 1 and 3 require percolation flow for effective impregnation. The mechanisms are dependent on fiber-resin distribution and deconsolidation severity, which is shown in the comparison of zones 1 and 3. It has been recognized that the degree of effective intimate contact increases with pressure. A model based on only squeeze flow is insensitive to a pressure increase and a model based percolation flow is sensitive to pressure. Suggesting that percolation flow is indeed occurring during consolidation. However, no model has been built and tested yet.

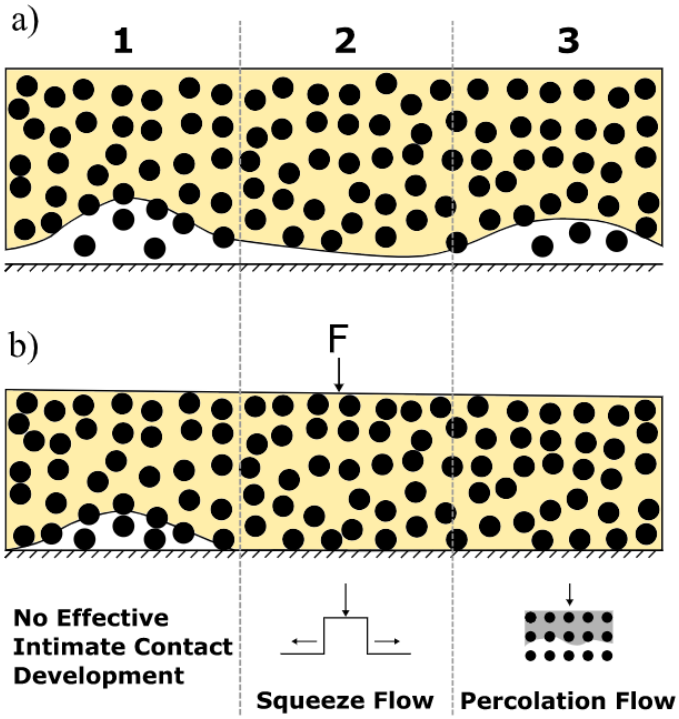

Figure 2.11: "Development of effective intimate contact and underlying mechanisms for initial surfaces with different microstructure. (a) Uncompressed composite tape,(b) compressed composite tape"[19]

Deconsolidation Resolvement

In a recent study by Slange [73], the consolidation of stamp forming blanks was investigated, where LAFP was one of the blank manufacturing techniques. The study showed that with sufficient pressure, temperature, and time, the deconsolidation effects can be resolved, resulting in a well-consolidated laminate. However, the process parameters that allowed for the resolving mechanisms to take place were not in line with LAFP. This is because during the post-consolidation step, the laminate was heated using conduction/convection, resulting in a different type of deconsolidation, and the temperature and pressure history were not consistent with what is expected in LAFP, where shorter times above the melting temperature and under compaction pressure are observed.

To further investigate the effect of deconsolidation on consolidation using LAFP, Çelik et al. [20] conducted an experimental study. In this study, deconsolidated tapes were subjected to constant pressure and temperature for a duration of time. Compared to Slange's study, Çelik et al. focused more on understanding the deconsolidation resolving mechanisms and the effect of process parameters. Through their experimental approach, they were able to gain insight into what deconsolidation form can be resolved under specific process parameters. The study findings were grouped into four categories based on the temperature range: mechanisms acting below and at T_g, between T_g and T_m, and above T_m. The study also examined the effect of pressure on consolidation. To efficiently summarize the results of this study, Table 2.2 has been provided.

What is most notable is that waviness and thickness is the only parameter that is affected below T_g. This is due to flexibility of the matrix and is confirmed by a drop in waviness and thickness at T_g when the matrix releases the stored compression energy. It has become clear that the time above T_m is really important to resolve the deconsolidation and form a good bond.

While the experimental results have shed light on the mechanisms behind consolidation, it is important to note that the set-up deviates significantly from the LAFP process. Specifically, the temperature and pressure histories are not representative of the actual LAFP process. In the study the previously

deconsolidated tapes have been kept under pressure while a heat cycle was applied, the process was in the order of minutes. In reality, the temperature history is shorter, and pressure is only applied under the roller. As a result, any further deconsolidation before and after the roller is ignored. Finally, due to spending more time in the processing temperature, the crystallinity is lower and thus the matrix mobility is higher. In the LAFP process, the crystallinity is expected to reduce less and thus the mobility is expected to be lower due to the shorter heating cycle. Additionally, the heating method in the LAFP process is different, as the fibers are heated. This leads to a temperature distribution within the composite that is dependent on local fiber density. The difference in temperature and mobility can have an impact on the local matrix mobility. The effectiveness of consolidation is overestimated, and the results from this study should therefore be used qualitatively rather than quantitatively.

Table 2.2: Influence of process parameters on deconsolidation forms. The upward (↑) arrow, downward (↓) arrow or horizontal bar (-) indicates the increase, decrease or in-effectiveness of the process parameter on the deconsolidation mechanism. The colour of the cell indicates whether that effect is positive(green) or neutral(yellow) to the consolidation quality. Two arrows indicate a more significant effect, a bar and arrow indicate a slight effect.

	Waviness	**Voids**	**DEIC**	**Roughness**	**thickness**
$<= T_g$	↓↓	-	-	-	↓↓
$T_g <> T_m$	-	-↓	-	-↓	-
$> T_m$	↓	↓↓	↑↑	↓↓	↓
P increase	-	↓	↑	↓↓	↓

2.5. Conclusion

In conclusion, this literature study has provided a comprehensive overview of the research conducted in advance of the current master thesis. The topics covered include consolidation, deconsolidation, and the effects of deconsolidation on the consolidation phase. The study has identified existing gaps in understanding and established a framework for the current research.

The consolidation phase was thoroughly discussed. This covered the origin, propagation and resolving mechanisms of voids, as well as bonding mechanisms and effects of process parameters. The bonding mechanisms can be summarized in two steps: first, intimate contact should be developed, then autohesion occurs bonding the tape and substrate. In addition, the literature covered the deconsolidation of TP composite tapes and the mechanisms that cause changes in micro- and meso-structure, such as fiber decompaction, void growth, thermal expansion, and specific volume change. These mechanisms result in changes in the form of increased thickness, surface roughness, volumetric void content, and waviness. Importantly, the negative effect of deconsolidation on the bond-forming ability during the consolidation phase was also highlighted.

Finally, the literature on consolidation after deconsolidation was studied. It was found that experimental studies have shown it is possible to reduce the negative effects of deconsolidation by applying extensive pressure and temperature during consolidation. The effect of LAFP type consolidation on resolving deconsolidation has remained unaddressed in literature. The effects of rapid laser deconsolidation currently limit the manufacturing quality that can be achieved with the LAFP process. The first step in improving the manufacturing quality is understanding the effect of LAFP type consolidation conditions on resolving deconsolidation. Overall, this literature study has provided a solid foundation for the methodology and interpretation of the results of the current research on LAFP.

3

Research Definition

Although significant research has been conducted to investigate rapid laser deconsolidation and its effect on compaction behavior, as demonstrated in the previous chapter, there are still several gaps in the current literature. This chapter aims to address these gaps by closely examining the covered literature and defining a research plan. To begin, relevant research gaps in current LAFP literature are identified. From the research gap, the research objective, and research questions will be deduced and described in detail in this chapter.

3.1. Research Gaps

These gaps highlight the limitations and shortcomings of previous research, and provide opportunities for further investigation. By closely studying the literature, three research gaps have been identified in the current state of research:

Deconsolidation of a Restrained Tape.
The current literature, as discussed by Choudhary [23] and Çelik et al. [13], suggests that deconsolidation during the LAFP process leads to out-of-plane deformation, exacerbating the temperature distribution and local deconsolidation. However, these studies were conducted on free-to-deform tape specimens, which may not fully recreate LAFP circumstances. Partial recognition has been found that tape tension and out-of-plane movement restriction results in less deformation [20, 22]. Moreover, it is expected that tape tension and roller back pressure during the LAFP process will result in less out-of-plane deformation. This suggests a gap in research regarding the uniformity and severity of tape deconsolidation during the LAFP process.

Resin-rich Surface Tape.
Research has been conducted by Blommert [72] regarding the investigation of resin-rich surface tapes earlier this year. The research indicated that such tapes can reduce the effects of deconsolidation and improve intimate contact development. However, the study did not determine the optimal amount of resin on the surface of the tapes, nor did it examine the feasibility of adding more resin. Additionally, the impact of the resin-rich surface on the overall laminate properties needs to be further quantified. Hence, there is a gap in understanding the optimal resin distribution on the surface of the tapes and its impact on the LAFP process and properties.

Effect of Deconsolidation on Consolidation Phase.
While the effect of rapid laser deconsolidation during LAFP has been studied, the ability of the LAFP consolidation phase to resolve these effects is not well understood. Çelik et al. [20] have identified the temperature and pressure ranges needed to resolve deconsolidation. However, there is a lack of knowledge regarding how capable the LAFP process consolidation phase is in resolving the deconsolidation forms. A better understanding of the limitations and capabilities of the consolidation phase in resolving different forms of deconsolidation, as well as the quantitative effect of process parameters on these forms, would greatly benefit the scientific community.

Based on the analysis of the identified research gaps, it is evident that further investigation is necessary to enhance the quality and reliability of the LAFP process. The effects of rapid laser deconsolidation currently limit the manufacturing quality that can be achieved with the LAFP process. Among the various research gaps, resolving deconsolidation during the consolidation phase appears to be the most pressing issue. The first step in improving the manufacturing quality is understanding the effect of LAFP type consolidation conditions on resolving deconsolidation. A thorough understanding of the consolidating capability and the impact of process parameters on deconsolidation forms would greatly benefit the advancement of the LAFP process. Once this understanding is established, potential improvement such as resin-rich surface tapes can be researched. The availability of fundamental scientific background information provides a solid foundation to build a comprehensive research framework.

3.2. Research Objective

The research objective is to develop a novel experimental setup capable of achieving variable laser-assisted fiber placement process parameters, analyze and compare the produced specimens, and acquire knowledge on the consolidation of rapid laser-deconsolidated thermoplastic composite tapes, as well as the effect of process parameters on the consolidation process.

3.3. Research Questions

From the research objective, the research questions can be computed. The main research question that will be solved in this thesis work reads as follows:

RQ: What is the effect of LAFP type temperature and pressure histories on the ability to resolve deconsolidation during the consolidation phase of the LAFP process?

From the research question, multiple sub-questions can be deduced that have to be answered. Per sub-question, another level of smaller questions can be formulated that together contribute to the answer of the sub-question:

SQ1: How can an experimental set-up mimic and apply LAFP temperature and pressure histories to thermoplastic composite tape?

- SQ1.1: What are specific parameters and variables that need to achievable with the experimental set-up to achieve relevant results?
- SQ1.2: How can the experimental set-up be designed and manufactured such that variable LAFP process temperature and pressure histories can be achieved?
- SQ1.3: How will the experimental set-up be verified to achieve the desired process parameters?

SQ2: What is the effect of applying different consolidation pressures and placement speeds on the void content, roughness, thickness and degree of effective intimate contact?

- SQ2.1: How can void content, roughness, thickness and degree of effective intimate contact be measured quantitatively?
- SQ2.2: How does the change in pressure and placement speed correlate with void content, roughness, thickness, and degree of effective intimate contact in the LAFP process?
- SQ2.3: What process parameter recommendations can be formulated from the experimental results in order to minimize the effect of deconsolidation on consolidation quality?

4

Experimental Set-up

The purpose of this research is to gain a better understanding on the ability of LAFP pressure and temperature histories to resolve deconsolidation forms. The research objective is twofold: first, to establish the capability to generate LAFP type pressure and temperature histories, and second, to utilize this ability to investigate the effectiveness of such conditions in resolving deconsolidation forms. This chapter focuses on the first objective, which involves designing and constructing an experimental setup capable of producing specimens subjected to LAFP type temperature and pressure histories.

The experimental set-up design method used in this study will be outlined, including the variables and requirements taken into consideration. Additionally, the process of concept selection utilized in the design of the experiment will be discussed. The details of the experimental set-up design will be delved into, followed by a discussion of any limitations that may affect the results. The potential impact of these limitations on the validity of the study's findings will also be addressed. Finally, a conclusion will summarize the key takeaways from the experimental set-up, highlighting its strengths and weaknesses. The aim of this chapter is to provide a comprehensive understanding of the experimental set-up, its design process, limitations, and implications on the study's findings, with a clear rationale behind the choices made.

4.1. Experimental Set-up Concept

The experimental set-up design process is structured according to the approach outlined in Figure 4.1. The first step is to clearly define the goal of the set-up, which serves as the foundation for determining the necessary requirements and variables. These requirements and variables are then used as the foundation for designing the experimental set-up and determining the methods for measuring the variables. This approach allows for a systematic and logical design process, ensuring that all necessary considerations are taken into account and that the specific goals of the study are met. The goal of the experimental set-up is to able to produce specimens that underwent LAFP type temperature and pressure histories.

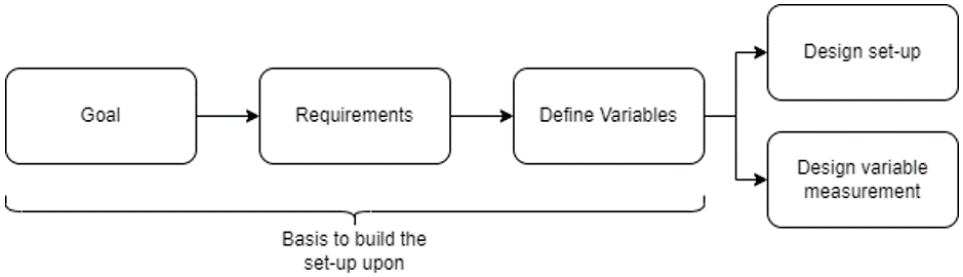

Figure 4.1: Experimental set-up design approach.

4.1.1. Requirements

The research goal provides specific requirements that the experimental set-up must fulfill in order to provide desired results. These requirements were taken into account in the design and development of the experimental set-up. Note that there is some overlap between requirements and the variables. The requirements are categorized in three categories:

Tape process conditions

- Rc1) The composite tape should be heated with infrared laser heating.
- Rc2) The experimental set-up should be able to apply LAFP compaction cycle durations, between 0.03 and 0.3 seconds.
- Rc3) The experimental set-up should be able to apply LAFP compaction pressures with a upper range in 500 to 1000 kPa.
- Rc4) The compaction cycle should be applied directly after the heating phase, with the exception of the shadow zone.

Rc2 is based on reported placement speeds ranging from 37.5 to 500 mm/s [13, 74–76] and Rc3 is based on reported higher end expected compaction pressures [19, 76].

Materials and equipment

- Re1) The compaction pressure should be applied with a flexible material.
- Re2) The infrared laser heating source should be a VCSEL.
- Re3) The set-up should be able to feed quarter-inch CF/PEEK composite material.
- Re4) The experimental set-up should allow for the placement of a FLIR A655sc thermal camera.

Measuring

- Rm1) The experimental set-up should be able to measure the visible nip-point temperature (closest point to the nip-point that is visible/measurable).

Project

- Rp1) The experimental set-up should be able to be manufactured with the equipment available in the ASM aircraft hall.
- Rp2) The experimental set-up should be able to be designed and manufactured within a 3 month time frame.
- Rp3) The experimental set-up should be adjustable for future research.
- Rp4) Operation of the experimental set-up should not cause disproportional risk of damage to instruments or operators.

4.1.2. Variables

From the research questions, it is possible to specify which variables will be measured (dependent variables) and which variables will be varied (independent variables) in the experimental set-up. This is crucial in the design process, as it ensures that the experimental set-up is equipped to measure the appropriate variables and that the experimental manipulation is able to effectively isolate and study the dependent variables. The variables of both types are listed below in two separate lists.

Independent variables

- Heating intensity
- Heating distribution
- Placement speed
- Compaction force

Dependent variables

- Visible nip-point temperature
- Compaction pressure
- Compaction time
- Heating time

4.1.3. Conceptual trade-off

Based on the set of requirements and variables, the experimental set-up will be designed. The process starts with five initial conceptual ideas as starting points. These concepts and their working mechanisms will be explained in detail. A trade-off analysis will then be conducted based on their ability to achieve movement, ability to apply pressure and how well they align with the actual LAFP process.

Concept 1 and 2

The first two concepts presented in this research are designed to closely align with the actual LAFP process. Conceptual drawings of these concepts can be found in Figure 4.2. Both concepts make use of a silicon roller to apply pressure. In concept 1 the instruments (laser, roller, tape feed, etc.) are stationary, fixed to the set-up frame. The movement required to roll the tape between from the tape feed to the roller and the tool, comes from the tool movement. Concept 2 is based on the same principle, however in this concept the instruments move in order to move the tape and the tool is stationary.

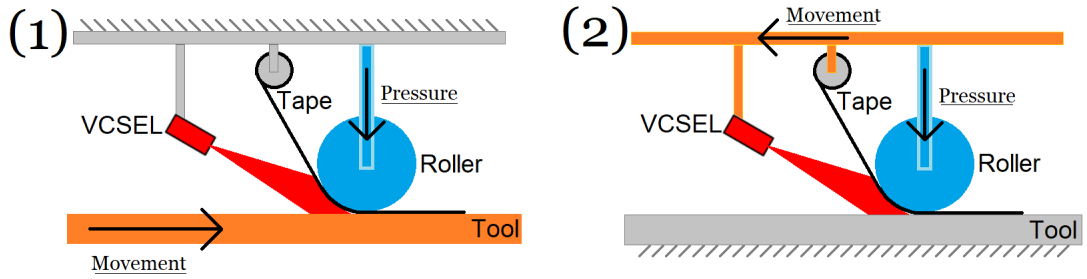

Figure 4.2: Experimental concepts: (1) stationary instruments, sliding tool. (2) Stationary tool, sliding instruments.

Concept 3 and 4

The next two concepts is based on a secondary moving tool that will provide the pressure that has to be applied. The two concepts are presented in Figure 4.3. For both concepts the tape is placed stationary on the tool. First the VCSEL will irradiate the tape, followed by a closing movement of the consolidation tool. When the tool is closed, the mechanism will apply the required pressure. In concept 3 the movement and pressure application of the consolidation tool is achieved via a rotational movement, and in concept 4 via a linear movement. Laser irradiation and consolidation tool movement would be performed in a pattern to mimic the LAFP shadow zone.

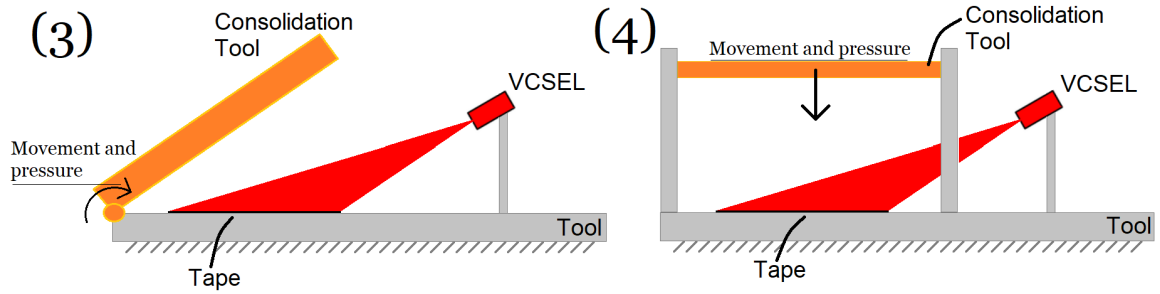

Figure 4.3: Experimental concepts: (3) stationary instruments and tool, rotating tool. (4) Stationary instruments and tool, horizontally moving tool.

Concept 5

The final conceptual idea is concept 5, of which a drawing is visible in Figure 4.4. In this concept the consolidation pressure will be applied via a silicon roller, onto a round tool. The tape movement originates from the rotation of the round tool which will pull the tape between the silicon roller and the tool.

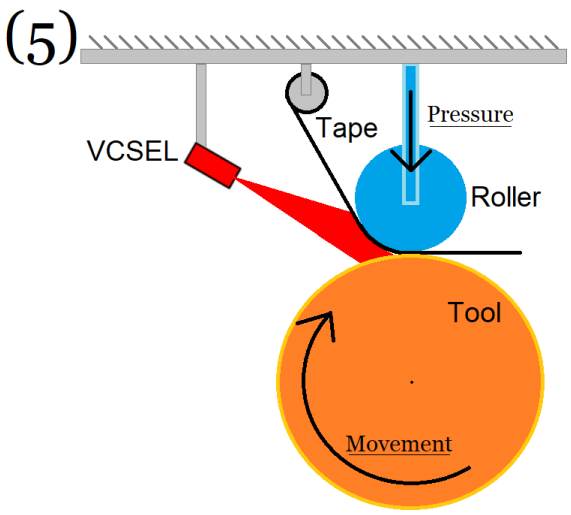

Figure 4.4: Experimental concept: (5) stationary instruments, rotating tool.

Final concept trade-off

The final trade-off between the concepts will be based on multiple criteria: complexity, construction time, safety, flexibility and how well it mimics LAFP conditions. These criteria originate from the set project requirements (Rp1-4). How well the concepts are expected to perform on the criteria is mainly based on the following few considerations:

- It is expected that the mechanisms required for Concepts 3 and 4 will be the most complex and thus time consuming. In order to minimize the time that the specimen will not be exposed to laser radiation before compaction (simulated shadow zone), the closing tool is expected to move relatively quick. To mimic the compaction time, the consolidation tool should be in the closing position for a short amount of time. The necessary deceleration and following acceleration to close and open the tool fast enough is expected to be significant. While the tool must move quickly, it also needs to apply pressure accurately. One potential approach to achieve such a mechanism would be to make use of pneumatic components, where the compaction force depends on the set pneumatic pressure. Consistent operation of a fast moving pneumatic system is expected to be difficult. The mechanism calibration is expected to be most time consuming for these two concepts and operator safety when interchanging tapes should be taken into account.

- The rotating tool mechanism of concept 5 is expected to be easier to realize and safer to operate than any other concept movement mechanism. It however limits the flexibility for future research as e.g. applying a heated tool surface or substrate material becomes more challenging on a round tool. Also the round tool compromises on the ability to mimic the LAFP process by changing the consolidation pressure profile.

- When instrument safety is considered, concept 2 is most challenging as the instruments will be in movement during operation. On the other hand concepts 1 and 5 provide a more stable construction for the instruments to operate in.

A trade-off table is generated, visible in Table 4.1, which provides an overview of how well the concepts are expected to perform per criteria. In this table it is clear that concept 3 and 4 are least fit, mostly due to the difficult mechanisms and not mimicking LAFP. Furthermore it can be seen that comparing concept 5 to concept 1 and 2, concept 5 provides the least potential to mimic LAFP and providing value for future research. Finally concept 1 is expected to be less difficult to construct and is safer in operation than concept 2. As mimicking LAFP conditions as close as possible and flexibility for further research is valued most, the decision is made to realize concept 1 in this research.

Table 4.1: Trade-off table comparing the five experimental set-up concepts. Per concept the trade off criteria are given a rating in the form of positive(+ or ++), negative (- or - -) or neutral (0) effect with respect to the other concepts. For Complexity and Construction Time, a positive effect(+ or ++) means less complex and less construction time, and vice versa.

Concept	Complexity	Construction Time	Safety	Flexibility	Mimic LAFP
1	+	+	+	++	++
2	0	-	-	++	++
3	- -	- -	-	-	0
4	-	-	-	-	0
5	++	++	++	0	+

4.2. Experimental Set-up Design

In this subsection it is described how the experimental set-up concept is translated into the final experimental set-up that will be used to generate experimental results. First the two main mechanisms of the set-up, namely the tool movement and pressure application are covered, followed by the complete experimental set-up and its functionalities.

4.2.1. Tool movement and pressure application

The design and manufacturing of the two mechanisms should take all requirements into account. There are however some important main considerations for these mechanisms and that is the availability of equipment and materials. It is important to consider availability when the experimental set-up should be designed and manufactured within the given time frame. First the design of the tool movement will be discussed.

The goal of the moving tool is to provide a stable linear movement. Furthermore the moving tool should adhere to the following posed requirements:

- The tool velocity should be able to achieve a maximum of 200 mm/s. (Originating from Rc2, combined with expected consolidation length of 10 to 30 mm.)
- The tool velocity should be variable.
- The tool should be stiff enough to not deform significantly under the applied pressure of the roller.
- The tool movement mechanism should be able to provide enough force to overcome the resistance applied by itself and the roller.

The experimental set-up requirements result in a linear sliding mechanism, modelled in Figure 4.5. The mechanism consists of an aluminium plate (red) that serves as the tool and working area, which slides over two linear guides (blue) using four linear bearings. The force required to move the tool is supplied by the ball screw linear actuator (green).

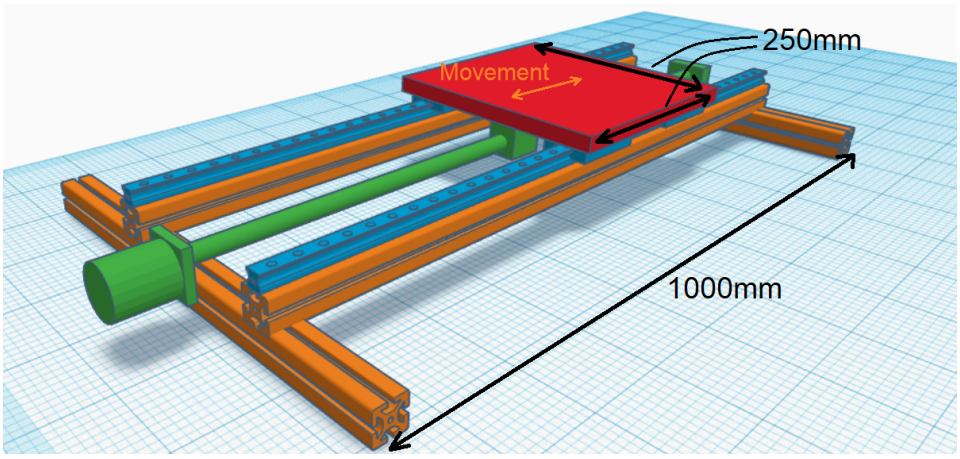

Figure 4.5: Schematic model of the tool movement mechanism

The ball screw linear actuator will translate rotational movement into linear movement by rotating a long screw to which the ball nut, which is attached to the tool, will move linearly along the screw. The rotation of the screw will be supplied by a stepper motor due to its excellent controllability and widely available documentation.

Following the design of the tool movement, the design of the pressure application will be discussed. The problem of applying variable pressure to the product has been split up into two parts, first a variable force should be able to be applied and secondly that force should be translated into pressure via the roller.

The application of a variable compaction force can be achieved in various different ways. Two solutions have been considered for the force application, a pneumatic cylinder or free weight. Initial tests using pneumatic cylinders showed that it was not possible to achieve consistent output force while providing the same input air pressure. At lower input pressures the pneumatic cylinder required a certain pressure build up before it started to move resulting in a stuttering type of force application, which rarely ended up at the same output value. Additionally when a pneumatic cylinder would be used, the set-up structure is required to be stiff and strong enough to provide the counter force to the cylinders reaction force. The second solution that was considered is free weight. In this case the general concept is to guide a variable free moving moving weight in vertical manner, such that the gravitational force is applied onto the roller. The benefit in this concept is in the simplicity, the limit is in the fact that it requires a volume and weight of a certain material to apply the force. The amount of weight that can be used safely could be limited. The free moving weight concept has been chosen for its consistency and simplicity.

In previous master thesis research performed at TU Delft, silicon rollers have been used for research on AFP [77]. The silicon material of which the rollers have been produced is SILASTIC RTV-4136-M Liquid Silicone Rubber [78]. The material hardness level of 59 sh is an average hardness level within expected hardness levels (30-85) for use during fiber placement [76]. Furthermore the material sensitivity to laser irradiation has been inspected, the material should not deteriorate nor should its temperature reach over the suggested 250 °C operational temperature. The material has been subjected to the expected process laser irradiation while being inspected visually and via thermal imaging. The material did not show any signs of deterioration nor did the material reach temperatures above 50 °C. For the aforementioned reasons the available rollers have been deemed fit for the purpose and will thus be used to translate compaction force to compaction pressure.

Again the mechanism has been modelled, see Figure 4.6. The pressure application mechanism has been oriented above the moving tool mechanisms, thus providing a clear view on their interaction. First, the roller is visible in the pink color, the roller is attached to yellow slide. On the top of the slide a plate is attached on which weight can be placed. The roller and slide are constrained in all directions except vertical movement via the linear guide and bearings, which are depicted in blue. The length of the yellow slide will be decided such that enough clearance can be supplied to instruments that have to be placed in front of the roller.

In the design phase of both mechanisms the availability of materials and components have been taken into account to reduce production time. The use of aluminium profiles significantly reduces production and construction time of structural elements. Furthermore the components such as screw, ball nut, linear guides and linear bearings were all available components and the mechanisms have been tailored around them.

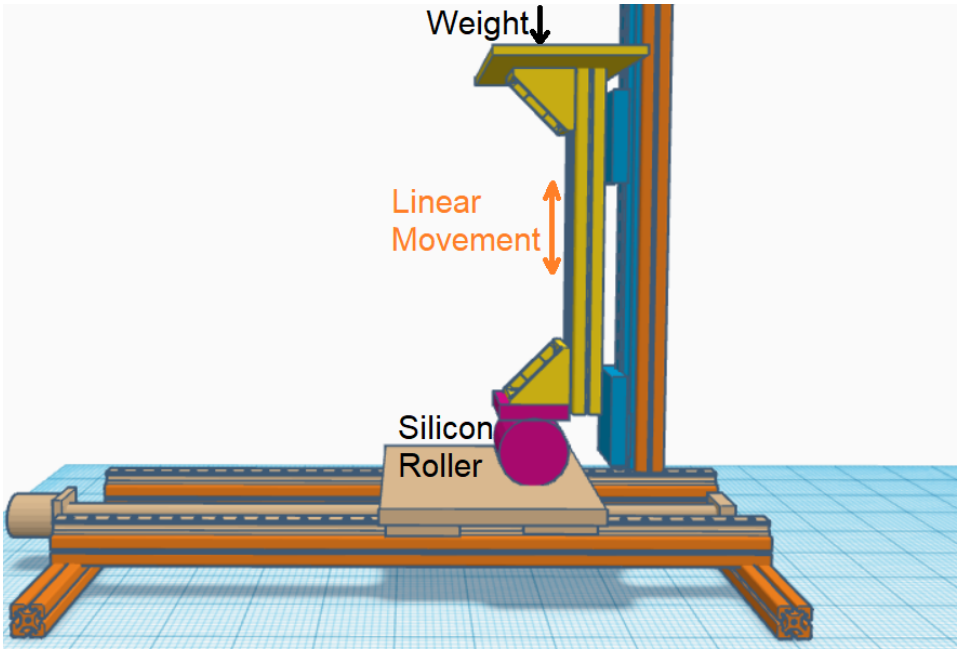

Figure 4.6: Schematic model of the pressure application mechanism

4.2.2. Laser placement considerations

The placement of the laser is important both for the design of the experimental set-up and the processing parameters. Each individual emitter in the available VCSEL (Philips Photonics GmbH. PPM412-12-980-24-c) has a 10-degree beam angle. As a result, the radiating intensity distribution decreases further away from the laser. The laser manual provides the intensity distributions and profiles shown in Figure 4.7 [79]. This figure reveals that the distance between the VCSEL and the material should be kept as short as possible and ideally should not exceed 100 mm to ensure the most efficient use of the available laser intensity. Furthermore, the placement of the laser should be optimized to minimize the shadow zone while ensuring a safety margin on the quick-moving tool beneath it.

4.2.3. Experimental set-up and functionalities

This subsection presents the final experimental set-up that has been designed and built. The experimental set-up has been carefully constructed to meet the specific requirements and variables identified during the design process. To provide a clear understanding of the experimental set-up, two pictures are included in Figure 4.8. The left picture provides an overview of the entire set-up, while the right picture shows a more detailed view of the working area. These figures will be used to illustrate and explain various aspects of the set-up.

Tool movement and pressure application

The experimental set-up relies on two primary mechanisms for its operation: tool movement and pressure application. The tool movement mechanism is located at the markers labeled 1 and 5 in Figure 4.8. The first marker shows the stepper motor and gearing necessary to achieve the desired placement speeds, while the sliding mechanism itself - consisting of linear guides, bearings, and the tool - is located at marker 5.

To provide more information about the tool movement mechanism, a NEMA23 stepper motor with a 1:5 gearing ratio gearbox is used to achieve the desired speeds. The motor is powered by a Leadshine DM556 stepper motor driver unit and controlled by an Arduino. The Arduino has been programmed to initiate tool movement by accelerating it to the desired speed, maintaining that speed for the working distance, and then decelerating it. The movement can be triggered using a switch, and limit switches have been installed on both ends of the linear guides for added safety measures to prevent the tool from moving beyond its intended range of motion. These switches immediately halt the movement to prevent any potential accidents.

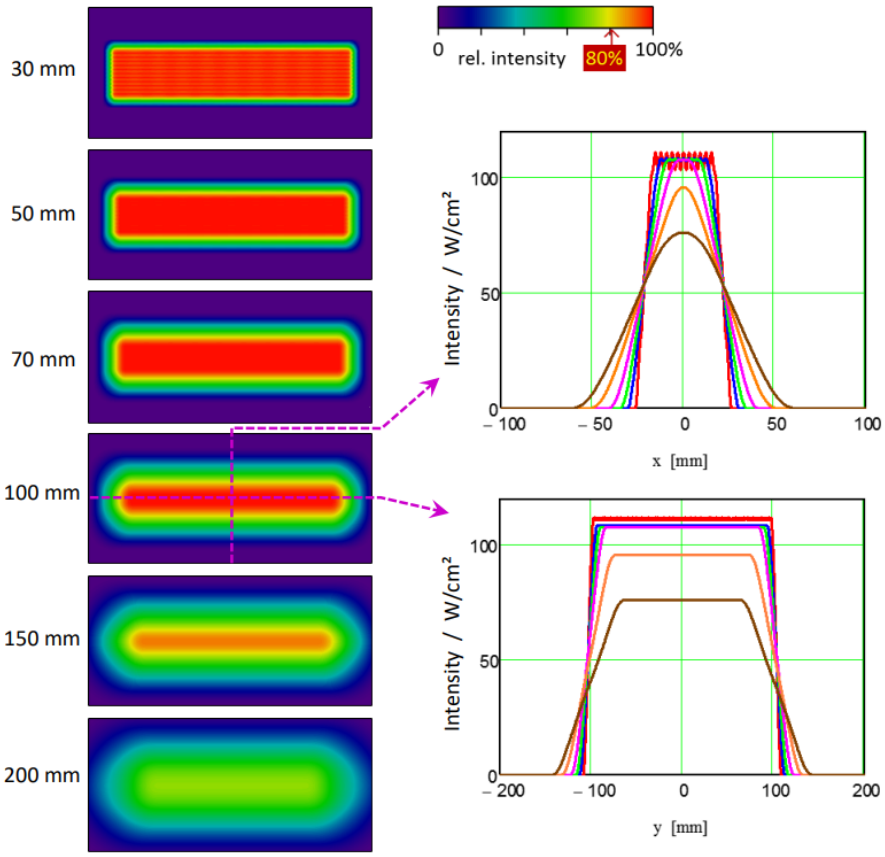

Figure 4.7: Intensity distributions (left) and intensity profiles (right) of the VCSEL [79]. Where the beam spread and thus intensity decrease of the laser is visible.

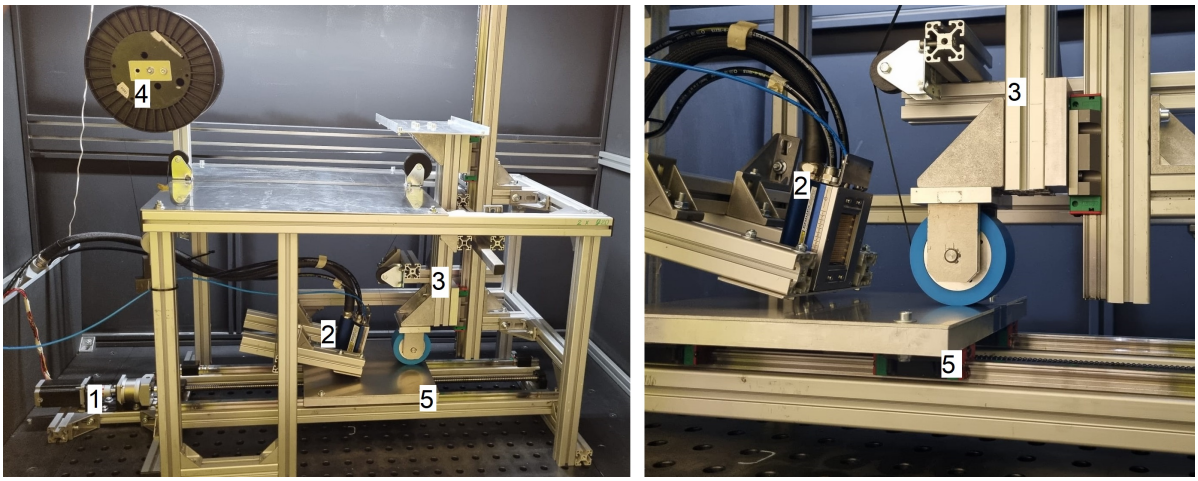

Figure 4.8: The experimental set-up as manufactured. 1) Stepper motor and gearbox. 2) VSCEL. 3) Pressure application slide. 4) CF/PEEK reel. 5) Linear sliding mechanism.

In Figure 4.8, the pressure application mechanism is indicated by marker 3. The mechanism comprises a fixed linear guide, bearings, and a slide. The slide is attached to the silicon roller on the bottom to translate force to pressure and a plateau on the top side to contain the necessary weight. Additionally, a part of the tape guiding system is also attached to the slide, as visible in the right picture of the figure. The reason for attaching the system to the slide is to ensure that the incidence angle of the tape remains constant, even if the height of the tool (and thus slide movement) changes. Additionally, to facilitate the

resetting of the set-up between runs, a handle has been constructed to reduce the effort required to lift the slide with weight on it. The handle allows the user to lift the slide by pushing down on it with a 7x weight reduction. Once the slide is lifted to a certain height, a mechanism falls into place and the slide is locked in the lifted position. After the set-up has been reset, the mechanism can be released and the slide can be lowered back into position. This feature is particularly useful when conducting multiple experiments and minimizing user fatigue.

VCSEL attachment and placement
Figure 4.8 showcases marker 2, which indicates the VCSEL and its attachment. The VCSEL is connected to four hoses, two for cooling, one for purge air, and the last one for powering the emitters. These hoses are rigid and require significant clearance to be navigated out of the laser room. An attachment bracket has been designed and manufactured to bring the laser as close to the tool surface and nip-point as possible. This bracket is attached to a system of aluminum profiles that allow for VCSEL angle and location variability. The laser has been positioned and angled in such a way that the lowest emitter line emits as close to the nip-point as possible, while also being as close to the material as possible. The laser distance form the incoming tape is between 80mm at the top to 150mm at the bottom, as is presented in Figure 4.11. It is worth noting that this setup allows for future modifications to the VCSEL's position and angle, which could be explored in future research work.

Tape guiding system
The final major component of the experimental set-up is the tape guiding system, identified by marker 4 in Figure 4.8. The material on which the experiments will be conducted is quarter inch CF/PEEK, which is supplied in the form of a continuous tape that unwinds from the reel seen where the marker 4 is placed in the figure. The tape enters the working area via a series of one pulley and three stationary rollers. Just below the reel, the tape passes through the pulley. The weight of the pulley can be adjusted to change the tape tension. The system is designed to allow for the braking of the reel, conducting the experiment, removing the specimen, and resetting the system by releasing the brake and extending the outgoing tape again.

Great care has been taken in designing all the major components of the experimental set-up, with the aim of providing flexibility for future research. Numerous factors have been considered in achieving this, such as the location and orientation of the VCSEL, the incidence angle of incoming material, the tape tension weight, the structure of the tool (to allow for heating or substrate material), placement speed, pressure, and more. All these elements have been designed with the possibility of further experimentation in mind.

4.2.4. Verification
To ensure the accuracy of the experimental setup, various verifications have been carried out. The VCSEL irradiation location, silicon roller alignment and pressure translation, and the placement speed have all undergone verification and will be discussed in more detail. Note that during the manufacturing of the set-up the structure and movements has measured continuously to be square and moving linearly.

VCSEL irradiation location
Although the VCSEL has been aligned with measuring tools, the exact irradiation location needed to be verified for added certainty. To achieve this, the top and bottom emitter lines were allowed to emit onto stationary material for a certain period of time. Thermal data from the process was recorded using a thermal camera. The irradiation location of the top and bottom emitter lines was then verified by analyzing the thermal data. This process confirmed that the lowest emitter line irradiates as close to the nip-point as possible.

Roller alignment and pressure application
The roller has been aligned to roll in line with the tool movement, in order to prevent any unrealistic diagonal forces from being applied to the material. Tests and calculations were carried out to measure how force translates to pressure via the roller. To achieve this, weight was placed on top of the plateau, and the roller was first stamped into an inkpad and then stamped on paper to leave a mark. This

procedure was repeated eight times, and the ink marks were measured to calculate the average area. The average pressure under the roller was then computed, based on the weight. This process was repeated eight times, each with a different weight, to produce a graph showing the average pressure over the total slide weight, as depicted in Figure 4.9. The start of the graph is at a weight of 6.9kg, the weight of the slide itself.

It is important to note that there is a distinction between static roller pressure and dynamic roller pressure. While the pressure tests have been conducted in a static form, the experiments will be performed in a dynamic form. Nevertheless, it can be considered that the rolling movement has a negligible effect on the pressure distribution, according to Jiang et al. [80].

Placement speed
The stepper motor driver, in conjunction with the Arduino, allows for precise determination of the placement speed. The driver can set the number of steps required for one stepper motor rotation, while the Arduino can communicate the exact amount of steps per second. This results in rotations per second. To verify that the translation, in combination with the gearbox ratio and ball screw linear actuator, results in the expected placement speeds, a mobile phone camera with slow-motion functionality was utilized. Colored squares, each with a width of 20mm, were placed on the tool. A specific speed was then inputted into the Arduino, and a run was performed while filming the tool. The footage was then analyzed to determine how many squares were moved with respect to a marker point in the span of a second, which confirmed that the input speed was the same as the realized speed. In Figure 4.10, two frames are presented that were recorded one second apart. It is clear that within that time frame, five squares of 20mm have passed. This observation verifies that the speed of the tool is 100mm/s, which is consistent with the input to the Arduino.

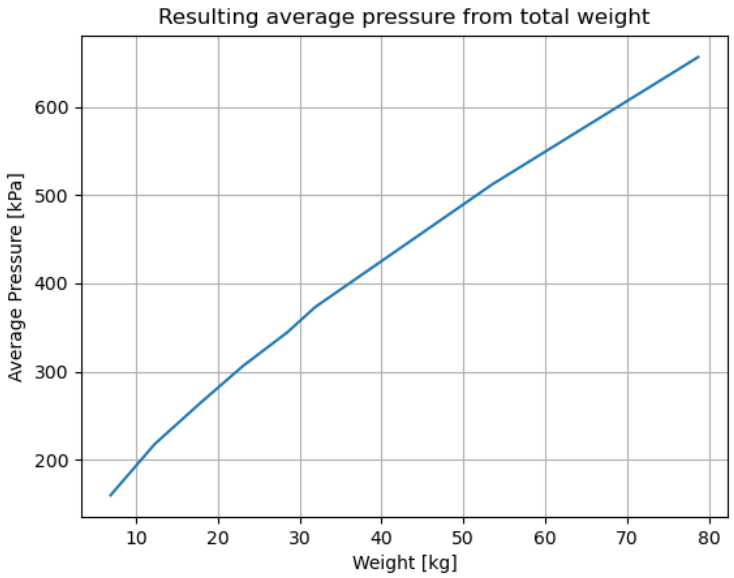

Figure 4.9: Graph showing the average pressure over the total slide weight.

4.3. Capabilities and Limitations

While the experimental set-up described in the previous sections has been designed with great care to allow for variability in many different ways, there are still some limitations to consider. These limitations may affect the accuracy and precision of the experimental results and should be taken into account when interpreting them. In this section, the operational limits of the set-up and potential sources of error that may affect the accuracy and precision of the results are discussed.

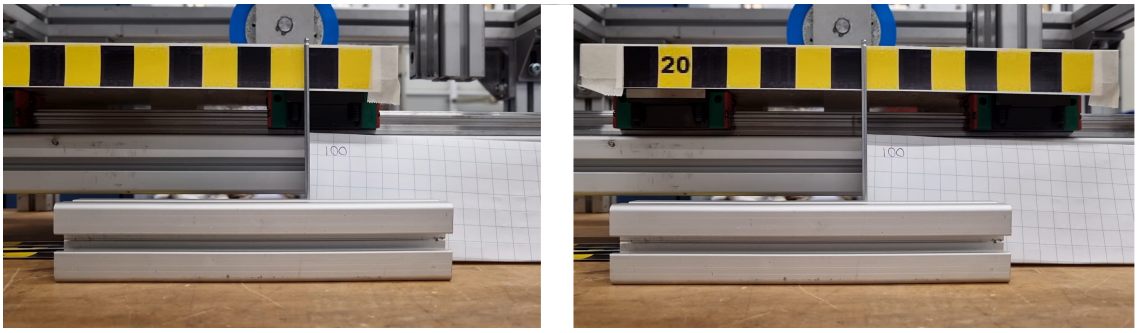

Figure 4.10: Placement speed verification measurement procedure. Two frames, one second apart.

Placement speed range

The experimental set-up has the capability of achieving a maximum a placement speed of 200mm/s. This speed is limited by the length of the working range and the output power of the stepper motor. Accelerating too quickly can cause power limitations on the motor, so a slower acceleration results in a longer acceleration distance, which in turn limits the available working range. To increase the placement speed further, a longer tool and/or a more powerful motor may be required.

Pressure range

The pressure application range that the experimental set-up is capable of applying is between 160kPa and 600kPa. The minimal pressure that can be applied is achieved when no weight is placed on top of the plateau, the 6.9kg slide weight results in an average pressure of 160kPa, as can be seen in Figure 4.9. For future work it would be possible to reduce the pressure by reducing the slide weight, or equipping the set-up with a constant force cylinder or spring to lift the slide and reduce the force experienced by the roller.

On the other hand, the maximum pressure that can be exerted on the material is limited by the weight that can safely be placed on top of the plateau, with stability, equipment and operator safety in mind. As such, the amount of weight that can safely be placed on top of the plateau is carefully considered. Currently, the maximum weight that can be added is limited to 62.0kg, which, when combined with the slide, totals to 68.9kg. This results in a pressure of 600kPa, as can be seen in Figure 4.9. However, it is possible to increase the pressure exerted on the material through a number of means. For example, one could redesign the setup to include a larger plateau or make use of weight materials with a higher density than the current (steel). Additionally, the setup could be equipped with a constant force cylinder or spring to push the slide down, thereby increasing the total force and resulting in a higher pressure.

Operational use

During an experimental run, operational timing is crucial. In operation, the first step is to trigger the Arduino using a switch to perform the predetermined tool movement. Following this the VCSEL should be turned on for a predetermined time, while the tool is moving. Turning on the VCSEL while the material is stationary would overheat the material. During this two step procedure, timing is important to prevent material overheating. Although consistent results were achieved, the risk of turning on the VCSEL while the tool is not moving is always present. The VCSEL is equipped with a trigger option. For future work it should be possible for the Arduino to trigger the laser right after the tool moves. Therefore minimizing the operational mistake probability.

VCSEL placement

The VCSEL placement has been optimized to limit the shadow zone length while operating as close to the incoming tape as possible. Figure 4.11 shows to placement and irradiation zone (indicated with two lines) achieved in this set-up. Due to the size of the casing and the general structure of the VCSEL laser, it is difficult to orientate the laser to irradiate as close to the nip-point as possible. Figure 4.11 provides a clearer view of the limited orientation freedom of the VCSEL due to its structure.

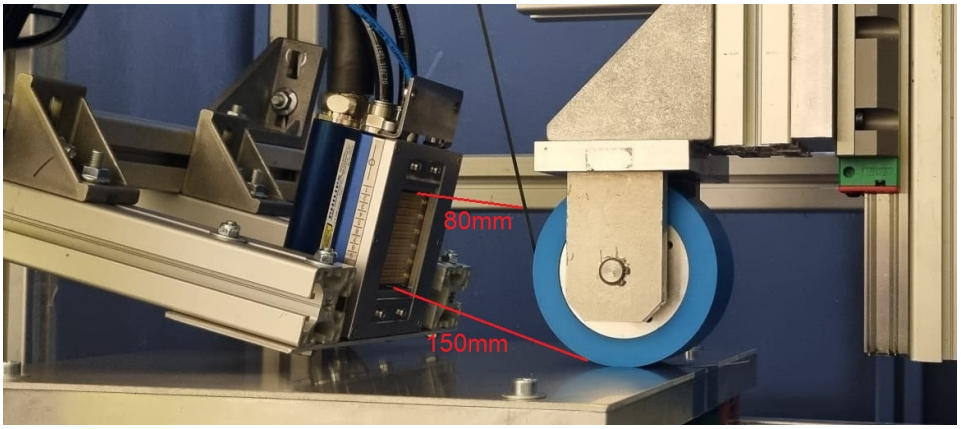

Figure 4.11: VCSEL placement and orientation including indication of the irradiation zone.

FLIR camera placement

In chapter 5, the in-situ measurement technique used to measure heating phase temperature temperature will be discussed. In Figure 4.12 the placement and view of the thermal camera is provided. However, it is important to note that the current design and size of the VCSEL and its attachment provide limited space for additional equipment near the heating side of the set-up. This restriction limits the placement of the FLIR camera, which needs to have a clear view of the material. While some limitations are inevitable, improvements could be made by redesigning the variable VCSEL attachment to provide a bigger clear view of the material.

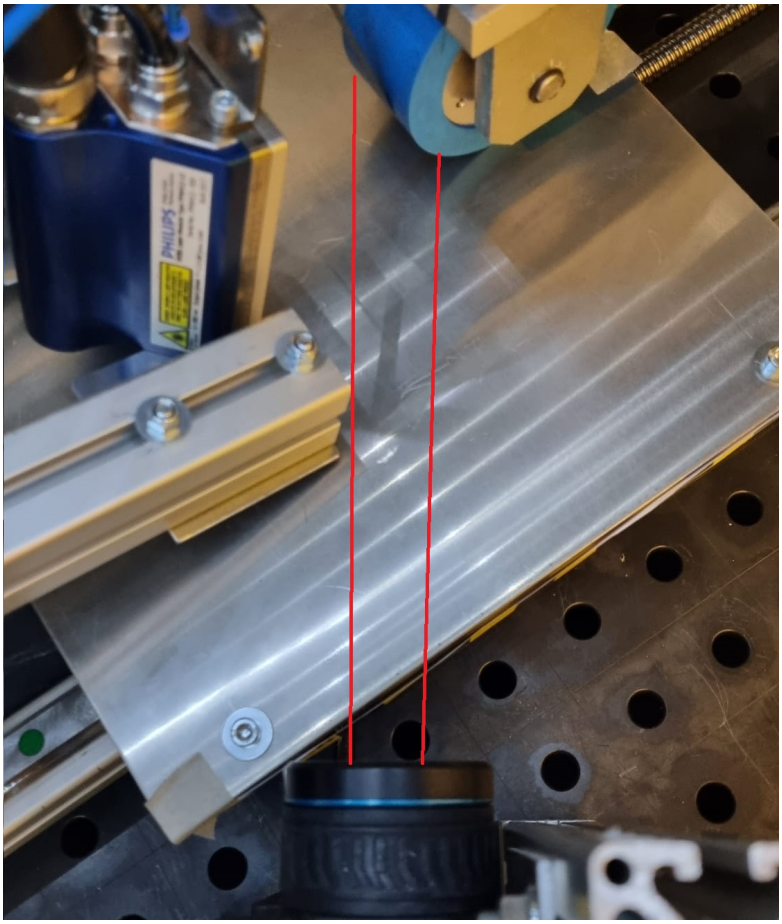

Figure 4.12: FLIR camera placement and view path indication through the set-up.

Heating capability

During the initial testing phase, it was discovered that the experimental set-up was sometimes limited by its heating capability. The VCSEL needs to be able to heat the incoming material to the desired processing temperature as close to the visible nip-point as possible. However, due to the VCSEL placement limitation, in combination with high placement speeds, the set-up was sometimes unable to achieve the desired temperature at the visible nip-point. It was observed that roller deformation due to pressure played a role in heating capability. As shown in Figure 4.13, a more deformed roller, resulting from higher pressure, led to longer irradiation of the material and a smaller shadow zone, which improved heating capabilities. At the lowest pressure (160kPa), the maximum placement speed at which the desired processing temperature could be achieved was 120mm/s. However, due to roller deformation, a placement speed of 200mm/s could be achieved at a pressure of 600kPa.

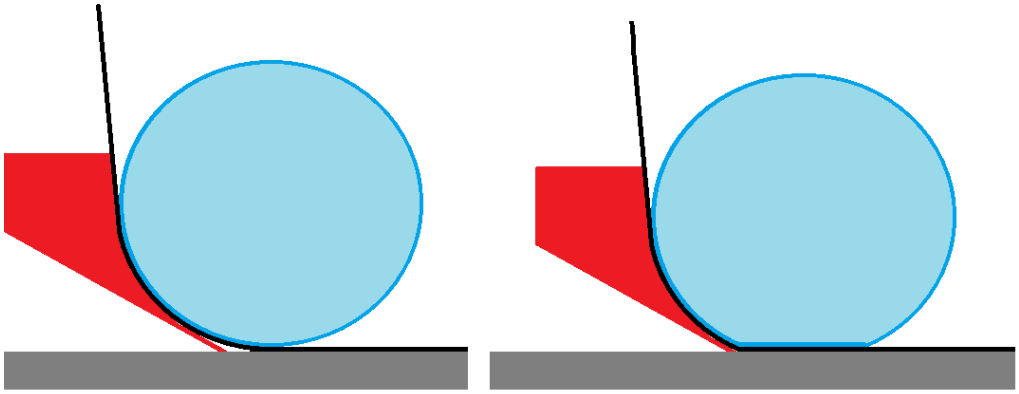

Figure 4.13: Effect of roller deformation on the VCSEL irradiation zone.

4.4. Experimental set-up Evaluation

The experimental set-up has been designed and manufactured with a set of requirements in mind. The set-up will be compared to the requirements which were presented in subsection 4.1.1. All requirements have been fulfilled, with the exception of Rc2, which has been partially met. Further details regarding Rc2 will be discussed in the following paragraph.

Tape process conditions

By using the VCSEL the material is heated via infrared laser heating, and Rc1 is met. Furthermore due to the maximum placement of 200 mm/s and a consolidation length between 9.62mm and 25.34mm (due to 160kPa and 600kPa being applied), the minimal achievable compaction cycle duration is between 0.05s and 0.13s depending on the applied pressure. It is thus possible to achieve cycle duration from 0.05s and upward. Compared Rc2, the requirement is met for the majority of the range, 0.05s to 0.3s. For the third requirement, Rc3, the upper limit of 600kPa falls within required range of 500kPa to 1000kPa. Finally due to the experimental design concept, the Rc4 is met as the compaction cycle is applied directly after the heating phase with the exception of the shadow zone.

Materials and Equipment

As described in subsection 4.2.3 the set-up has been manufactured including a VCSEL laser, can feed quarter-inch CF/PEEK tape, allows for the placement of the FLIR and makes use of the silicon roller, resulting in achieving all of the four material and equipment requirements(Re1-4).

Measuring

Due to placing the thermal camera in line with the tool, a view between the roller and the tool was achieved. The thermal camera is hereby able to measure the temperature at the visible nip-point, meeting Rm1.

Project

The manufacturing of the experimental set-up has been achieved within the 3 month time frame, and

was fully constructed with the equipment available in the ASM aircraft hall. The limited availability of resources such as external help, materials, components and time did not affect the outcome or quality of the experimental set-up. Adjustability has been part of the design and manufacturing, and a lot of operational freedom is achieved. Finally risk of damage to instruments or personal has been minimized. For the operator it is physically impossible to operate and be in the set-up danger zone at the same time. All moving parts are linearly constrained and not in line with any other vital instrument. The VCSEL is protected from any moving part or free weight. Hereby all project requirments are met.

4.5. Conclusion

The objective in this research phase was to design and construct an experimental set-up capable of producing specimens subjected to LAFP type temperature and pressure histories. Initially the first research sub-question (SQ1) corresponding to this research phase has been answered: How can an experimental set-up mimic and apply LAFP temperature and pressure histories to thermoplastic composite tape? This question was answered in steps leading from initial concepts to the final design. As a result of this process an experimental set-up has been constructed.

The set-up was designed and manufactured to mimic the LAFP process as closely as possible. By first heating the tape with a VCSEL, followed by a shadow zone and finally compaction under a flexible roller, the tape undergoes temperature and pressure histories that are expected for the LAFP process. The experimental set-up is able to achieve variable LAFP relevent process parameters: placement speed up to 200mm/s and compaction pressures between 160kPa and 600kPa. The set-up has been successfully manufactured with the available equipment, materials and time while not compromising on quality and being flexible for future research modifications and advancements.

Overall, the experimental set-up has been designed with a clear goal and a comprehensive understanding of its capabilities. It is expected that the experimental set-up will be instrumental in achieving the second objective of this research, which is to investigate the effectiveness of LAFP type temperature and pressure histories in resolving deconsolidation forms.

5

Experimental Details

The purpose of this chapter is to provide a detailed explanation of the experimental work that will be conducted. The chapter will begin by discussing the material that will be used in the experiments. This will be followed by a description of the specimens that will be produced. And finally, it is explained how the forms of deconsolidation (deconsolidation forms) will be quantified using material characterization techniques.

5.1. Material

Polyether-ether-ketone (PEEK) is a high performance thermoplast that is often utilized in aerospace applications due to its structural performance and high operational temperatures. In addition, recent relevant LAFP research work has predominantly used CF/PEEK material, making it an ideal reference material for this research. Quarter-inch TenCate Cetex TC1200 PEEK AS-4 will be used in the research of this thesis. The as-received (AR) material has the following global material properties as presented in Table 5.1.

Table 5.1: As-received (AR) material properties of TenCate Cetex TC1200 PEEK AS-4 quarter inch tape [81].

Material	Tg[°C]	Tm[°C]	Tp[°C]	Width[mm]	Thickness[mm]
CF/PEEK AS-4	143	343	370-400	6.35	0.14

An overview of the full cross-sectional view of the AR tape is presented in Figure 5.1. The microscopy picture was recorded using a Keyence VHX-2000 microscope with a VH-Z100 lens at 300x magnification.

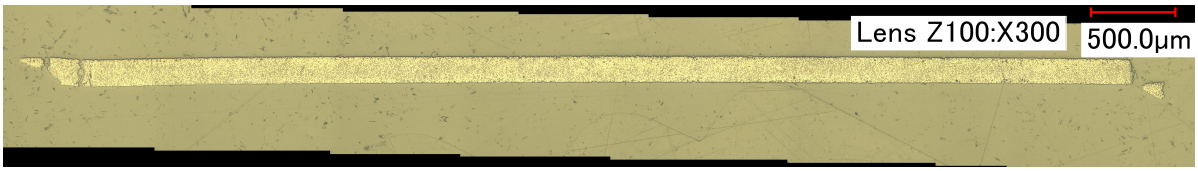

Figure 5.1: Full cross-sectional view of the AR tape.

When analyzing more detailed figures, it becomes clear that the fiber volume fraction exhibits high local variability, which can have an impact on the heating and compaction behavior during the heating and consolidation phase. Two examples of the local fiber volume density difference are provided in Figure 5.2, where low and high local fiber volume fraction locations are marked. These microscopy images have been recorded using a Keyence VK-X1000 LSCM at 50x magnification. It should be noted that the two figures presented here are two locations with significant difference in local fiber volume fraction, this behaviour is not found to be consistent throughout the material.

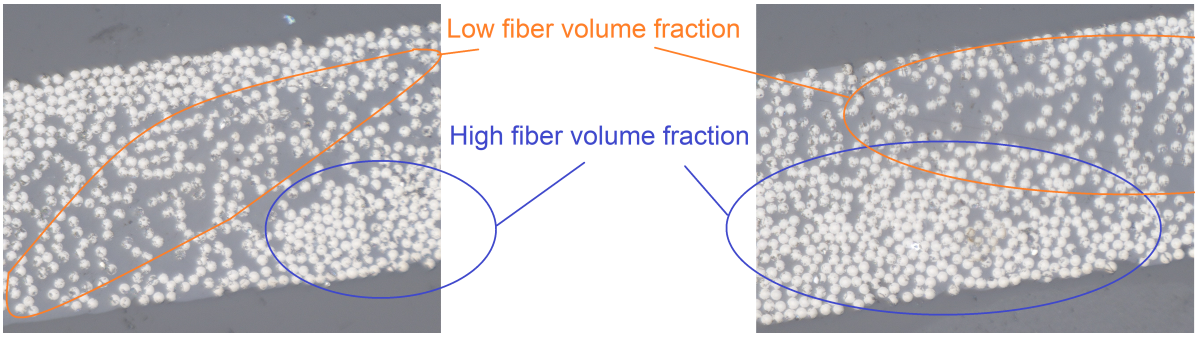

Figure 5.2: Fiber volume fraction local difference AR tape.

5.2. Specimens

This section aims to provide specific details on the process parameter settings that will be used to generate the data points. Additionally, the set-up configuration to achieve said process parameter settings will be outlined. And finally the extraction and preparation of the samples is discussed.

5.2.1. Process Parameters

Determining what process parameters will be tested depends on the limitations of the set-up and the relevance for LAFP research. First the limitations of the experimental set-up are taken into account. The experimental set-up enables varying the placement speed between 0 to 200 mm/s and the average compaction pressure between 160 to 600 kPa while using room temperature aluminium as the tool material.

The suggested processing temperature range in Table 5.1 provides the opportunity to test multiple visible nip-point temperatures to observe the differences in material behavior. However, in a recent study by Çelik et al. [19], it was found that a small temperature increase within the processing temperature range did not significantly affect the intimate contact development. The suggested reason is the short time above the melting temperature. The tool used in that study was heated to $155°C$, and it had a quenching effect on the material due to its rapid cooling. Since the tool in the experimental set-up is not heated, it is expected that the quenching effect will be even more pronounced. Furthermore, temperature differences on the surface of the tape are expected due to the deformation of the tape surfaces and local differences in fiber volume fraction, which affects the temperature distribution. Therefore, it is decided to set the visible nip-point temperature in the middle of the material processing temperature range. The aim is to have a visible nip-point temperature of $385°C$, which will leave a tolerance of $\pm 15°C$ for any local deviation while still being within the processing temperature range.

Furthermore, the relevance of the process parameters for LAFP research and industry is taken into account. In literature a wide range of placement speeds and consolidation pressures are evaluated. Commonly used placement speeds range from 37.5 to 500 mm/s [13, 74–76] and consolidation pressures have been tested up to 1MPa [19, 76]. Note that these finding were the basis for the experimental set-up requirements.

The available process parameter range of the experimental set-up is in line with the reported process parameters. It is thus decided to test to full operational range of the experimental set-up. The lowest and highest settings of both placement speed and pressure will be combined, resulting in 4 data points. However, due to heating limitations, the combination of 160kPa and 200mm/s is not possible, and it will only be possible to produce the remaining 3 specimens. To improve data analysis and correlation searching, an additional set of data points is added, consisting of 160kPa, 300kPa, and 600kPa all at 120mm/s. This will allow us to observe a better relation between consolidation and pressure, and consolidation and placement speed as with these 6 data points there will be 3 placement speeds at 600kPa, and 3 pressures at 120mm/s. The AR tape will also be analysed, bringing the total amount of data points to 7. The data points are summarized in Table 5.2 below.

Table 5.2: Process parameters settings used in experiments.

Visible nip-point temperature[°C]	Consolidation pressure[kPa]	Placement speed[mm/s]
385	160	40
		120
	300	120
	600	40
		120
		200

5.2.2. Setting up the experimental set-up

To operate the experimental set-up, it needs to be configured for the desired process parameters. The input setting for the placement speed is controlled by the Arduino, while the pressure can be adjusted by adding the appropriate weight on the plateau. To achieve the required processing temperature, the VCSEL settings need to be selected carefully.

Using Figure 4.9, the three pressure values to be tested (160kPa, 300kPa, and 600kPa) can be translated to the corresponding additional weights (0 kg, 15.4 kg, and 62.0 kg) that need to be added to the plateau.

Since both the placement speed and pressure (due to roller deformation) affect the heating phase, the VCSEL settings need to be tailored to each data point. The VCSEL consists of 12 emitter lines, each with a maximum power of 200W. The goal when designing the heating settings was to minimize unnecessary long heating and to reach the desired processing temperature only at the visible nip-point, not before it. The laser settings were optimized by testing different configurations, analyzing thermal data, and adjusting the settings accordingly. Table 5.3 provides an overview of the VCSEL settings used for each data point.

Table 5.3: Laser settings used to achieve process parameter settings.

	Process parameters [mm/s-kPa]					
Emitter line	**40-160**	**40-600**	**120-160**	**120-300**	**120-600**	**200-600**
1	0	0	60	60	60	0
2	0	0	60	60	60	120
3	0	0	60	60	60	140
4	0	0	60	60	60	180
5	0	0	60	60	60	180
6	0	0	140	140	60	200
7	0	0	200	200	140	200
8	160	10	200	200	180	200
9	200	200	180	180	190	200
10	200	200	200	190	200	200
11	200	200	200	200	200	200
12	200	200	200	200	200	200
Total power [W]:	960	810	1620	1610	1470	2020

5.2.3. Specimen preparation

After the experimental procedure is completed, the samples must be extracted from the set-up. This involves three steps. First, the material must be removed from the experimental set-up by lifting the roller and cutting off the material. Second, the location of the material with the correct temperature history must be determined. The material at the start and end of the run has only been partially irradiated by the VCSEL and has not reached the required processing temperature, so it must be avoided. The correct location can be determined by analyzing video recordings and thermal data of the experiment, where it can be indicated what tape location has seen the full heat cycle. Additionally a change in tape width is observed where the tape becomes wider if the tape has reached processing temperature (minus a transition area), which is visible in picture 2 of Figure 5.3. Finally, three samples must be extracted

from the material. The samples are marked with numbers 1 to 3 to indicate the order in which they were placed in the run and have a length of approximately 25mm. An example of the sample extraction procedure is shown in Figure 5.3. First the processed tape on the tool, which is than extracted and cut on the marker lines to form 3 data points.

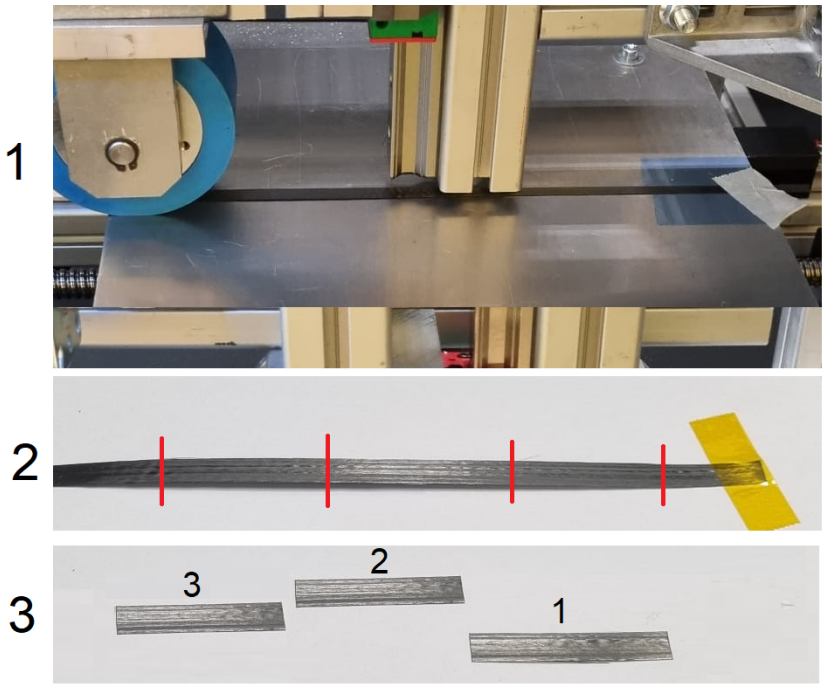

Figure 5.3: Sample extraction method

The sample surface will then be analysed for roughness and DEIC, which will be further explained in section 5.3. Once the surface analysis has been performed, the sample cross-section will be analysed for void content and thickness, which agian will be further explained in section 5.3. In order to analyse the cross-section, the samples will be embedded in embedding resin and the cross-section is polished.

All three of the samples per data point are secured in a clip and placed in a mould. Epofix embedding resin is poured into the mould which is then left to harden for 24 hours. Once the resin is hardened the samples undergo grinding and polishing steps to result in a surface that can be analysed. The steps of this procedure are visualized in Figure 5.4. For the grinding and polishing, the Struers Tegramin Automatic Preparation System is used. The grinding and polishing is performed in steps, where the surface fineness is decreased up to 0.25μm grid.

5.3. Material Characterization

This section will explain how thermal data is recorded in-situ, and how the samples will be post analyzed to quantify the deconsolidation forms. This quantitative data is utilized to draw conclusions of the effectiveness of process parameters in resolving deconsolidation forms and find correlations between them.

5.3.1. In-situ measurement: Thermal analysis heating phase

The FLIR A655sc High-Resolution Science Grade LWIR Camera is used for thermal analysis, with a resolution of 640x480 pixels and an accuracy of temperature measurement of $\pm 2°C$ or $\pm 2\%$ (whichever is greater) in the calibrated range of 100-650°C. The thermal data is recorded to ensure the desired processing temperature is achieved and to identify any correlation between temperature and tape properties. As mentioned in section 4.3, the location for the placement of the camera was limited. This

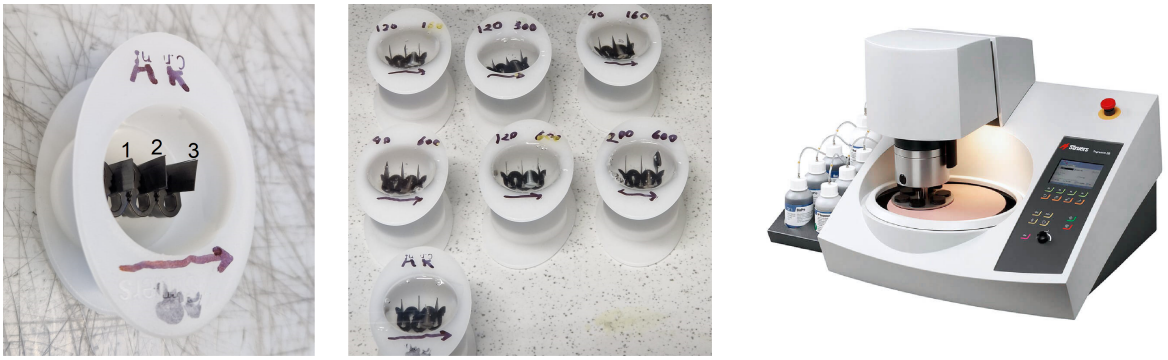

Figure 5.4: Steps for embedding samples, samples placed in moulds, moulds are embedded and the final grinding and polishing step on the Struers Tegramin.

location as well as the reflection of the aluminium tool makes it difficult to analyze the footage near the nip-point. Therefore, a reliable point before the nip-point (visible nip-point) is chosen to determine if the appropriate processing temperature is reached. The analysis of the thermal data is presented in Figure 5.5. Here a section of the heatmap of the material is visible on the left figure, where two areas are marked. Rectangular area Ar1 covers the entire material and circular area El1 covers the visible nip-point. The processing temperature is determined by the average temperature of the visible nip-point area. The right figure shows the visible nip-point temperature in a graph over time. Also the maximum temperature achieved in both areas are provided, providing valuable information on temperature distribution and temperature peak location.

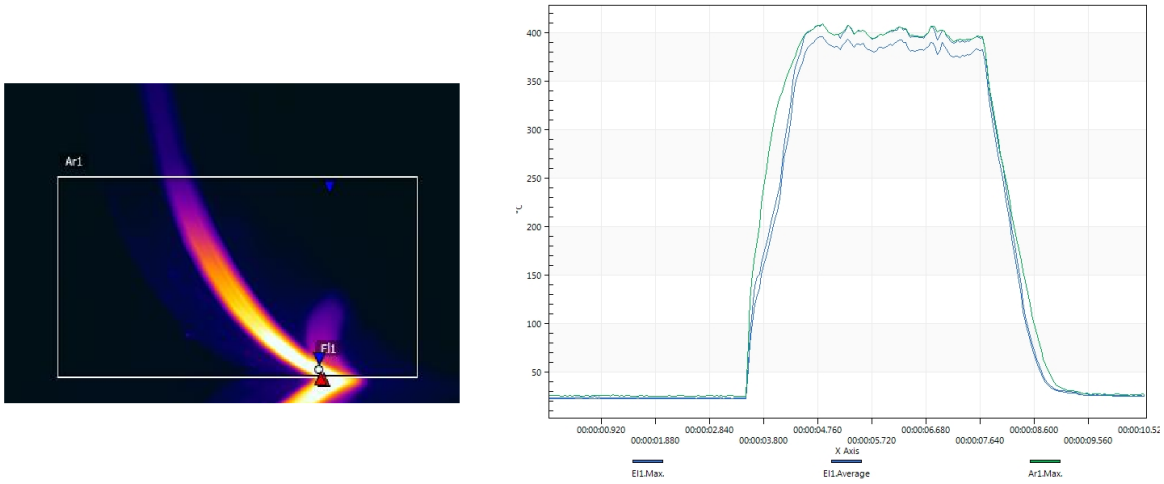

Figure 5.5: Heating phase thermal analysis figures. Left figure showing a heat map of the incoming tape with two areas, Right figures shows the average and maximum temperature values of these areas over time.

5.3.2. Post Experiment Measurements

The post measurements are split up into two parts, first the heated side of the tape surface is analysed for roughness and DEIC. Then the aforementioned embedding step is performed followed by the cross-sectional analysis to measure the void content and width.

Surface Microscopy

Roughness

The surface roughness analysis is performed using a Keyence VK-X1000 Laser Scanning Confocal Microscope (LSCM) with a 20x lens. The image size resulting from the analysis is 0.53x$0.70mm^2$. The roughness and waviness are distinguished according to ISO-4287 guidelines with a recommended 0.8mm cut-off wavelength. The measurement frequency and location is derived from the ISO standard, Figure 5.6 has been provided to provide a clear understanding of the following measurement descrip-

tion: A total of 3 locations, at 20%, 50%, and 80% of the sample length, are evaluated for each sample, visible as the blue lines in the first picture. To meet the standard's requirement of at least 5 samplings (image analyses), 7 samplings are performed per measurement location (picture 2). Each sampling involves the analysis of the multi-line roughness with 11 lines that are 80μm apart (picture 3). The LSCM software is used to calculate the R_a (mean roughness) and R_q (root mean square roughness) of each sampling, which are later averaged to obtain an R_a and R_q per location. The R_a and R_q of the 3 locations is averaged to achieve the R_a and R_q of the sample.

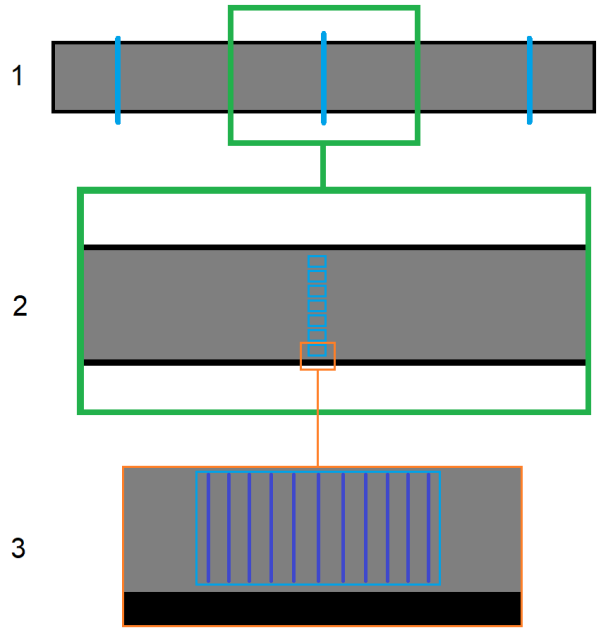

Figure 5.6: Roughness analysis sampling method. 1) three measurement locations, 2) 7 samplings per location and 3) line roughness analysis using 11 lines.

Degree of Effective Intimate Contact

The Keyence VHX-2000 digital microscope, with VH-Z100 lens at 200x magnification is utilized to evaluate the DEIC, resulting in an image size of 1.2x$1.6mm^2$. To determine the DEIC, the method of Çelik et al. [19] was used as a starting point. The method consists of three steps, which will be discussed and accompanied by Figure 5.9 illustrating the steps using the native software of the microscope. The first step is to convert pixel value of the original image to a grey scale histogram. The second step is to select the grey scale values that resemble the resin. During this step, difficulty was experienced in using the original method as described by Çelik et al., and the selection procedure was altered. The original method stated to mark the cut-off point between fibers and resin as the lowest point between the two peaks of the histogram, as has been visualized in the second figure of Figure 5.7. However this low-point moves depending on the amount of resin and fibers that is present, and in some cases there is no low point at all, as visualized in the 3th and 4th figure. For this reason it has been decided to keep a constant cut off point, right after the end of the carbon fiber peak. By doing so, the determination of what is considered resin or fiber is independent of their respective amounts.

Now that all the resin coloured pixels of the image are selected, the third step is performed: filtering. Dry fibers at the surface of the material can reflect light in such a way that they are included in the resin selection, to eliminate the presence of these fibers in the resin content analysis, a filter is applied. Following the method of Çelik et al., all subareas smaller than 500 μm^2 are excluded from the analysis. All of these steps are performed using the native software on the microscope. Finally, the software sums up the resin area and determines its percentage compared to the total analyzed area, resulting in the DEIC percentage.

To ensure the validity of the results, an additional comparison was performed to confirm that the change

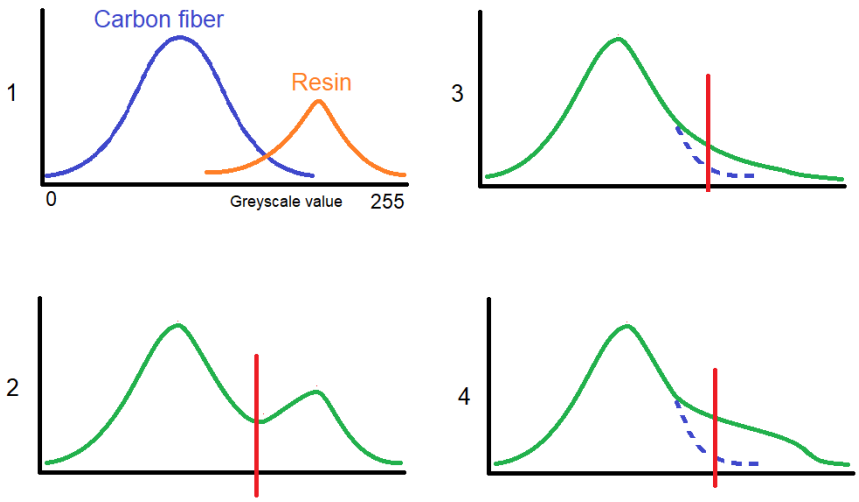

Figure 5.7: DEIC grey scale histogram cut-off point determination using a fixed cut-off point.

in selection method did not affect the results. The VK-X1000 LSCM and VHX-2000 microscope have been set up to capture the exact same picture of a specimen. The VK-X1000 is able to provide a better resolution picture where material and texture can be visually interpreted more easily. The resulting figure was visually compared to the figure and DEIC analysis method performed on the VHX-2000 to evaluate how well the analysis method recognized resin and filtered out fibers. An image comparison is presented in Figure 5.8, where what is recognized in the left picture as resin and fiber, is clearly visible in the right picture as a colour difference. During the analysis method as shown in Figure 5.9, the filtering step has been visually compared to the figures of Figure 5.8 to confirm that the filtering step filters out surface resin.

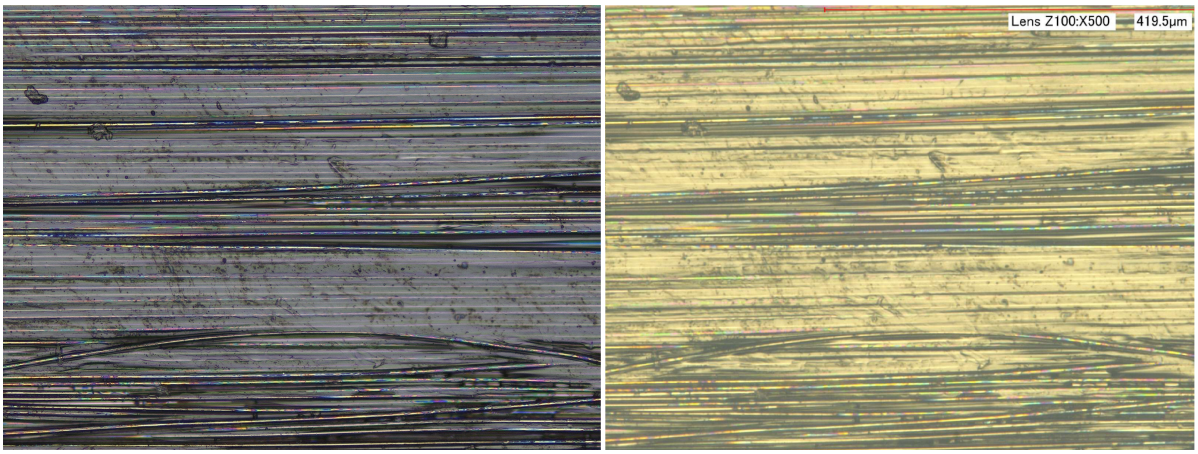

Figure 5.8: Image comparison of Keyence VK-X1000 LSCM (left) compared to Keyence VHX-2000 (right). Where re

Finally, the DEIC is determined for each microscopy picture. This is done at three locations along the sample length: 20%, 50%, and 80%. At each location, two pictures are taken, resulting in a total of six pictures. The final DEIC value for the sample is calculated as the average of the six evaluations.

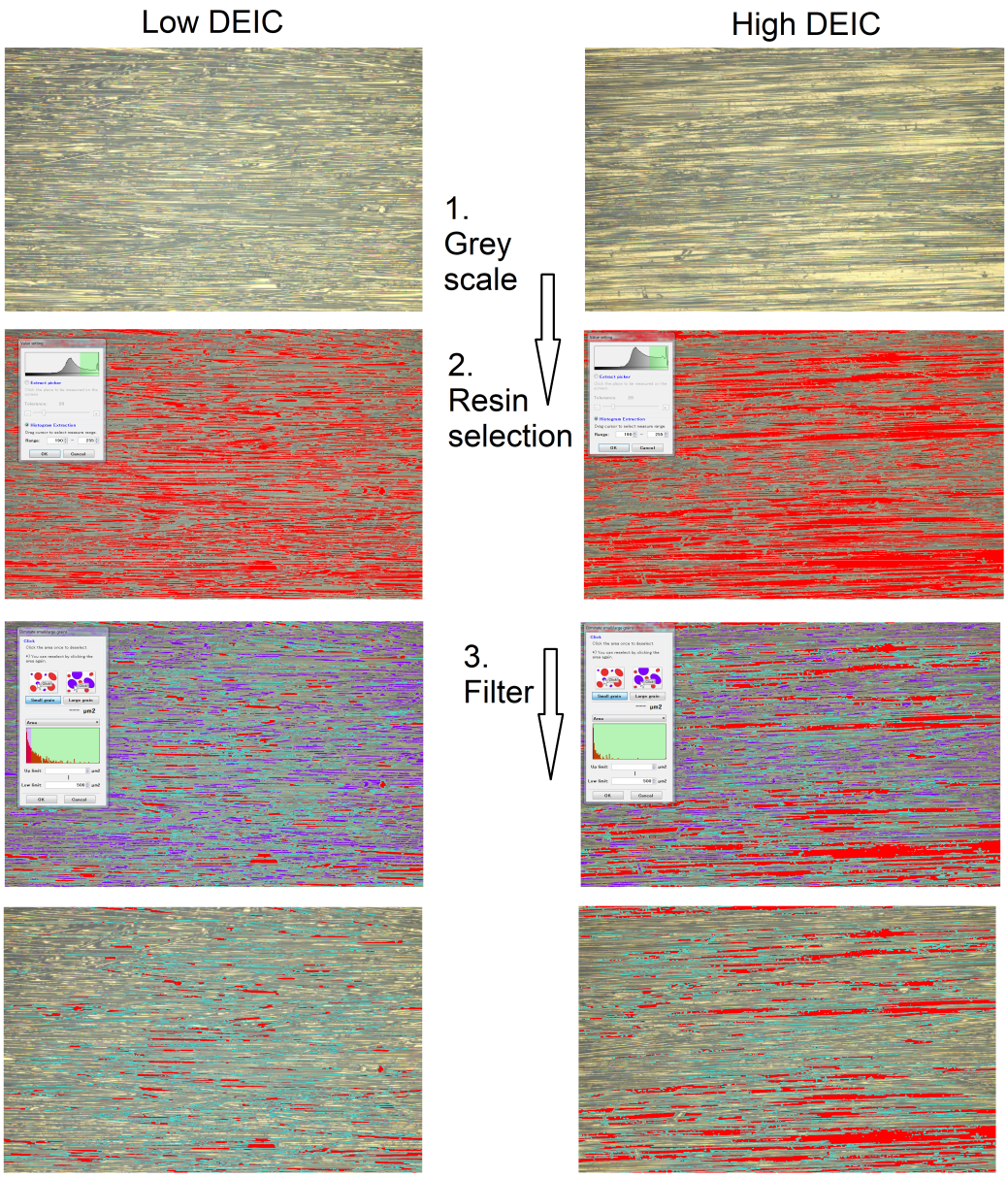

Figure 5.9: DEIC evaluation method. 1) Produce grey scale histogram from picture 2) Select the grey values of resin 3) filter out small areas.

Cross-sectional Microscopy

Following the surface microscopy, the samples undergo cross-sectional microscopy analysis. As detailed in section 5.2, the samples are embedded and prepared in order to be able to be evaluated. Due to the grinding and polishing procedure in the sample preparation, the estimated evaluation location of each sample is approximately at 50% of the sample length.

Void Content

The void content analysis is performed using a Keyence VK-X1000 LSCM with a 50x lens. The image size resulting from the analysis is $0.21\text{x}0.28mm^2$. For the figure analysis, ImageJ was used. The void content analysis is based on the grey scale value of the materials. The analysis method consist of three steps, which will be discussed and accompanied by Figure 5.10 illustrating the steps using the ImageJ software. The first step is to select the evaluation area. The second step is to convert the pixel values of the selected area into a grey scale histogram. The grey scale histogram has clear peaks on the values for PEEK and fibers, and the void value is easily identified. Finally the grey scale values for

voids is selected and the void content is calculated by the program. The void content is a percentage value representing the void area of the total selected area.

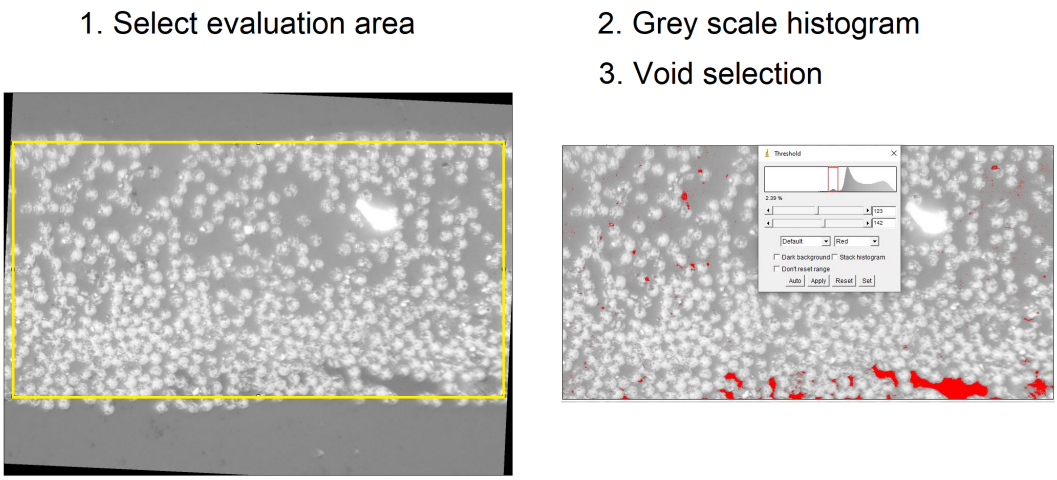

Figure 5.10: Void content analysis steps. 1) select evaluation area, 2) convert to grey scale histogram and 3) select the grey value for voids.

As discussed in chapter 2, voids can be classified into two types: intra- and interlaminar voids. Since the current experimental setup does not bond two specimens together, the interlaminar voids cannot be evaluated. However, it is observed that cavities appear on the heated side of the tape, such as on the bottom right of the evaluation area in the figure. The cavities have a high probability of being interlaminar voids if it would have been consolidated with another specimen. Therefore, these cavities present on the surface of the tape are included in the void content analysis, assuming that they would be considered interlaminar voids.

Multiple cross-sectional pictures are captured to ensure that the entire sample width is covered. Detached fibers and bundles at the ends of the cross-section are however excluded from the evaluation. Depending on the sample width this is in the range of 15 to 20 pictures, these pictures are not overlapping. To maintain high resolution and analysis quality, the use of stitched images is avoided. The void content is determined for each picture individually, and the void content value is averaged over all the pictures. This results in a void content value for the sample at a single cross-section location.

Thickness

The thickness evaluation is conducted using the Keyence VHX-2000 digital microscope with a VH-Z100 lens at 500x magnification. The resulting image size is 0.49x$0.65mm^2$. The thickness measurements are performed using the native software of the microscope. The thickness is measured at 8 locations across the width of the sample. Per location 3 measurements are performed and these are averaged to obtain the average local thickness. The local thickness is recorded for all 8 locations and averaged to determine the sample thickness.

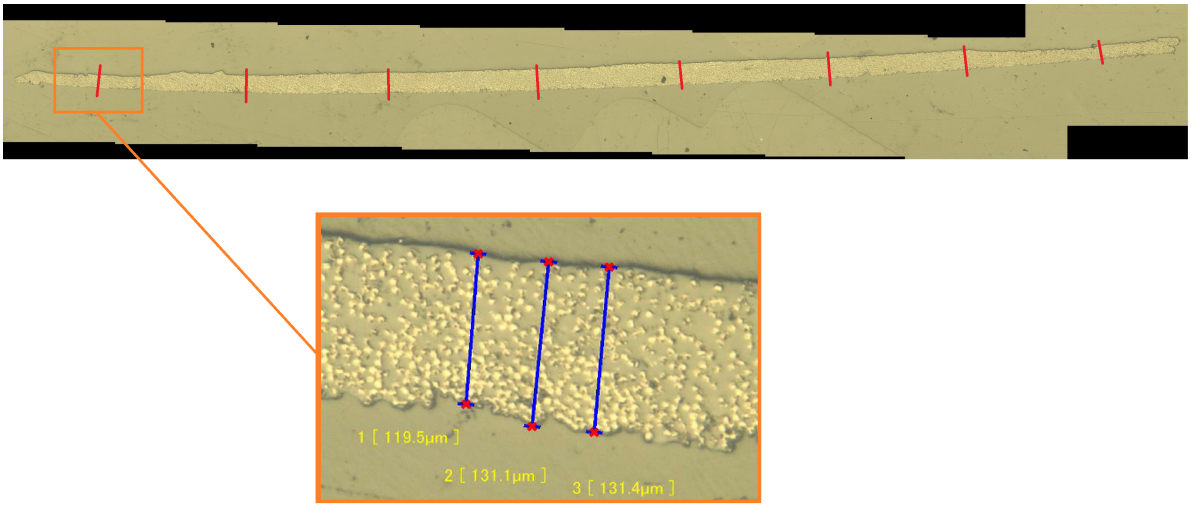

Figure 5.11: Thickness evaluation method. A total of 8 measurement locations along the tape width, 3 thickness measurements per location.

6

Results and Discussion

Using the experimental set-up, which has been designed and constructed as described in chapter 4, experiments and material characterization was conducted as detailed in chapter 5. The resulting data will be presented and analyzed in this chapter, with the goal of gaining a better understanding of the effect of LAFP process parameters on the deconsolidation forms. The chapter is organized to first present the results and observations for each deconsolidation form individually, starting with roughness, followed by Degree of Effective Intimate Contact (DEIC), void content and thickness. The results are followed by a general discussion.

Per deconsolidation form a total of four graphs will be presented. The first two graphs plot the values over the placement speed and the remaining two plot the values over pressure. Although the data value is similar, it allows to see the relationship with respect to the process parameter more clearly. The structure of the two graphs per process parameter remains the same for all deconsolidation forms: Graph (a) displays the value per data point, including their extreme values (minimum and maximum), while graph (b) proposes curves that have been fit to the data points. These curves present the expected relationship between the process parameter and the deconsolidation form. Each graph contains two curves, first the curve for the data set with three points is computed. It is then assumed that the relationship behaviour between the second data set and the process parameter is the same as the first set, so a curve with equal behaviour is assumed to the second data set which only has two data points. For the placement speed graphs the curve is extrapolated to extend to the same length, which is indicated in the figure. All the graphs have been provided with the as-received property value for reference. In section 9.2 the raw data for each sample is provided without being plotted in graphs.

6.1. Roughness

The roughness analysis of all data points was conducted, and the root-mean-squared (RMS) roughness (R_q) values are presented in Figure 6.1 and Figure 6.2. The effect of placement speed and pressure is evaluated individually. Literature suggests that the main contributor to roughness is fiber decompaction [13], as has been presented in Figure 2.10. For roughness to be reduced, re-compaction of the material would have to be performed. The R_q value of AR samples was analysed to be $1.69 \mu m$. Previous studies suggest that deconsolidated tape has an R_q of 6 to 10 μm [20].

6.1.1. The Effect of Placement Speed on Roughness

In Figure 6.1a, a decrease in roughness with an increase in placement speed is visible. Moreover, when comparing the roughness of equal pressures, the extreme values of the data points do not overlap. No overlap in extreme values indicates that there is a clear difference in value, and if the extremes would overlap, there is more uncertainty that the difference is true. Additionally, as the placement speed increases, the roughness of the samples per data point appear to be closer together as the extreme magnitude decreases. In Figure 6.1b, two curve fits are proposed for the placement speed sets that underwent equal pressures. The curves that are proposed for the data set of 600 kPa and 160 kPa pressure show an initial fast decrease in roughness which is expected to level out beyond 200 mm/s.

The curve for 600 kPa data set seems to be decreasing in roughness faster than for the 160 kPa set.

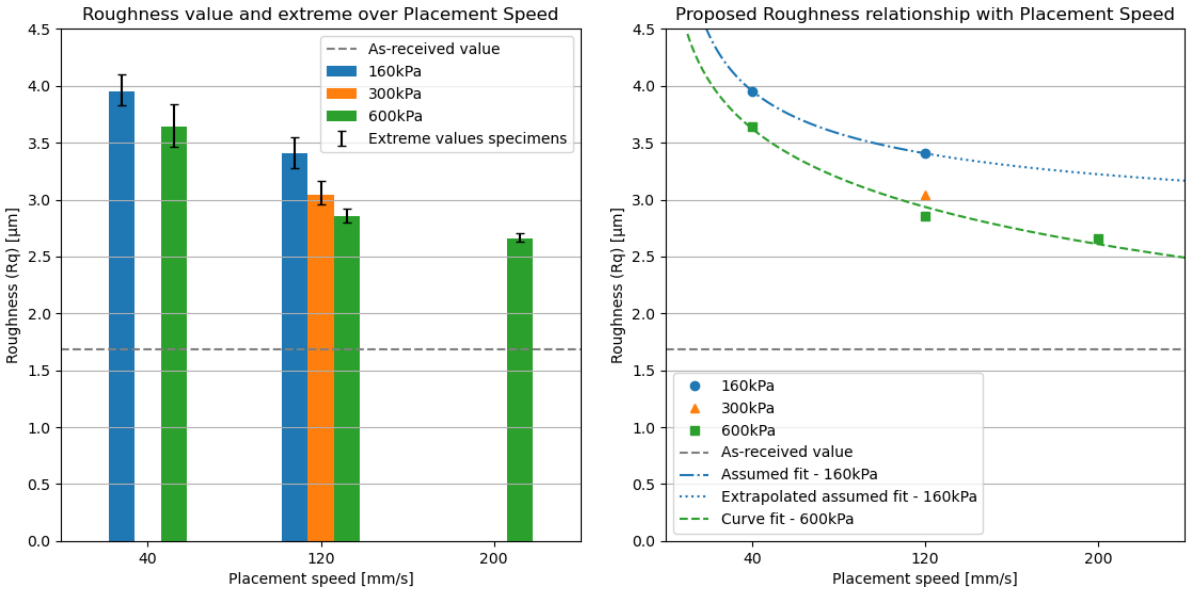

(a) Data point average roughness (R_q) and their extreme (minimum and maximum) values, plotted over placement speed.

(b) Fit, assumed and extrapolated proposed curves to the R_q data point sets of equal pressures.

Figure 6.1: Data point roughness values over applied placement speed.

6.1.2. The Effect of Pressure on Roughness

In Figure 6.2a, a decrease in roughness due to an increase of consolidation pressure is observed when the placement speed remains constant. With an increase in pressure, the extreme values of the data points decrease without overlap in extreme values. In Figure 6.2b, two curve fits are proposed for the sets of pressures that underwent equal placement speeds, 40mm/s and 120mm/s. The curves show an initial fast decrease in roughness, which is expected to level out beyond 600 kPa.

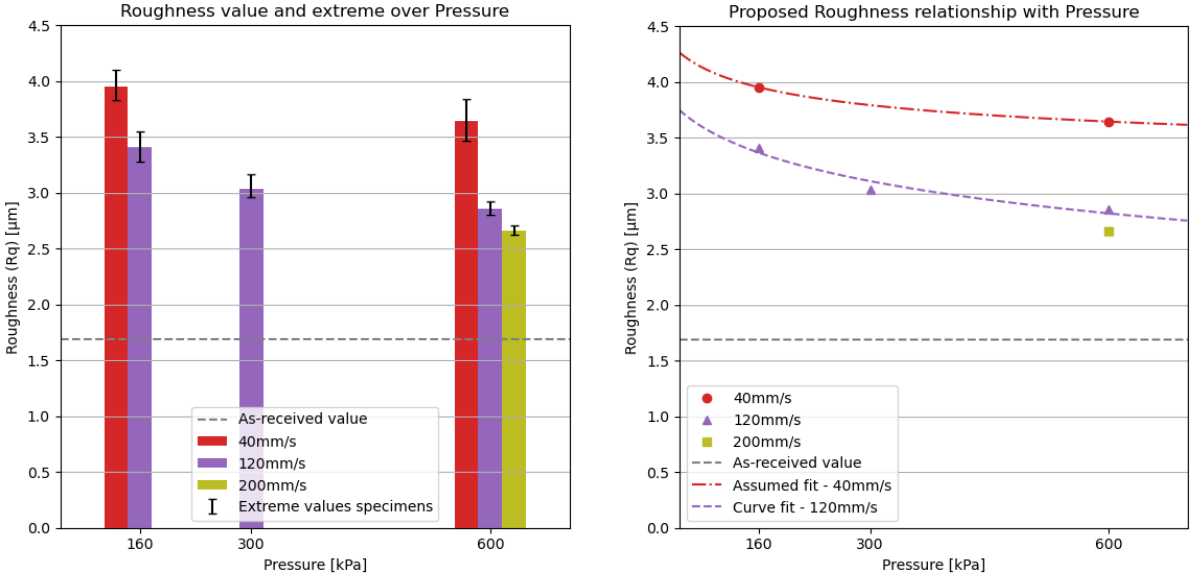

(a) Data point average roughness (R_q) and their extreme (minimum and maximum) values, plotted over consolidation pressure.

(b) Fit, assumed and extrapolated proposed curves to the R_q data point sets of equal placement speeds.

Figure 6.2: Data point roughness values over applied consolidation pressure.

6.2. Degree of Effective Intimate Contact (DEIC)

The DEIC analysis of all data points was conducted, and the DEIC values are presented in Figure 6.3 and Figure 6.4. The effect of placement speed and pressure is evaluated individually. The DEIC will increase when more resin has been able to flow to re-impregnate fibers and cover the surface. The suggested flow mechanism that take place during the consolidation, squeeze flow, through-thickness and in-plane percolation flow [19], are dependent on the matrix mobility and the compaction pressure that is applied. The DEIC in the AR tape has been analysed to be 25.9%, which is relatively high compared to previously recorded 5.9% [20] for the same material. This difference can be contributed to the change in measuring technique. Çelik et al. [19] have measured the DEIC of the same material in deconsolidated state to be 0.2%.

6.2.1. The Effect of Placement Speed on DEIC

In Figure 6.3a, an increase in DEIC is visible when the placement speed is increased. When considering the data points where the applied consolidation pressure is constant a clear increase in value is visible with no overlap in extreme values. The magnitude of the extreme values is spread throughout the data set. In Figure 6.3b, two curve fits are proposed for the placement speed sets that underwent equal pressures, being 160 kPa and 600kPa. For both curves the increase in placement speed results in an increase in DEIC, where it is expected that the curve will level off at some point beyond 200 mm/s.

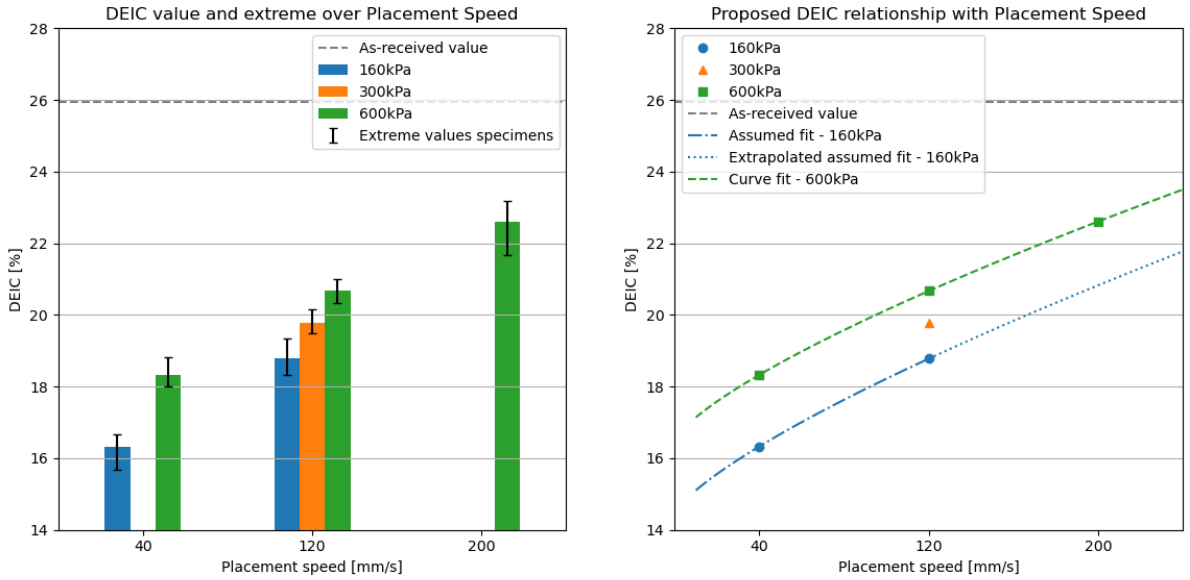

(a) Data point average DEIC and their extreme (minimum and maximum) values, plotted over placement speed.

(b) Fit, assumed and extrapolated proposed curves to the DEIC data point sets of equal pressures.

Figure 6.3: Data point DEIC values over applied placement speed.

6.2.2. The Effect of Pressure on DEIC

When comparing the data points that underwent equal placement speed presented in Figure 6.4a, an increase DEIC due to the increase in pressure is visible. The extreme values of these data points do not overlap. The difference in DEIC between 160 kPa and 600kPa is 1.9 and 2.0 % respectively for 40 mm/s and 120 mm/s. In Figure 6.4b, two curve fits are proposed for the pressure sets that underwent equal placement speeds, being 40 mm/s and 120 mm/s. As the difference between the data points of these 2 curves is almost equal, the curves look similar with an offset. The curves show an increase in DEIC with an increase in consolidation pressure.

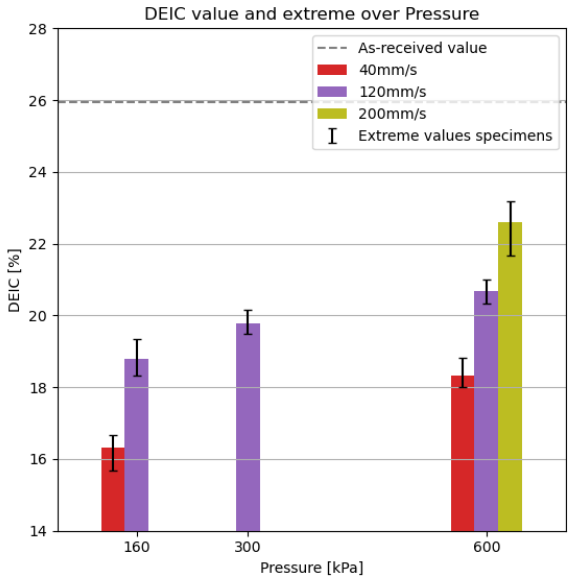

(a) Data point average DEIC and their extreme (minimum and maximum) values, plotted over consolidation pressure.

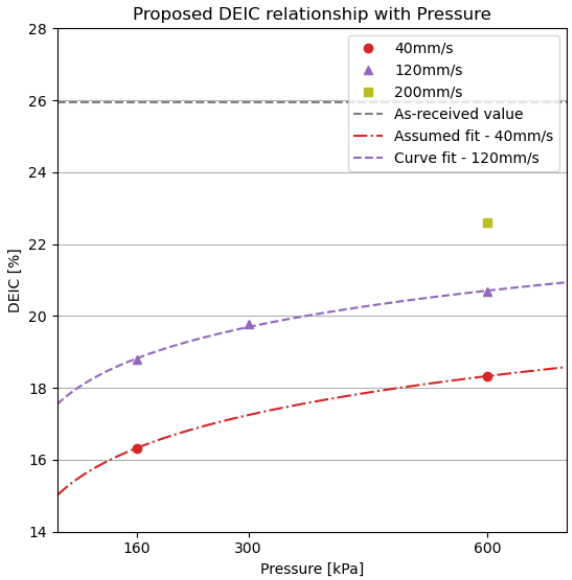

(b) Fit, assumed and extrapolated proposed curves to the DEIC data point sets of equal placement speeds.

Figure 6.4: Data point DEIC values over applied consolidation pressure.

6.3. Void Content

The void content analysis of all data points was conducted, and the measured void content is presented in Figure 6.5, Figure 6.6 and Figure 6.7. The effect of placement speed and pressure is evaluated individually. During deconsolidation, expansion of intralaminar voids and decompaction are the deconsolidation mechanisms that cause an increase in void content [13], as presented in Figure 2.10. As discussed in section 5.3, the void content analysis includes surface cavities in void content, as they resemble interlaminar voids when consolidated against another ply. In the AR state, solely intralaminar void content is analysed, as no cavities are present, which has been measured to be 0.46%. Çelik et al. [13] have measured the average void content of the same material in deconsolidated state, being between 3.3% to 4.3%. To reduce the effects of deconsolidation, intralaminar void compression, recompaction and re-impregnation of the surface layer should take place.

6.3.1. The Effect of Placement Speed on Void Content

In Figure 6.5 the data point void content values and extremes are visible. For both a compaction pressure of 160 and 600 kPa, a decrease in average void content is recorded between placement speeds 40 mm/s and 120 mm/s, however the extreme values of the 160 kPa data points are fully overlapping. The data point of 600 kPa and 200 mm/s has an higher average void content than at 600kPa and 120 mm/s, however the extreme values are overlapping.

In Figure 6.6, four curve fits are proposed for the placement speed sets that underwent equal pressures, being 160 kPa and 600kPa. As described in the chapter introduction, the curves for the compaction pressure of 600 kPa are proposed first. As the average void content of the 200 mm/s data point is higher then the 120 mm/s data point, it could be that a minimum void content has been achieved. For when this is the case, a parabolic curve fit has been proposed to both data sets in Figure 6.6a. However, as the extreme values of the data points are overlapping, it could also be the case that a minimum is not necessarily achieved, and the void content is expected to decrease and level out further. If this is the case, a power curve fit to the data points is more appropriate, which has been presented in Figure 6.6b.

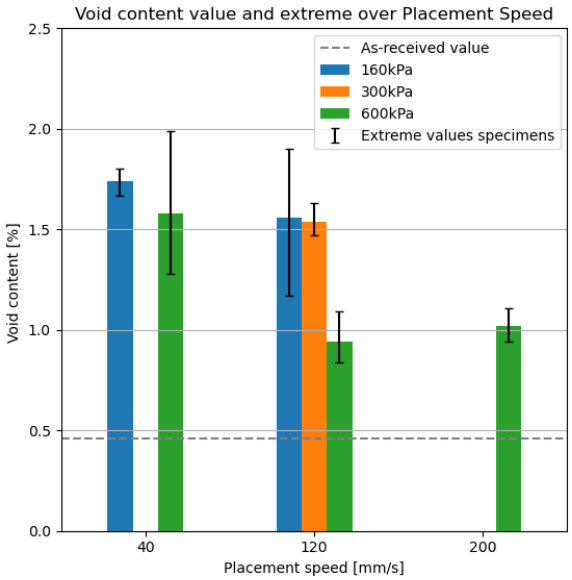

Figure 6.5: Data point average void content and their extreme (minimum and maximum) values, plotted over placement speed.

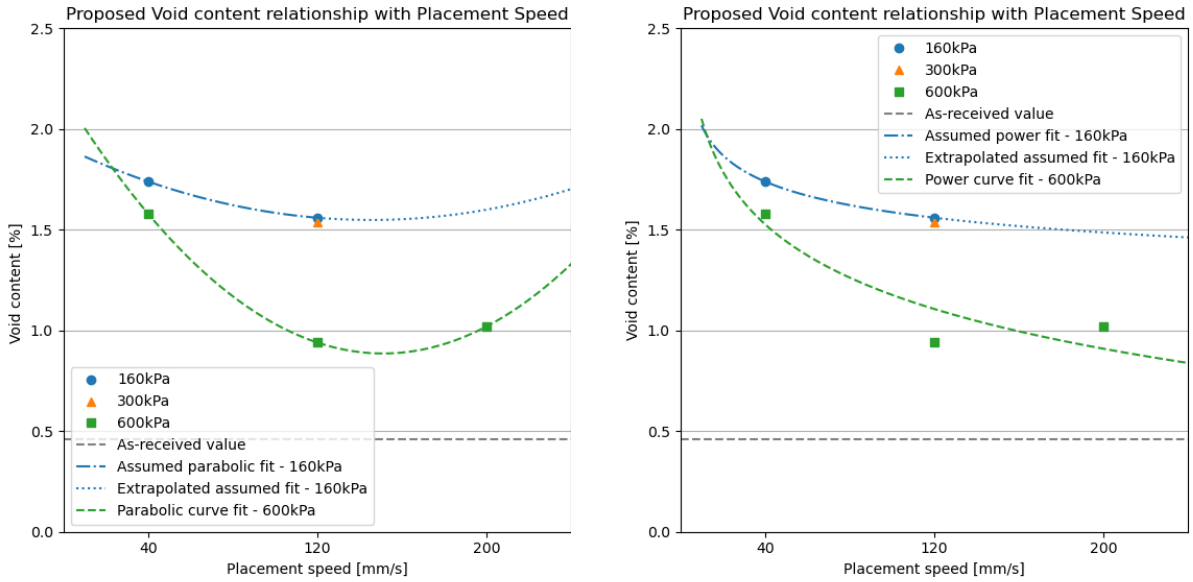

(a) Parabolic relationship

(b) Power relationship

Figure 6.6: Fit, assumed and extrapolated proposed curves to the void content data point sets of equal consolidation pressures.

6.3.2. The Effect of Pressure on Void Content

In Figure 6.7a a general decrease in average void content value can be seen. It can however be seen that the extreme values of the data points are overlapping. In Figure 6.7b two curve fits have been proposed for the pressure sets that underwent equal placement speed, being 40 mm/s and 120 mm/s. The relationship initially has a fast decrease in thickness, followed by a curve that decreases in void content when pressure is increased, which is leveling out.

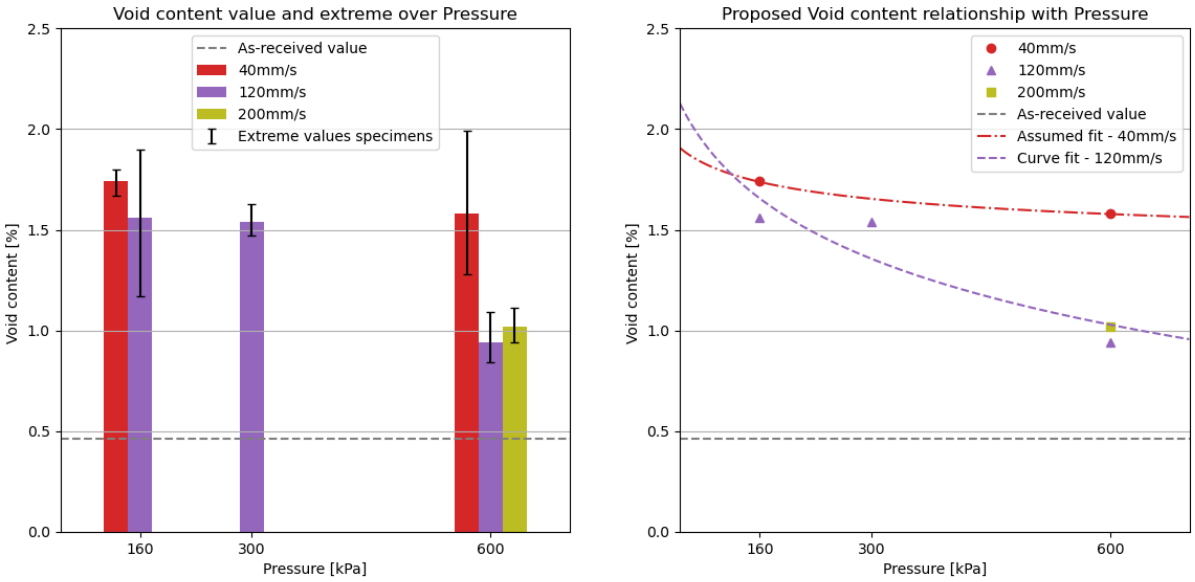

(a) Data point average void content and their extreme (minimum and maximum) values, plotted over consolidation pressure.

(b) Fit, assumed and extrapolated proposed curves to the void content data point sets of equal placement speeds.

Figure 6.7: Data point void content values over applied consolidation pressure.

6.4. Thickness

The thickness analysis of all data points was conducted, and the thickness is presented in Figure 6.8 and Figure 6.9. First an observation will be presented, followed by the individual effect of placement speed and pressure on thickness.

During deconsolidation multiple mechanisms will cause an increase in thickness. Fiber decompaction, specific volume change and void growth all contribute to the increase in thickness [13], as has been presented in Figure 2.10. The specific volume of PEEK is expected to increase with around 21% at 385 °C compared to room temperature [82]. This increase in specific volume will cause a geometry change during the heating phase, however the specific volume is again reduced to the original state once the material is cooled to room temperature again. The final mechanism that causes an increase in thickness is the expansion of intralaminar voids. The decompaction and void expansion mechanisms are considered when evaluating the thickness results. The AR tape thickness has been measured to be 0.153mm. While in deconsolidated state the thickness is expected to be in the range of 0.175 to 0.3 mm for the same tape [13, 20].

6.4.1. The Effect of Placement Speed on Thickness

In Figure 6.8a a decrease in thickness with an increase in placement speed is observed. There is an overlap in extreme values for the data points tested at 160kPa. The magnitude of the extremes of the data points decreases with the increase of placement speed. In Figure 6.8b two curves are presented that have been fit to the data points that underwent constant pressure (160 kPa and 600 kPa). Initially there is a steep decrease in thickness expected, followed by decrease in evolution when placement speed progresses. It is observed that the curve of 600 kPa has a steeper decrease in thickness when placement speed is increased.

6.4.2. The Effect of Pressure on Thickness

In Figure 6.9a a decrease in thickness due to an increase in consolidation pressure is observed. The magnitude of the extreme values per data point decrease with the increase in pressure. In Figure 6.9b two curves are presented that depict the relationship between thickness and pressure, here the placement speed is constant. Initially the thickness decreases relatively fast, after which the evolution of the thickness decrease due to pressure increase decreases. The thickness decreases faster for the data set where the placement speed is 120 mm/s.

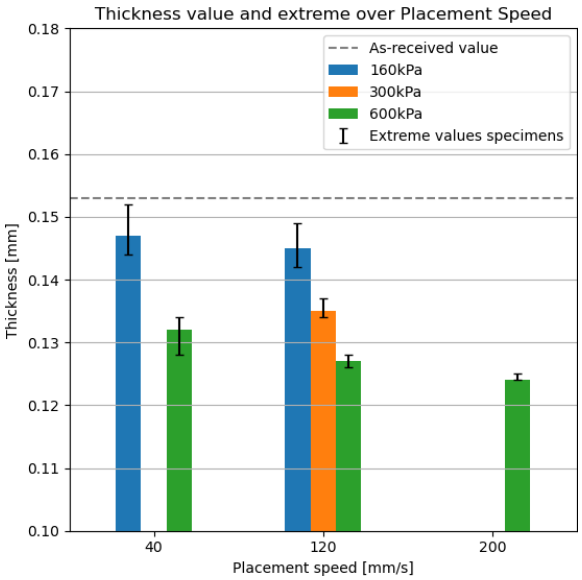

(a) Data point average thickness and their extreme (minimum and maximum) values, plotted over placement speed.

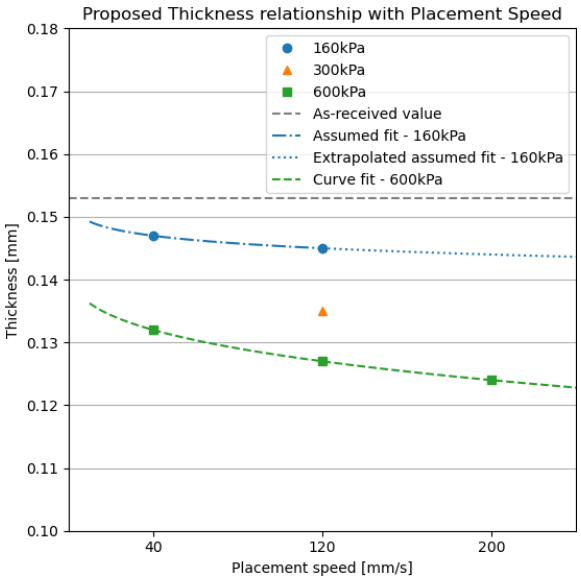

(b) Fit, assumed and extrapolated proposed curves to the thickness data point sets of equal pressures.

Figure 6.8: Data point thickness values over applied placement speed.

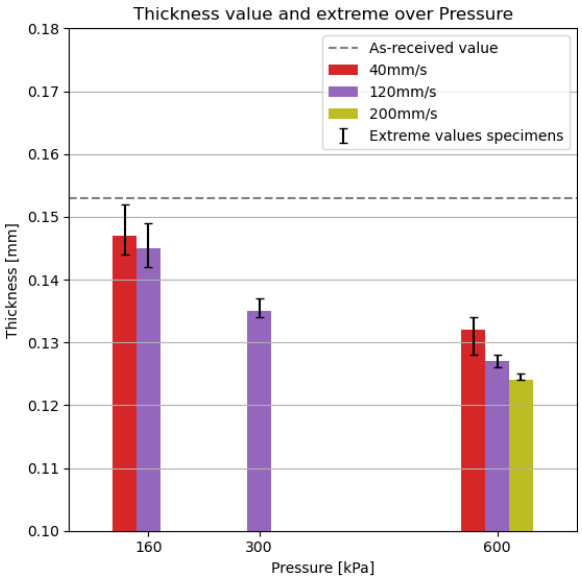

(a) Data point average thickness and their extreme (minimum and maximum) values, plotted over consolidation pressure.

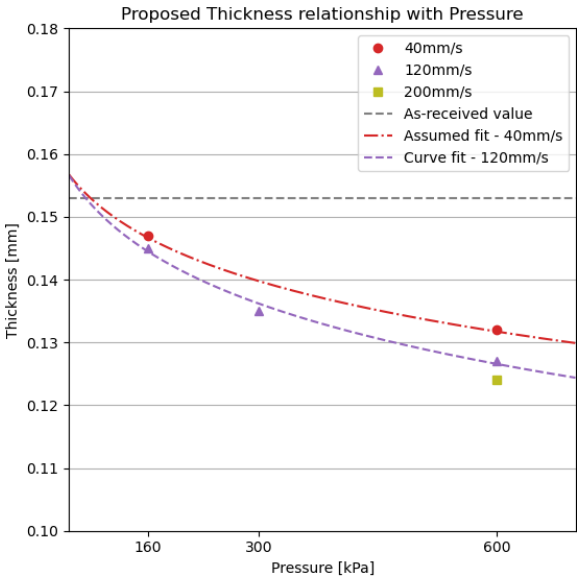

(b) Fit, assumed and extrapolated proposed curves to the thickness data point sets of equal placement speeds.

Figure 6.9: Data point roughness values over applied consolidation pressure.

6.5. Discussion

In this section the results are discussed. In the results section each deconsolidation form has been discussed separately, however in this section the results are combined. Before the results will be discussed, an overview of the achieved deconsolidation forms values and level of deconsolidation resolvement is provided for the lowest and highest process settings in Table 6.1. Initially the implication of the visible nip-point processing temperature will be discussed. Followed by the effect of placement speed, the effect of consolidation pressure and finally other findings.

Table 6.1: Deconsolidation form values, showing the base line as well as the achieved value and level of deconsolidation resolvement at the lowest and highest utilized process settings. Deconsolidation resolvement is with respect to the increase between AR and deconsolidated.

Deconsolidation Form	Reference values		Low settings (40 mm/s, 160 kPa)		High settings (200 mm/s, 600 kPa)	
	As-Received	Expected Decon-solidated [19, 20]	**Value**	**Decon-solidation resolved[%]**	**Value**	**Decon-solidation resolved[%]**
Roughness[μm]	1.69	6 - 10	3.954	47.5 - 72.8	2.659	77.5 - 88.3
DEIC[%]	25.9	0.2	16.33	62.8	22.61	87.2
Void content[%]	0.46	3.3 - 4.3	1.74	54.9 - 66.7	1.02	80.3 - 85.4
Thickness[mm]	0.153	0.175 - 0.3	0.147	...	0.124	...

Implications of visible nip-point processing temperature
Before conclusions can be drawn on the effects of the processing parameters, the resulting behaviour of setting the processing temperature at the visible nip-point should be discussed. In section 5.3 it was described that the visible nip-point is measured during set-up operation. The laser operation is optimized to achieve the same processing temperature for all of the data points at the visible nip-point. However, the actual nip-point temperature that is achieved depends on the time spent in the shadow zone, between the visible nip-point and the actual nip-point. The time spent in the shadow zone is dependant on both the placement speed and the length of the shadow zone.

When the placement speed is increased, the time spent in the shadow zone is decreased and the achieved nip-point temperature is higher. In chapter 4, with the help of Figure 4.13, it was explained that due to an increase in pressure, the roller deformation causes an decrease in shadow zone length. As a result the time spent in the shadow zone is decreased when pressure is increased, causing an increase in nip-point temperature.

In Figure 2.10, it is described what deconsolidation mechanisms are the causes for what deconsolidation forms. In reverse it is expected that for resolvement of deconsolidation to take place, re-compaction of the fibers, void compression and surface layer re-impregnation is necessary. All these mechanisms partially depend on the mobility of the matrix, as movement of fibers or flow of resin is necessary. Increasing the nip-point temperature increases the matrix mobility and thus the ability to resolve deconsolidation forms more efficiently. It must therefore be considered that part of the effectiveness of increasing the placement speed and pressure can be devoted to an increase in nip-point temperature.

In section 2.4 of the literature study, it was found that increasing the consolidation pressure has a positive effect of resolving consolidation, on the other hand the placement speed was found to have a negative effect. For all the deconsolidation forms the results show an increase in deconsolidation resolvement with an increase in placement speed, which is different from the expected behaviour. In work presented by Çelik et al. [19], similar behaviour was found. This study measured the DEIC, the average DEIC increased with placement speed, which correlates with the results that were found. Similar to the measurement techniques that have been used, this study also measured the visible nip-point.

It is expected that part of the effectiveness of increasing the placement speeds and consolidation pressure in resolving deconsolidation forms is due to an increase in nip-point temperature.

6.5.1. The effect of placement speed

For all the measured deconsolidation forms, the severity has decreased with respect to the expected deconsolidated state and the severity is decreasing when the placement speed is increased. The relationship between the deconsolidation forms severity and the placement speed increase yield an initial fast decrease. This decrease can be seen in the form of an approximate 50% deconsolidation resolvement in the lowest process settings as presented in Table 6.1. It is expected that when the placement speed increases further, the effect of the decrease in shadow zone time is decreased and the nip-point temperature will become closer to the visible nip-point temperature. Hereby minimizing the effect of the nip-point temperature increase, and the relationship thus appears to level off. If the

placement speed would be increased beyond 200 mm/s, it would be possible that the consolidation phase becomes so short that the material is above T_g in the release phase. When the temperature of the tape is above T_g in the release phase, void expansion and decompaction will be able to occur. As a result it is expected that when the placement speed is increase too much, the deconsolidation severity will increase again. It can thus be expected that the relationship between the deconsolidation severity and the placement speed is of a bathtub or parabolic type of curve.

6.5.2. The effect of consolidation pressure

For all the measured deconsolidation forms, the severity has decreased with respect to the expected deconsolidated state and the severity is decreasing when the consolidation pressure is increased. It is expected that for resolvement of deconsolidation to take place, re-compaction of the fibers, void compression and surface layer re-impregnation is necessary. Not only is matrix mobility required for the movement of fibers or flow of resin, but also force needs to be applied to the material to displace or deform it into the desired position. According to Figure 2.10, the main contributor to an increase in roughness is the decompaction of the fibers. The decrease in roughness due to increased pressure indicates that pressure is able to re-compact the fiber bed better with higher pressure. And the increase in DEIC with an increase in pressure, indicates that the surface layer is being re-impregnated more efficiently with a higher pressure. When cross-sectional figures are compared between lower and higher pressure, an increase in surface re-impregnation is visible, see Figure 6.10. This is supported by literature suggesting that an increase in pressure results in an increase in (effective) intimate contact and autohesion [19, 22, 41, 42], indicating that re-impregnation of the surface fiber bed is increasing at higher pressures.

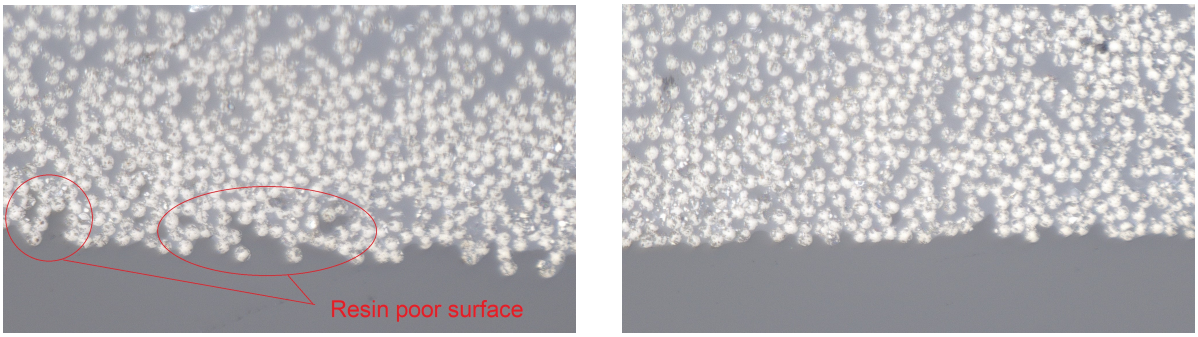

(a) Cross-section figure of 120 mm/s and 160 kPa data point.

(b) Cross-section figure of 120 mm/s and 600 kPa data point.

Figure 6.10: The difference in surface layer impregnation at two different pressure and constant placement speed. Laser heated side.

The relationship between the deconsolidation forms severity and the consolidation pressure increase yield an initial fast decrease. As no intralaminar voids have been observed, it is expected that the positive effect of pressure can be contributed to an increases in re-compaction and re-impregnation capabilities. For both of these mechanisms to take place, force has to be applied to the material. Çelik et al. [19] suggest that initially, the rougher surface has less contact area with the tool, resulting in a high local pressure. As a result more re-compaction and re-impregnation occurs at these locations. When more material starts to make contact with the tool, the local pressure decreases and the effectiveness of the applied consolidation pressure decreases, reducing re-compaction and re-impregnation capabilities. This behaviour can be observed in the results, where the relationship between the deconsolidation forms severity and the consolidation pressure, seems to be levelling off. The presented relationship curves of the four deconsolidation forms to consolidation pressure, all show a continued decrease in severity. It is however expected that a limit will be reached where more pressure does not result in an increase in surface quality. The relationship between the deconsolidation forms and the consolidation pressure is expected to be of a power curve, an fast initial decrease in severity followed by the decrease in evolution until it stalls.

6.5.3. Other findings

Intralaminar void compression

Figure A in Figure 6.11 shows what can be an expected deconsolidated tape state (same material, higher temperature achieved in the range of 395–511°C), where clear intralaminar expanded voids are visible. During the void content analysis it was remarked that almost all of the void content increase compared to AR void content, originated from the formation of surface cavities at the heated side. No intralaminar void expansion increase was visually recognized in any processed sample, figure B presents how a processed sample does not show a sign of void expansion. All of the tested placement speeds and pressures have shown to provide enough matrix mobility and force to perform void compression. The measured decrease in void content can thus be devoted to the decrease in surface cavities, meaning that the increased nip-point temperature and pressure enhances re-compaction and re-impregnation of the surface layer.

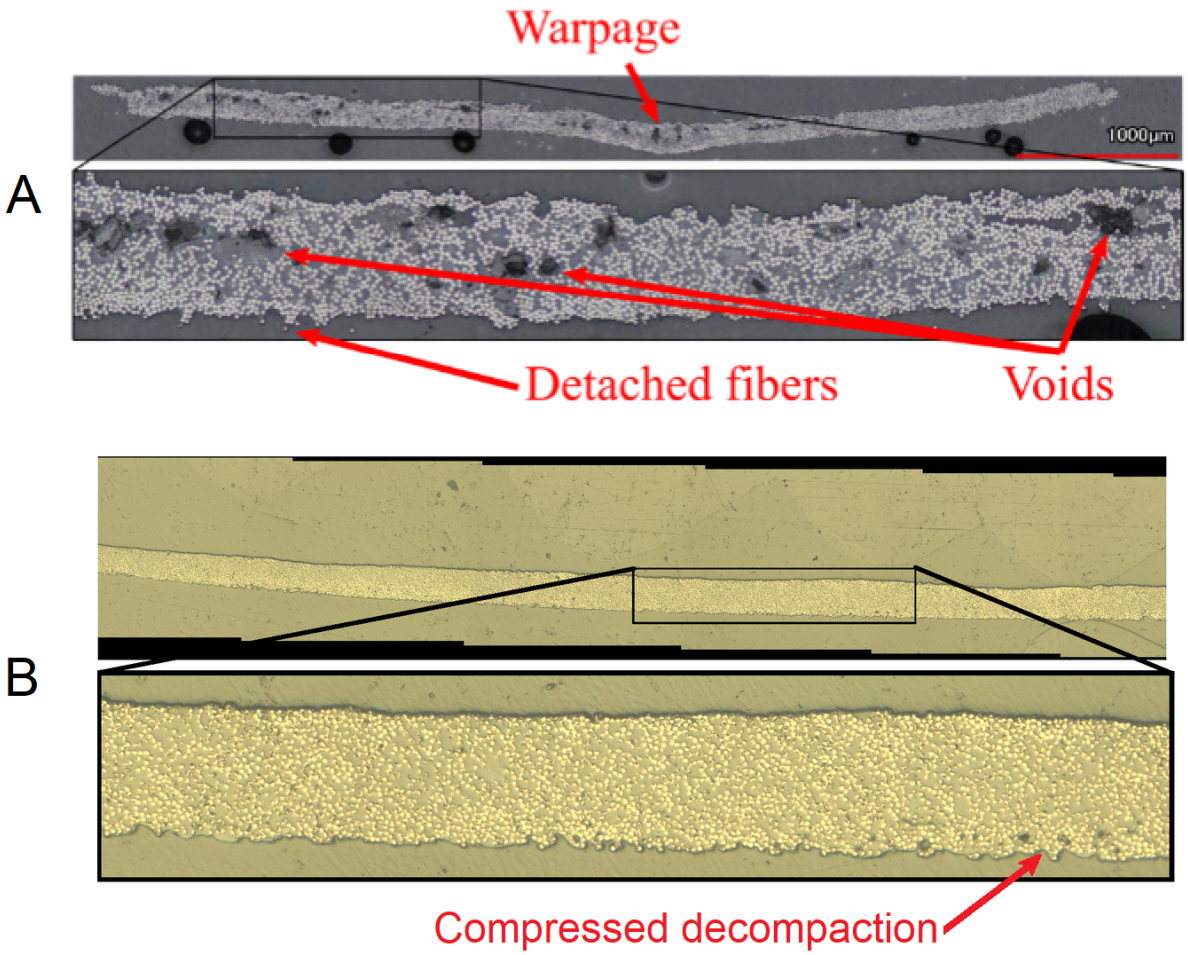

Figure 6.11: Comparison of (A) deconsolidated state [20] and (B) consolidated tape (placement speed = 40 mm/s, consolidation pressure = 160 kPa).

Initial decrease in deconsolidation severity

In Table 6.1 the values of the deconsolidation forms at the lowest process settings are compared to the expected deconsolidated tape state value. An significant improvement is made for this process setting, resolving in the order of 50% of the deconsolidation severity. In the deconsolidated state, fibers or small bundles detach from the material surface and intralaminar voids expand [13]. However, during cross-sectional analysis, these phenomena were not observed, as is presented in the comparison given in Figure 6.11. This indicates that the lowest tested placement speed and pressure can successfully resolve the void expansion and initial detachment of fibers or small bundles, which is recognized in the fast initial decrease in deconsolidation form severity.

An adequate placement speed is required to obtain a sufficient nip-point temperature that allows for sufficient matrix mobility. Furthermore, a minimum pressure is essential to provide the force required to compress voids and move detached fibers or bundles back into the material. The minimum value for both process parameter while using this set-up have not been identified, as detachment or significant de-compaction has not been observed.

Tape thickness decrease
The results presented in this study show much lower thickness values than the expected deconsolidation state, visible in Table 6.1. A decrease below the AR thickness is achieved for all of the data points. As the void content and roughness of processed tapes are higher than the AR tape values, the thickness of the tape should theoretically have increased as well. The decrease of the thickness below the AR thickness, indicates that the tape is being flattened and thus the width is increasing. When full cross-sectional figures of the samples are analysed, a clear increase in width is recorded. In Table 6.2 the decrease in thickness combined with an increase in width is presented. The cross sectional area of the specific samples are provided here as well. Here the averaged measured thickness is multiplied by the width of the sample. The change in area can be contributed to the increase in void content, decompaction and measurement error.

Table 6.2: Thickness, width and cross-sectional area of As-recieved, low (placement speed = 40 mm/s, consolidation pressure = 160 kPa) and high (placement speed = 200 mm/s, consolidation pressure = 600 kPa) process settings.

	As-Received	Low settings	High settings
Thickness[mm]	0.153	0.147	0.124
Width[mm]	6.3	7.3	8.4
Cross-section area [mm^2]	0.97	1.06	1.05

When the cross-sectional width and thickness is inspected, a re-occurring phenomena is found. There is a clear step in thickness found near the edges of the tape width, on both sides of the tape. An example of this is presented in Figure 6.12, in the top figure two blue arrows indicate the location where the decrease in thickness starts. The close up presents two dotted lines that indicate the transition region more closely. This phenomena occurs for all the tested specimens, however it is more clearly present at low placement speeds and high pressures. The width of the thicker region is consistent throughout the data points, being around 5.8mm. It is theorized that the room temperature roller acts as a heat sink to the cool side of the tape, keeping the temperature of that side of the tape below processing temperature. As a result only the heated side is able to deform and flatten to increase the width, it is not identified how much of the thickness is able to deform. As the width of the thicker region has been measured to be smaller than the AR tape width, it is thought that the edges of the tape can be irradiated by the laser from the side, allowing for more mobility locally. The transition region indicated in the figure could be the result of the side heating, as more consistent width is found beyond dotted line 2.

When Çelik et al. studied the resolvement of deconsolidation, no significant decrease in thickness with respect to the AR tape was observed [20]. The difference between the test set-ups is the movement, where Çelik et al. had a stationary pressure set-up, and this set-up is rolling. The movement of the roller could be introducing specific directional forces that enhances tape flattening. In the study of Çelik et al. resin was squeezed out of specimen in the length direction, as flow with the fibers is easier than against the fibers. In a continues placement set-up that is utilized here, there is no easy way out for the resin and only lateral movement is possible.

Relation between placement speed and consolidation pressure
It is observed that increasing both placement speed and pressure simultaneously yield a more positive effect on the deconsolidation resolvement for roughness, void content, and thickness, than an individual increase of either process parameter. This suggested positive effect can be deduced to the combined effect of reducing the time spent in the shadow zone by increasing placement speed and decreasing shadow zone length with higher pressure.

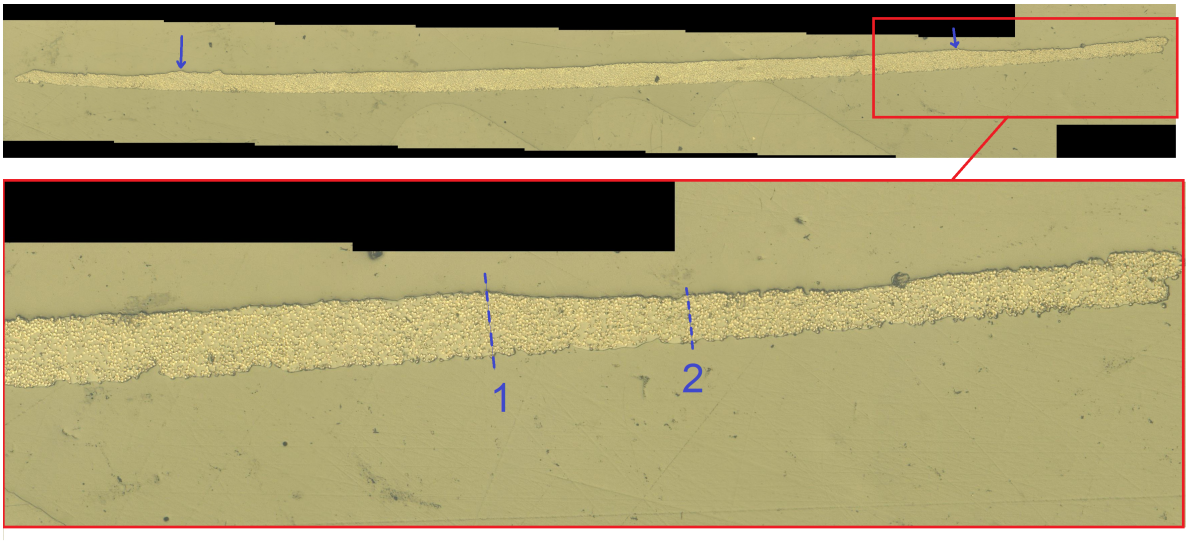

Figure 6.12: Tape widening with a clear step in thickness. Placement speed = 40 mm/s, consolidation pressure = 600 kPa.

By comparing how fast a deconsolidation form severity decreases with placement speed and consolidation pressure, the effectiveness of the process parameters can be compared. For example the effect of placement speed on R_q is observed to be more significant than the effect of pressure. This is deduced from the steeper decreasing curves of constant pressure in Figure 6.1b compared to the less steep constant placement speed curves of Figure 6.2b and a larger offset between the constant placement speed curves. This analysis is performed for all the graphs resulting in the following found relationships as presented in Table 6.3.

Table 6.3: Influence of placement speed and consolidation pressure increase on deconsolidation forms. The upward (↑) arrow, downward (↓) arrow indicates the increase or decrease of the process parameter on the deconsolidation form. The green colour of the cell indicates that its effect is positive to the consolidation quality. Two arrows indicate a more significant effect than the other parameters

	Roughness	**DEIC**	**Voids**	**Thickness**
Placement speed increase	↓↓	↑↑	↓	↓
Pressure increase	↓	↑	↓	↓↓

The results are compared to the results of both Çelik et al. [20], presented in Table 2.2, and various other studies, presented in Table 2.1. Please note that to meaning of a double arrow is different between the tables. In both tables from the literature study, the increase in consolidation pressure shows an decrease in deconsolidation severity. And the decrease in deconsolidation severity due to the placement speed increase was unexpected but can be justified by the nip-point temperature increase.

Furthermore Çelik et al. found that the nip-point temperature should be above T_m for improvement to occur in DEIC and thickess. Table 2.1 presents an increase in bond forming capabilities and decrease in void content when the nip-point temperature is increased. As improvements are made for all the tested data points, it can thus be concluded that the nip-point temperature has been above T_m for all tested data points. The behaviour that is presented in Table 6.3 is in correlation with literature, when the effect on nip-point temperature is taken into account.

Extreme values

When the extreme values are compared between data points, two main trends have been identified. First roughness and thickness decrease in extreme value magnitude as process parameters are increased. Secondly void content and DEIC have a random distribution of extreme value magnitude

throughout the tested realm. The effect of the latter is particularly interesting for the uncertain relationship between placement speed and void content. The increase in average void content at the placement speed of 200 mm/s could suggest that the material has been above T_g in the release phase. As no thermal data of the material in the release phase is available to confirm this, and the extreme values of the data points of both void content and DEIC are overlapping, a different influence can be considered.

The AR material was presented in chapter 5, where it was observed that there is significant difference in local fiber volume fraction. When the cross-sectional figures of processed tapes are analysed, significant difference in fiber volume distribution was found. A clear example is presented in Figure 6.13, where Figure 6.13a shows a section of the tape with a low fiber volume fraction, and Figure 6.13b shows a section of the tape with a high fiber volume fraction.

(a) Low fiber volume fraction, high surface resin

(b) High fiber volume fraction, low surface resin

Figure 6.13: Correlation between fiber volume fraction and surface resin content at the laser heated side. (placement speed = 200 mm/s, consolidation pressure = 600kPa)

As a result there are locations with high fiber volume content and minimal surface resin content and vice versa. This is also visible when the tape surface is analysed, for example in Figure 5.9, the high DEIC case has patches of high resin content and low resin content, resulting in local variation of DEIC. As only six DEIC analysis are performed per sample, there is a high dependency on the local fiber volume fraction. To achieve more consistent results, full surface analysis should be performed.

In literature it was found that local high fiber volume fractions would result in more severe deconsolidation, which is caused by a difference in temperature [13]. During the analysis of the void content, it has been remarked that almost all surface cavities occur at locations where the local fiber volume fraction is high. In the appendix, section 9.1, a total of 8 figures of severe deconsolidation are provided, showing a local high fiber volume fraction as well. Relating this information to the uncertainty in void content, in depth void content data analysis is performed. In Table 6.4 more complete void content data of each sample is provided of data points 120 mm/s and 200 mm/s at 600 kPa.

Table 6.4: Detailed void content data of two 600 kPa consolidation pressure data points.

	120 mm/s				200 mm/s			
Sample	1	2	3	Average	1	2	3	Average
Average void content [%]	1.09	0.84	0.88	0.94	0.94	1.11	1.00	1.02
Max void content [%]	2.20	2.38	2.59	**2.39**	1.56	1.94	2.39	**1.97**
No. figures where void content >1.0% [-](total No. figures)	8(18)	5(16)	4(16)	**5.7(16.7)**	8(17)	9(18)	8(17)	**8.3(17.3)**

For each sample the full cross section is captured in a number of figures and each figure is analysed for void content individually. Per figure, the void content depends on the presence and severity of the cavities. In Table 6.4 the void content of the figure with the largest void content and the number of figures

where the void content is above 1.0% are provided per sample. The 1.0% cut off point is a value which will filter out which figures have surface cavities, as the void content will only surpass this value when cavities are present. It can be seen that the average maximum void content of the 120 mm/s data point is larger than that of the 200 mm/s data point. The amount of figures where the recorded void content is larger than 1.0% can depict the amount of cavities that are present in a sample. From the provided data we can see that the amount of cavities is lower for the 120 mm/s data point compared to the 200 mm/s data point. What can be concluded from this information is that the 120 mm/s data point has less but more severe cavities, and the 200 mm/s data point has more but less severe cavities. It could thus be the case that even though a placement speed of 200 mm/s has the ability to resolve cavities more efficiently, as the cavities are found to be less severe, more local high fiber distributions have resulted in more cavities, which results in a higher average void content. For this reason and the fact that the other deconsolidation forms do not show an increase as well, it is assumed that the void content is not necessarily larger for 200 mm/s data point, and a power curve relationship would be more applicable. For more consistent results it is suggested to perform a volumetric void content analysis or increase the amount of measured cross-sections per sample.

The decrease in the magnitude of the extreme values of roughness and thickness are a result of a decrease in local deviation of roughness and thickness. From the previous argumentation it is expected that in deconsolidated state, decompaction is a local phenomena dependant on the fiber volume distribution. As a result the thickness and roughness are also higher in value where (severe) deconsolidation occurs. A decrease in local deviation thus suggest that the difference in value is leveled out as the process parameters are increased. This behaviour can be justified by the increase in matrix mobility and pressure enabling a better redistribution and re-compaction of the material.

7

Conclusion

Although significant research has been conducted to investigate rapid laser deconsolidation and its effect on compaction behavior, there is a lack of knowledge regarding how capable the laser assisted fiber placement (LAFP) process is in resolving deconsolidation. A thorough understanding of the consolidating capability and the impact of process parameters on deconsolidation severity would greatly benefit the advancement of reliability and quality of the LAFP process. Therefore, the research objective is to develop a novel experimental setup capable of achieving variable laser assisted fiber placement process parameters, analyze and compare the produced specimens, and acquire knowledge on the consolidation of rapid laser-deconsolidated thermoplastic composite tapes, as well as the effect of process parameters on the consolidation process.

The research objective was split up into two research activities. First, the goal was to design and construct an experimental set-up that has the capability to make specimens undergo LAFP type temperature and pressure histories. Secondly, utilizing the set-up to investigate the effect of LAFP process parameters on the rapid laser heating deconsolidation forms. The experimental set-up is utilized to produce CF/PEEK tape samples that have undergone six different combinations of placement speed (in the range of 40 mm/s to 200 mm/s) and consolidation pressure (in the range of 160 kPa to 600kPa). During post processing, four deconsolidation forms, roughness, degree of effective intimate contact (DEIC), void content and thickness of the six data points are characterized using microscopy. The results of the characterization are used to acquire knowledge on consolidation of rapid laser deconsolidated thermoplastic composite tapes.

The set-up that has been designed and constructed is capable of mimicking LAFP temperature and pressure histories. First the incoming tape is heated with a vertical-cavity surface-emitting laser (VCSEL), after which it moves through a shadow zone to then be consolidated between a silicon roller and a moving tool surface that provides the linear placement movement. The heating profile, placement speed and consolidation pressure are variable. The set-up makes use of a room temperature aluminium tool surface, 60sh silicon roller and is capable of varying placement speed up to 200 mm/s, and consolidation pressure between 160 kPa and 600 kPa. The proper application of placement speed, consolidation pressure and laser heating is verified. The experimental set-up has been designed and constructed to meet the research goal, while also maintaining flexibility for future modifications and advancements.

It is found that for when both consolidation pressure and placement speed are increased, the severity of the deconsolidation forms are decreased. Roughness, thickness and void content all show a general decrease in value, while DEIC shows an increase when the placement speed is increased. The increase in consolidation pressure and placement speed shortens the time in the shadow zone. As a result, the temperature decrease in the shadow zone is reduced and as the process temperature was set equal before the shadow zone, the nip-point temperature is increased. The higher nip-point temperature allows for an increase in matrix mobility and time above melting temperature during consolidation, increasing the re-compaction and re-impregnation capabilities. Increasing the nip-point temperature by

increasing the consolidation pressure and placement speed in this set-up has shown to have a positive effect on the resolvement of deconsolidation.

The decrease in deconsolidation severity when placement speed is increased is believed to be due to the resulting increase in nip-point temperature. It is expected that increasing the placement speed further does not yield additional benefits as there is an optimum for placement speed. An optimum in placement speed is achieved when time above melting temperature in the consolidation phase is maximized without the release temperature exceeding the glass transition temperature. This optimum is not found in these results, as it is expected that the room temperature tool cools the material quicker than the consolidation phase duration.

Increasing the consolidation pressure, results in a decrease of the severity of the deconsolidation forms. During cross-sectional analysis, no expected intralaminar void growth was recognized when comparing processed to as-received tapes. Deconsolidation resolvement is dependent on the re-compaction of the fiber bed and flow of the matrix material, for both these mechanisms, consolidation pressure plays a significant role. Increasing the consolidation pressure shows to have a positive effect on the resolvement of deconsolidation. An increase in pressure beyond 600 kPa is expected to yield even better results, however the evolution of the positive increase is expected to start stalling as re-compaction becomes more difficult. It must be considered that part of the effectiveness of the pressure increase can be devoted to an increase in nip-point temperature.

When the quantitative values of roughness and DEIC are analysed, it is found that the roughness and DEIC are almost returned to the as-received state and are expected achieve as-received values beyond the tested realm. Regarding the void content it is found that intralaminar void content can be brought back to the as-received state, but surface cavities, which are expected to turn into interlaminar voids in a laminate, have remained. The thickness has decreased below the as-received thickness, which can be contributed to both re-compaction and tape flattening. The local decompaction that causes significant thickness and void content increase shows to keep decreasing when the process parameters are increased, however the relationship evolution indicates it is more difficult to fully resolve these deconsolidation forms. It is expected that with an increase in process parameters beyond the tested realm, as-received values can be achieved for roughness and DEIC, but surface cavities due to decompaction will remain difficult to be fully resolved. For final production quality it should be considered that the tape structure should maybe be improved beyond the as-received state, for example for DEIC which is preferably 100%, not the as-received 25.9%.

All deconsolidation forms show to have improved from the expected deconsolidated state significantly, even at the lowest tested process setting (placement speed = 40 mm/s, consolidation pressure = 160 kPa). In deconsolidated state, intralaminar void growth, significant decompaction with detachment of fibers or bundles and thickness increase is expected, but none were observed. The main deconsolidation that was observed via cross-sectional microscopy was surface decompaction of the fiber bed, which also caused cavities to form. Within the tested process parameter realm, initial severe deconsolidation can be resolved, leaving a certain level of surface decompaction and cavities to be resolved.

During cross-sectional analysis it was observed in the void content and thickness data, that at locations where the local fiber volume fraction was higher, increased void content and thickness was observed. In the as-received material analysis a distribution in fiber volume content was found, with locations where the fiber volume fraction was relatively high or low. The VCSEL has the property to heat the carbon fibers and not the PEEK, as a result in locations where more fibers are present, more heat accumulates. It can be concluded that the increase in cavities and thickness at local high fiber volume locations is a result of more severe local deconsolidation. It would be expected that a more equal distribution in fiber volume would result in less severe deconsolidation spots or regions in the material.

The experimental set-up is able to vary the LAFP process parameters being applied to the samples. The set-up translates the process parameters to temperature and pressure histories that mimic those of LAFP. The set-up is therefore able to produce samples that underwent variable LAFP conditions. The set-up was able to successfully provide samples as per objective of this research. Furthermore

the set-up does have limitations but has been designed to maintain flexibility for future modifications and advancements, ensuring to be of significant value to future research in LAFP. Within the tested process parameter realm, initial severe deconsolidation can be resolved, leaving a certain level of decompaction and cavities to be resolved. Increased placement speed and consolidation pressure have shown to reduce the negative effects of rapid laser deconsolidated thermoplastic composite tapes, although partially due to increasing the nip-point temperature. The optimum process parameters have not been found in this study nor would the achieved quality meet the current aerospace standards. It is expected that the consolidation can be optimized to achieve as-received values for roughness and DEIC.

8

Recommendations

In this chapter recommendations for future work are provided. About half of the time spent in this research was dedicated to the design and construction of an experimental set-up that has proven to be able to mimic LAFP conditions. A majority of the recommendations are possible to be conducted with the use of the experimental set-up.

The effect of tool temperature

The literature study suggested that higher placement speed has a negative effect on the deconsolidation. It is believed this relation (besides different nip-point temperatures) was not achieved due to the quench cooling effect of the room temperature tool. The data of Çelik et al. [19] shows the same behaviour. Longer useful consolidation time could be achieved when the tool surface is heated, and then also a decrease in quality when placement speed is increased can be expected due to the higher release temperature. The removable tool surface of the set-up allows to build a heated bed section into the tool, allowing to investigate the effect of different tool temperatures. With the tool temperature increase investigation, the material temperature in the release phase should be recorded as well for a complete understanding.

Consolidation with substrate material

In this study the specimens have been consolidated against an aluminium tool. The expected consolidation behaviour is different between an aluminum tool and another ply of the same material. The increase in void content measured in this research is believed to be due to the presence of surface cavities. It is believed these surface cavities result in interlaminar voids when consolidated with another ply. To confirm this believe, and to investigate if the void quantity shows similar results, consolidation with the same material is suggested.

Tape width increase

It was found that the rolling motion of the set-up resulted in significant tape flattening. The flattening of tapes is an important mechanism to understand, when it is not well understood it could cause overlaps or gaps between tapes when used in industry. The influence of the roller material could be added to the research.

Set-up heating phase efficiency and measurement

To improve the experimental set-up as it is, the heating and temperature measurement should be optimized. The shape of the VCSEL did not allow for optimal placement and as a result the shadow zone is larger then necessary and the heating capability is reduced. To improve this, a different VCSEL unit could be considered, which has a more focused irradiation, Phillips also supplies LAFP dedicated VCSEL units. Or the VCSEL irradiation should be directed toward the nip-point more effectively via i.e. a reflective tool surface (keep laser safety in mind). The temperature measurement is limited due to the location of the FLIR and the incidence angle of the tape near the nip-point. No specific suggestion is considered.

Increasing set-up process parameter limits

The consolidation pressure of the set-up can be increased. For example, one could redesign the setup to include a larger plateau or make use of weight materials with a higher density than the current steel. Additionally, the setup could be equipped with a constant force cylinder or spring to push the slide down, thereby increasing the total force and resulting in a higher pressure. The placement speed on the other hand is expected to be more difficult to increase. For one the VCSEL would have to be operated by the Arduino to make sure the VCSEL is only on when the tool is moving. Secondly the hardware should have to be improved. A stepper motor (and accompanied driver) supplying more torque would be required to be able to accelerate faster.

Setting the nip-point temperature equal

As the processing temperature was equalized in the visible nip-point (before the shadow zone), the nip-point temperature was never equal between different process parameters. Due to the change in real nip-point temperature, the true effect of placement speed, consolidation pressure and nip-point temperature could not be investigated separately. To investigate the effect of placement speed, consolidation pressure and real nip-point temperature, the real nip-point temperature should be set equal for all the data points.

Tape structure and deconsolidation

The significance of the fiber volume fraction for deconsolidation became apparent in this research. Previously there has been some work performed on the investigation of resin rich surface layers. It was found to reduce fiber detachment and improve intimate contact development. An investigation towards optimizing the tape structure could fast track the improvement of the consolidation quality significantly if local severe deconsolidation could be eliminated. With more consistent tape behaviour, process optimization for the LAFP process can be performed more efficiently.

Comparing to achieved deconsolidation

In this research the achieved deconsolidation form values have been compared to an expected deconsolidated state. The deconsolidated state deconsolidation form values have been produced by Çelik et al. [20], who measured tape state after severe deconsolidation was performed. Although the exact same material was used, combined with using the same measurement techniques(except minor alterations) a direct deconsolidated state comparison can not be made. In the heating process that has been used in this study the deconsolidated state should be different for all tested process settings. In order to get a more accurate idea on the amount of deconsolidation that was originally present and how much of this has been resolved, the deconsolidated state should be recorded while a similar heating phase has been applied to the tape.

Measuring crystallinity

At the moment difficulty is found in accurately measuring the temperature history during the LAFP process. Understanding the temperature history would improve the understanding of the individual process parameter effects. In the literature study the behaviour of the material crystallinity of a thermoplastic material during the LAFP process has been covered in detail. By measuring the crystallinity of consolidated tapes, it might be possible to deduced more information regarding the undergone temperature history.

References

1. Airbus. *Global Market Forecast 2022-2041* https://www.airbus.com/en/products-services/commercial-aircraft/market/global-market-forecast (2022).
2. Boeing. *Commercial Market Outlook 2022–2041* https://www.boeing.com/commercial/market/commercial-market-outlook/index.page (2022).
3. Salas, E. B. *Number of jets added to the global aircraft fleet from 1999 to 2021, by manufacturer (in units)** https://www.statista.com/statistics/622779/number-of-jets-delivered-global-aircraft-fleet-by-manufacturer/ (2022).
4. Commission, E. Flightpath 2050 Europe's Vision for Aviation (2011).
5. Hellard, G. *Composites in Airbus—A Long Story of Innovations and Experiences* in *Airbus Global Investor Forum, Seville, Spain* (2008).
6. Miller, A. *The Boeing 787 Dreamliner* in *Seattle: American Society for Composites Technical Conference* (2007).
7. CompositesWorld. *Consolidating thermoplastic composite aerostructures in place, Part 1* https://www.compositesworld.com/articles/consolidating-thermoplastic-composite-aerostructures-in-place-part-1 (2022).
8. Hou, M., Ye, L. & Mai, Y. Manufacturing process and mechanical properties of thermoplastic composite components. *Journal of Materials Processing Technology* **63,** 334–338. ISSN: 0924-0136. https://www.sciencedirect.com/science/article/pii/S0924013696026441 (1997).
9. Comer, A. *et al.* Mechanical characterisation of carbon fibre–PEEK manufactured by laser-assisted automated-tape-placement and autoclave. *Composites Part A: Applied Science and Manufacturing* **69,** 10–20. ISSN: 1359-835X. https://www.sciencedirect.com/science/article/pii/S1359835X14003133 (2015).
10. Stokes-Griffin, C. & Compston, P. A combined optical-thermal model for near-infrared laser heating of thermoplastic composites in an automated tape placement process. *Composites Part A: Applied Science and Manufacturing* **75,** 104–115. ISSN: 1359-835X. https://www.sciencedirect.com/science/article/pii/S1359835X14002395 (2015).
11. Stokes-Griffin, C. & Compston, P. Investigation of sub-melt temperature bonding of carbon-fibre/PEEK in an automated laser tape placement process. *Composites Part A: Applied Science and Manufacturing* **84,** 17–25. ISSN: 1359-835X. https://www.sciencedirect.com/science/article/pii/S1359835X16000038 (2016).
12. Kok, T., Grouve, W. J., Warnet, L. L. & Akkerman, R. *Quantification of tape deconsolidation during laser assisted fiber placement* in *3rd International Symposium on Automated Composites Manufacturing, ACM 2017* (2017).
13. Çelik, O., Choudhary, A., Peeters, D., Teuwen, J. & Dransfeld, C. Deconsolidation of thermoplastic prepreg tapes during rapid laser heating. *Composites Part A: Applied Science and Manufacturing* **149,** 106575. ISSN: 1359-835X. https://www.sciencedirect.com/science/article/pii/S1359835X21002967 (2021).
14. Bussink, T. Effect of Rapid Laser Deconsolidation on Intimate Contact Development. *Delft University of Technology* (2021).
15. Stokes-Griffin, C. M., Compston, P., Matuszyk, T. I. & Cardew-Hall, M. J. Thermal modelling of the laser-assisted thermoplastic tape placement process. *Journal of Thermoplastic Composite Materials* **28,** 1445–1462 (2015).
16. Weiler, T., Emonts, M., Striet, P., Gronenborn, S. & Janssen, H. *Optical modelling of VCSEL-assisted thermoplastic tape placement* in *ECCM17—17th European Conference on Composite Materials* (2016).

17. Moench, H. *et al. High-power VCSEL systems and applications* in *High-Power Diode Laser Technology and Applications XIII* **9348** (2015), 267–276.

18. Moench, H. *et al.* High-power VCSEL systems and applications. *Proceedings of SPIE - The International Society for Optical Engineering* **9348** (Mar. 2015).

19. Çelik, O., Peeters, D., Dransfeld, C. & Teuwen, J. Intimate contact development during laser assisted fiber placement: Microstructure and effect of process parameters. *Composites Part A: Applied Science and Manufacturing* **134,** 105888. ISSN: 1359-835X. https://www.sciencedirect.com/science/article/pii/S1359835X20301263 (2020).

20. Çelik, O., Bussink, T., Peeters, D., Teuwen, J. & Dransfeld, C. The effect of Laser-Induced deconsolidation on the compaction behavior of thermoplastic composite tapes. *Composites Part A: Applied Science and Manufacturing* **151,** 106670. ISSN: 1359-835X. https://www.sciencedirect.com/science/article/pii/S1359835X21003870 (2021).

21. Brasington, A., Sacco, C., Halbritter, J., Wehbe, R. & Harik, R. Automated fiber placement: A review of history, current technologies, and future paths forward. *Composites Part C: Open Access* **6,** 100182. ISSN: 2666-6820. https://www.sciencedirect.com/science/article/pii/S2666682021000773 (2021).

22. Kok, T. On the consolidation quality in laser assisted fiber placement: the role of the heating phase (2018).

23. Choudhary, A. Thermal deconsolidation of thermoplastic prepreg tapes during Laser-Assisted Fiber Placement (2019).

24. Donough, M. J., Shafaq, St John, N. A., Philips, A. W. & Gangadhara Prusty, B. Process modelling of In-situ consolidated thermoplastic composite by automated fibre placement – A review. *Composites Part A: Applied Science and Manufacturing* **163,** 107179. ISSN: 1359-835X. https://www.sciencedirect.com/science/article/pii/S1359835X22003608 (2022).

25. Mehdikhani, M., Gorbatikh, L., Verpoest, I. & Lomov, S. V. Voids in fiber-reinforced polymer composites: A review on their formation, characteristics, and effects on mechanical performance. *Journal of Composite Materials* **53,** 1579–1669. eprint: https://doi.org/10.1177/0021998318772152. https://doi.org/10.1177/0021998318772152 (2019).

26. Comer, A. *et al.* Mechanical characterisation of carbon fibre–PEEK manufactured by laser-assisted automated-tape-placement and autoclave. *Composites Part A: Applied Science and Manufacturing* **69,** 10–20 (2015).

27. Ghiorse, S. Effect of void content on the mechanical properties of carbon/epoxy laminates. *SAMPE quarterly* **24,** 54–59 (1993).

28. CompositesWorld. *PEEK vs. PEKK vs. PAEK and Continuous Compression Molding* https://www.compositesworld.com/articles/peek-vs-pekk-vs-paek-and-continuous-compression-molding (2022).

29. Schledjewski, R. & Schlarb, A. In-situ consolidation of thermoplastic tape material effects of tape quality on resulting part properties. *International SAMPE Symposium and Exhibition (Proceedings)* **52** (Jan. 2007).

30. Tierney, J. & Gillespie Jr, J. W. Modeling of heat transfer and void dynamics for the thermoplastic composite tow-placement process. *Journal of Composite Materials* **37,** 1745–1768 (2003).

31. Gruber, M. B. *et al. Thermoplastic in situ placement requires better impregnated tapes and tows* in *Proceedings of the 2012 SAMPE conference and exhibition, Baltimore, MD* (2012).

32. Ranganathan, S., Advani, S. G. & Lamontia, M. A. A non-isothermal process model for consolidation and void reduction during in-situ tow placement of thermoplastic composites. *Journal of Composite Materials* **29,** 1040–1062 (1995).

33. Saenz-Castillo, D., Martín, M., Calvo, S., Rodriguez-Lence, F. & Güemes, A. Effect of processing parameters and void content on mechanical properties and NDI of thermoplastic composites. *Composites Part A: Applied Science and Manufacturing* **121,** 308–320 (2019).

34. Lundstrom, T., Gebart, B. & Lundemo, C. Void formation in RTM. *Journal of reinforced plastics and composites* **12,** 1339–1349 (1993).

35. Park, C. H. & Woo, L. Modeling void formation and unsaturated flow in liquid composite molding processes: a survey and review. *Journal of reinforced plastics and composites* **30,** 957–977 (2011).

36. Simacek, P., Advani, S. G., Gruber, M. & Jensen, B. A non-local void filling model to describe its dynamics during processing thermoplastic composites. *Composites Part A: Applied Science and Manufacturing* **46,** 154–165. ISSN: 1359-835X. https://www.sciencedirect.com/science/article/pii/S1359835X1200334X (2013).

37. Pitchumani, R., Ranganathan, S., Don, R., Gillespie Jr, J. & Lamontia, M. A. Analysis of transport phenomena governing interfacial bonding and void dynamics during thermoplastic tow-placement. *International journal of heat and mass transfer* **39,** 1883–1897 (1996).

38. Yang, F. & Pitchumani, R. Interlaminar contact development during thermoplastic fusion bonding. *Polymer Engineering & Science* **42,** 424–438. eprint: https://onlinelibrary.wiley.com/doi/pdf/10.1002/pen.10960. https://onlinelibrary.wiley.com/doi/abs/10.1002/pen.10960 (2002).

39. Butler, C. A., Mccullough, R. L., Pitchumani, R. & John W. Gillespie, J. An Analysis of Mechanisms Governing Fusion Bonding of Thermoplastic Composites. *Journal of Thermoplastic Composite Materials* **11,** 338–363. eprint: https://doi.org/10.1177/089270579801100404. https://doi.org/10.1177/089270579801100404 (1998).

40. Kim, Y. H. & Wool, R. P. A theory of healing at a polymer-polymer interface. *Macromolecules* **16,** 1115–1120. eprint: https://doi.org/10.1021/ma00241a013. https://doi.org/10.1021/ma00241a013 (1983).

41. Çelik, O. *et al.* The influence of inter-laminar thermal contact resistance on the cooling of material during laser assisted fiber placement. *Composites Part A: Applied Science and Manufacturing* **145,** 106367 (2021).

42. Dara, P. H. & Loos, A. C. *Thermoplastic matrix composite processing model* tech. rep. (1985).

43. Lee, W. I. & Springer, G. S. A model of the manufacturing process of thermoplastic matrix composites. *Journal of composite materials* **21,** 1017–1055 (1987).

44. Mantell, S. C. & Springer, G. S. Manufacturing process models for thermoplastic composites. *Journal of Composite Materials* **26,** 2348–2377 (1992).

45. Yang, F. & Pitchumani, R. A fractal Cantor set based description of interlaminar contact evolution during thermoplastic composites processing. *Journal of materials science* **36,** 4661–4671 (2001).

46. Stokes-Griffin, C. & Compston, P. An inverse model for optimisation of laser heat flux distributions in an automated laser tape placement process for carbon-fibre/PEEK. *Composites Part A: Applied Science and Manufacturing* **88,** 190–197. ISSN: 1359-835X. https://www.sciencedirect.com/science/article/pii/S1359835X16301713 (2016).

47. Mantell, S. C., Wang, Q. & Springer, G. S. Processing Thermoplastic Composites in a Press and by Tape Laying—Experimental Results. *Journal of Composite Materials* **26,** 2378–2401. eprint: https://doi.org/10.1177/002199839202601603. https://doi.org/10.1177/002199839202601603 (1992).

48. Schaefer, P., Guglhoer, T., Sause, M. & Drechsler, K. Development of intimate contact during processing of carbon fiber reinforced Polyamide-6 tapes. *Journal of Reinforced Plastics and Composites* **36,** 593–607. eprint: https://doi.org/10.1177/0731684416687041. https://doi.org/10.1177/0731684416687041 (2017).

49. Khodaei, A. & Shadmehri, F. Intimate contact development for automated fiber placement of thermoplastic composites. *Composites Part C: Open Access* **8,** 100290. ISSN: 2666-6820. https://www.sciencedirect.com/science/article/pii/S2666682022000548 (2022).

50. Yang, F. & Pitchumani, R. Healing of thermoplastic polymers at an interface under nonisothermal conditions. *Macromolecules* **35.** Cited by: 142, 3213–3224. https://www.scopus.com/inward/record.uri?eid=2-s2.0-0037046321&doi=10.1021%2fma010858o&partnerID=40&md5=e03ac3331531af8be086ad343a188c76 (2002).

51. Lamèthe, J.-F., Beauchêne, P. & Léger, L. Polymer dynamics applied to PEEK matrix composite welding. *Aerospace Science and Technology* **9,** 233–240. ISSN: 1270-9638. https://www.sciencedirect.com/science/article/pii/S1270963805000180 (2005).

52. Tardif, X. *et al.* Experimental study of crystallization of PolyEtherEtherKetone (PEEK) over a large temperature range using a nano-calorimeter. *Polymer Testing* **36,** 10–19. ISSN: 0142-9418. https://www.sciencedirect.com/science/article/pii/S0142941814000713 (2014).

53. Sonmez, F. O. & Hahn, H. T. Modeling of Heat Transfer and Crystallization in Thermoplastic Composite Tape Placement Process. *Journal of Thermoplastic Composite Materials* **10,** 198–240. eprint: https://doi.org/10.1177/089270579701000301. https://doi.org/10.1177/089270579701000301 (1997).

54. Gao, S.-L. & Kim, J.-K. Correlation among crystalline morphology of PEEK, interface bond strength, and in-plane mechanical properties of carbon/PEEK composites. *Journal of Applied Polymer Science* **84.** Cited by: 29, 1155–1167. https://www.scopus.com/inward/record.uri?eid=2-s2.0-0037138329&doi=10.1002%2fapp.10406&partnerID=40&md5=2f8d46b20ebdcc1042c8dde7efd55040 (2002).

55. Koutras, N., Amirdine, J., Boyard, N., Fernandez Villegas, I. & Benedictus, R. Characterisation of crystallinity at the interface of ultrasonically welded carbon fibre PPS joints. *Composites Part A: Applied Science and Manufacturing* **125,** 105574. ISSN: 1359-835X. https://www.sciencedirect.com/science/article/pii/S1359835X19303239 (2019).

56. Pistor, C. M. & Güçeri, S. I. Crystallinity of On-Line Consolidated Thermoplastic Composites. *Journal of Composite Materials* **33,** 306–324. eprint: https://doi.org/10.1177/002199839903300401. https://doi.org/10.1177/002199839903300401 (1999).

57. Tierney, J. J. & Gillespie Jr., J. Crystallization kinetics behavior of PEEK based composites exposed to high heating and cooling rates. *Composites Part A: Applied Science and Manufacturing* **35,** 547–558. ISSN: 1359-835X. https://www.sciencedirect.com/science/article/pii/S1359835X04000028 (2004).

58. Gao, S.-L. & Kim, J.-K. Cooling rate influences in carbon fibre/PEEK composites. Part III: impact damage performance. *Composites Part A: Applied Science and Manufacturing* **32,** 775–785. ISSN: 1359-835X. https://www.sciencedirect.com/science/article/pii/S1359835X00001895 (2001).

59. Chadwick, A., Kotzur, K. & Nowotny, S. Moderation of thermoplastic composite crystallinity and mechanical properties through in situ manufacturing and post-manufacturing tempering: Part 1 – Mechanical characterisation. *Composites Part A: Applied Science and Manufacturing* **143,** 106286. ISSN: 1359-835X. https://www.sciencedirect.com/science/article/pii/S1359835X21000166 (2021).

60. Khan, M. A., Mitschang, P. & Schledjewski, R. Parametric study on processing parameters and resulting part quality through thermoplastic tape placement process. *Journal of Composite Materials* **47,** 485–499. eprint: https://doi.org/10.1177/0021998312441810. https://doi.org/10.1177/0021998312441810 (2013).

61. M. Brzeski, R. H. & Schledjewski, R. Effect of tool temperature on laminate properties during in situ consolidation placement process. *SAMPE Symposium and Exhibition (SAMPE 2010)* (2010).

62. Agarwal, V., McCullough, R. & Schultz, J. The thermoplastic laser-assisted consolidation process-mechanical and microstructure characterization. *Journal of thermoplastic composite materials* **9,** 365–380 (1996).

63. Henninger, F., Ye, L. & Friedrich, K. Deconsolidation behaviour of glass fibre-polyamide 12 composite sheet material during post-processing. *Plastics, Rubber and Composites Processing and Applications* **27,** 287–292 (1998).

64. Wolfrath, J., Michaud, V. & Månson, J.-A. Deconsolidation in glass mat thermoplastic composites: Analysis of the mechanisms. *Composites Part A: Applied Science and Manufacturing* **36,** 1608–1616. ISSN: 1359-835X. https://www.sciencedirect.com/science/article/pii/S1359835X05001363 (2005).

65. Ye, L., Lu, M. & Liu, H.-Y. in *Polymer Composites: From Nano- to Macro-Scale* 233–254 (Springer US, Boston, MA, 2005). ISBN: 978-0-387-26213-0. https://doi.org/10.1007/0-387-26213-X_13.
66. Ye, L., Lu, M. & Mai, Y.-W. Thermal de-consolidation of thermoplastic matrix composites—I. Growth of voids. *Composites Science and Technology* **62,** 2121–2130. ISSN: 0266-3538. https://www.sciencedirect.com/science/article/pii/S0266353802001446 (2002).
67. Lu, M., Ye, L. & Mai, Y.-W. Thermal de-consolidation of thermoplastic matrix composites—II. "Migration" of voids and "re-consolidation". *Composites Science and Technology* **64,** 191–202. ISSN: 0266-3538. https://www.sciencedirect.com/science/article/pii/S0266353803002331 (2004).
68. Brzeski, M. Experimental and analytical investigation of deconsolidation for fiber reinforced thermoplastic composites (2014).
69. Slange, T., Warnet, L., Grouve, W. & Akkerman, R. Deconsolidation of C/PEEK blanks: on the role of prepreg, blank manufacturing method and conditioning. *Composites Part A: Applied Science and Manufacturing* **113,** 189–199. ISSN: 1359-835X. https://www.sciencedirect.com/science/article/pii/S1359835X18302628 (2018).
70. Krämer, E., Grouve, W., Koussios, S., Warnet, L. & Akkerman, R. Real-time observation of waviness formation during C/PEEK consolidation. *Composites Part A: Applied Science and Manufacturing* **133,** 105872. ISSN: 1359-835X. https://www.sciencedirect.com/science/article/pii/S1359835X2030110X (2020).
71. Ye, L., Chen, Z.-R., Lu, M. & Hou, M. De-consolidation and re-consolidation in CF/PPS thermoplastic matrix composites. *Composites Part A: Applied Science and Manufacturing* **36,** 915–922 (2005).
72. Blommert, Y. Deconsolidation of thermoplastic prepreg tapes during the heating phase of LAFP: An experimental investigation into the effect of a resin-rich surface and tape pre-tension (2022).
73. Slange, T. K. Rapid Manufacturing of Tailored Thermoplastic Composites by Automated Lay-up and Stamp Forming: A Study on the Consolidation Mechanisms (2019).
74. Engelhardt, R., Irmanputra, R., Brath, K., Aufenanger, N. & Drechsler, K. Thermoset Prepreg Compaction during Automated Fiber Placement and Vacuum Debulking. *Procedia CIRP* **85.** 2nd CIRP Conference on Composite Material Parts Manufacturing, 10-11 October 2019, Advanced Manufacturing Research Centre, UK, 153–158. ISSN: 2212-8271. https://www.sciencedirect.com/science/article/pii/S2212827119312855 (2019).
75. Chen, J. *et al. Science and Engineering of Composite Materials* **22,** 165–173. https://doi.org/10.1515/secm-2013-0257 (2015).
76. Bakhshi, N. & Hojjati, M. Effect of compaction roller on layup quality and defects formation in automated fiber placement. *Journal of Reinforced Plastics and Composites* **39,** 3–20. eprint: https://doi.org/10.1177/0731684419868845. https://doi.org/10.1177/0731684419868845 (2020).
77. Zhou, P. Numerical Simulation for the Pressure Distribution of the Compaction Roller in in-situ consolidation processes. *TU Delft* (2018).
78. dow.com. *SILASTIC™ RTV-4136-M Base and Curing Agent* https://www.dow.com/en-us/pdp.silastic-rtv-4136-m-base-and-curing-agent.04107127h.html#overview (2023).
79. Aachen, P. P. G. Laser System with Laser Module PPM412-48-980-96 Reference and Installation Manual V 1.8 (2018).
80. Jiang, J., He, Y. & Ke, Y. Pressure distribution for automated fiber placement and design optimization of compaction rollers. *Journal of Reinforced Plastics and Composites* **38,** 860–870. eprint: https://doi.org/10.1177/0731684419850896. https://doi.org/10.1177/0731684419850896 (2019).
81. Composites, T. A. Toray Cetex TC1200 PEEK Product Data Sheet (2019).
82. Zoller, P., Kehl, T., Starkweather, H. W. & Jones, G. A. The equation of state and heat of fusion of poly(ether ether ketone). *Journal of Polymer Science Part B* **27,** 993–1007 (1989).

9

Appendices

9.1. Decompaction and cavities at high fiber volume locations - 2 data points compared

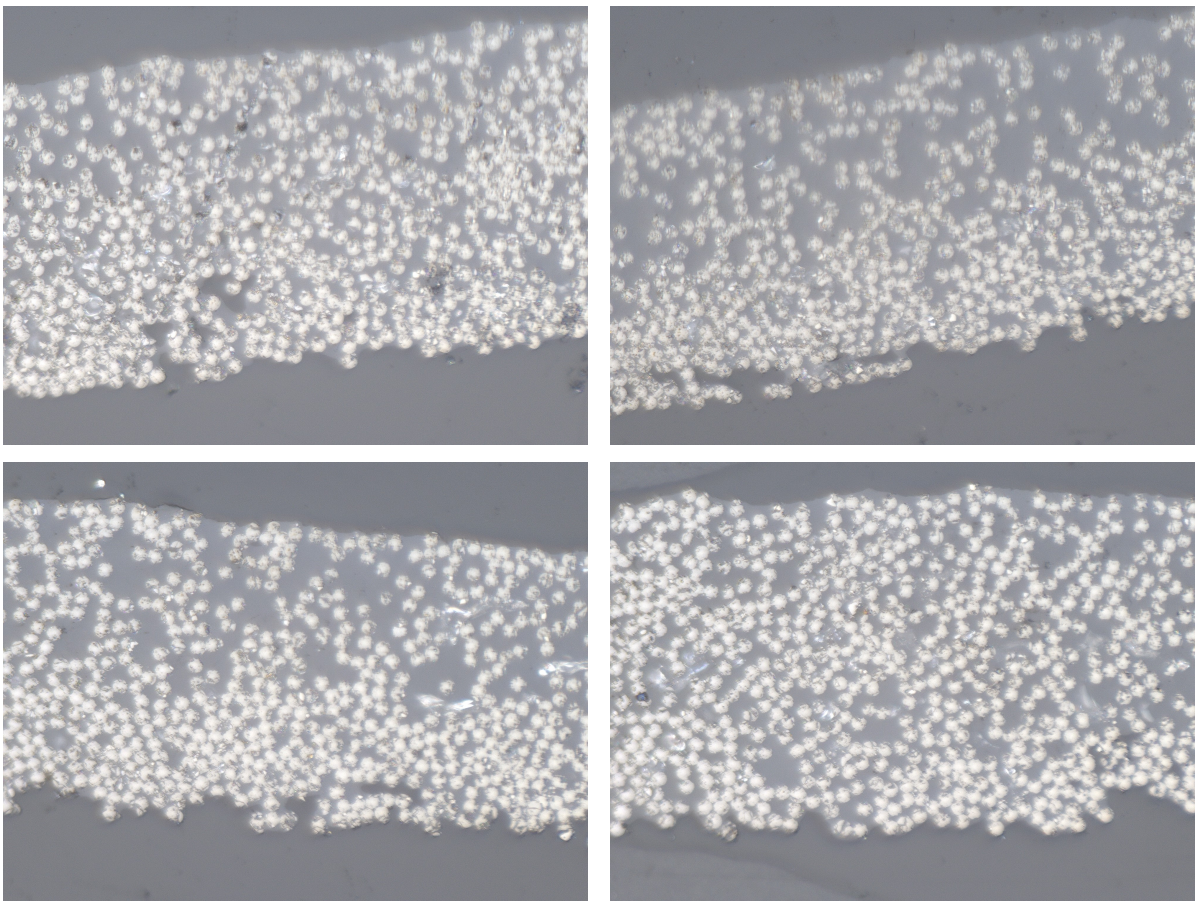

Figure 9.1: Four examples of decompaction and cavities at high fiber volume locations. Placement speed = 40 mm/s, consolidation pressure = 160 kPa

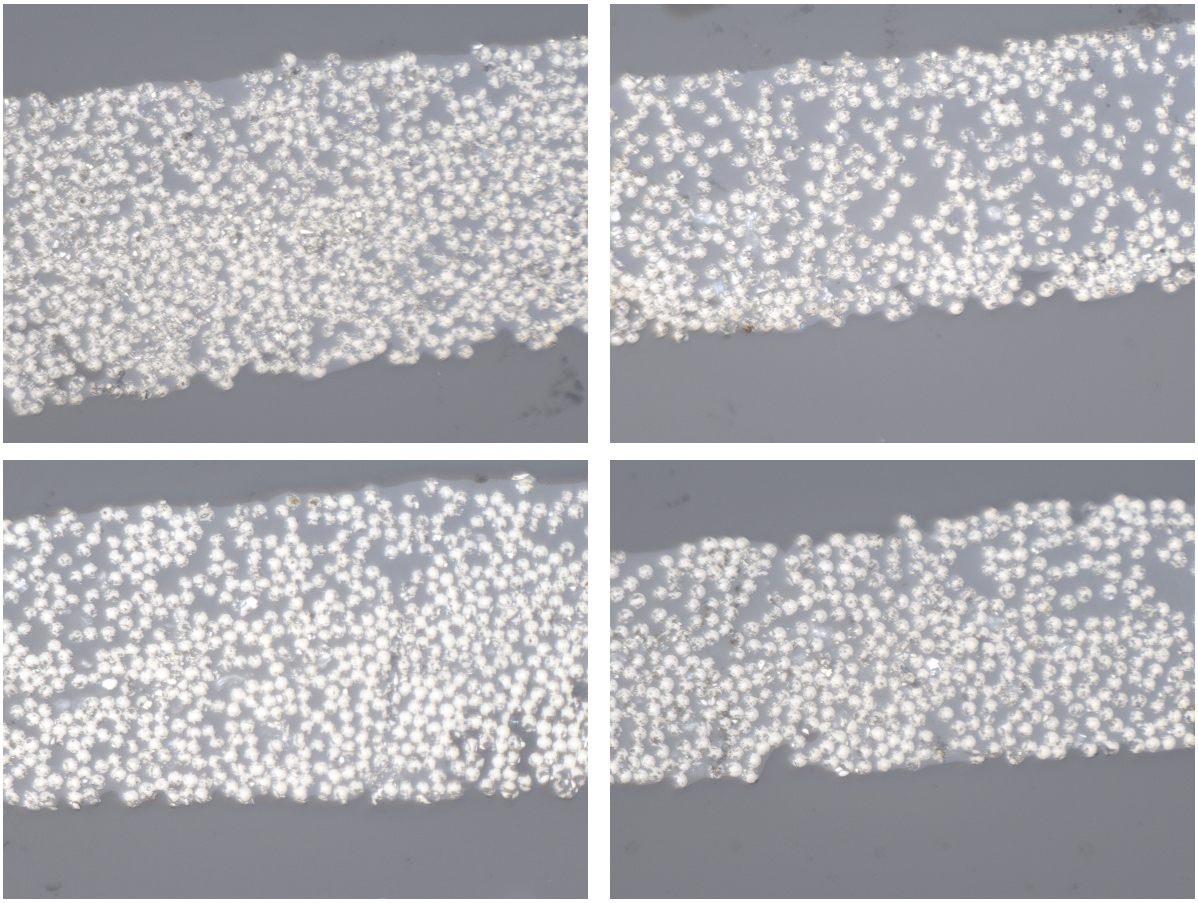

Figure 9.2: Four examples of decompaction and cavities at high fiber volume locations. Placement speed = 200 mm/s, consolidation pressure = 600 kPa

9.2. All deconsolidation form values

As-Received

DEIC

Sample	Value
1	27.50%
2	27.67%
3	22.67%
Average:	**25.95%**

Roughness

sample	Ra	Rq
1	1.284	1.650
2	1.308	1.680
3	1.342	1.733
Average	**1.311**	**1.688**

Thickness

Sample	Value [um]
1	152.9
2	151.4
3	153.6
Average:	**152.633**

Void

Sample	Value
1	0.42%
2	0.53%
3	0.42%
Average:	**0.46%**

Figure 9.3: All deconsolidation form values per sample of the As-Received data point. Ra and Rq are in [μm]

40mm/s - 160kPa

DEIC

Sample	Value
1	16.67%
2	16.67%
3	15.67%
Average:	**16.33%**

Roughness

sample	Ra	Rq
1	3.254	4.105
2	3.059	3.833
3	3.087	3.923
Average	**3.133**	**3.954**

Thickness

Sample	Value [um]
1	145.3
2	153
3	143.5
Average:	**147.267**

Void

Sample	Value
1	1.80%
2	1.62%
3	1.76%
Average:	**1.72%**

Figure 9.4: All deconsolidation form values per sample of the 40 mm/s - 160 kPa data point. Ra and Rq are in [μm]

40mm/s - 600kPa

DEIC

Sample	Value
1	18.00%
2	18.17%
3	18.83%
Average:	**18.33%**

Roughness

sample	Ra	Rq
1	2.895	3.635
2	2.755	3.463
3	3.051	2.841
Average	**2.900**	**3.313**

Thickness

Sample	Value [um]
1	133.2
2	127.9
3	133.9
Average:	**131.667**

Void

Sample	Value
1	1.28%
2	1.99%
3	1.49%
Average:	**1.58%**

Figure 9.5: All deconsolidation form values per sample of the 40 mm/s - 600 kPa data point. Ra and Rq are in [μm]

120mm/s - 160kPa

DEIC

Sample	Value
1	19.33%
2	18.33%
3	18.67%
Average:	**18.78%**

Roughness

sample	Ra	Rq
1	2.598	3.275
2	2.721	3.390
3	2.799	3.552
Average	**2.706**	**3.406**

Thickness

Sample	Value [um]
1	141.6
2	145.2
3	149
Average:	**145.267**

Void

Sample	Value
1	1.17%
2	1.60%
3	1.90%
Average:	**1.56%**

Figure 9.6: All deconsolidation form values per sample of the 120 mm/s - 160 kPa data point. Ra and Rq are in [μm]

120mm/s - 300kPa

DEIC

Sample	Value
1	19.67%
2	19.50%
3	20.17%
Average:	**19.78%**

Roughness

sample	Ra	Rq
1	2.496	3.164
2	2.377	2.959
3	2.383	2.992
Average	**2.419**	**3.038**

Thickness

Sample	Value [um]
1	134
2	137.1
3	134
Average:	**135.033**

Void

Sample	Value
1	1.63%
2	1.47%
3	1.52%
Average:	**1.54%**

Figure 9.7: All deconsolidation form values per sample of the 120 mm/s - 300 kPa data point. Ra and Rq are in [μm]

120mm/s - 600kPa

DEIC

Sample	Value
1	21.00%
2	20.67%
3	20.33%
Average:	**20.67%**

Roughness

sample	Ra	Rq
1	2.265	2.842
2	2.218	2.802
3	2.297	2.924
Average	**2.260**	**2.856**

Thickness

Sample	Value [um]
1	127.9
2	125.8
3	128.1
Average:	**127.267**

Void

Sample	Value
1	1.09%
2	0.84%
3	0.88%
Average:	**0.94%**

Figure 9.8: All deconsolidation form values per sample of the 120 mm/s - 600 kPa data point. Ra and Rq are in [μm]

200mm/s - 600kPa

DEIC

Sample	Value
1	23.17%
2	21.67%
3	23.00%
Average:	**22.61%**

Roughness

sample	Ra	Rq
1	2.079	2.628
2	2.142	2.705
3	2.100	2.645
Average	**2.107**	**2.659**

Thickness

Sample	Value [um]
1	125
2	123.6
3	123.9
Average:	**124.167**

Void

Sample	Value
1	0.94%
2	1.11%
3	1.00%
Average:	**1.02%**

Figure 9.9: All deconsolidation form values per sample of the 200 mm/s - 600 kPa data point. Ra and Rq are in [μm]